Characteristics and Bioavailability of Dissolved Natural Organic Matter in a Boreal Stream during Storm Flow

Alexander Håland

Thesis for the Master's
Degree in Chemistry

60 study points

Department of Chemistry
Faculty of Mathematics and Natural Sciences

UNIVERSITY OF OSLO

06 / 2017

Abstract

DNOM (Dissolved Natural Organic Matter) is characterized as a heterogeneous mixture of organic macromolecules. DNOM is naturally formed in soils, sediments and natural waters by decay and alteration through biodegradation of plant and microbial remains in a process called humification. The material has a profound influence on water chemistry and thus plays an important role in the natural environment. A main characteristic of DNOM is its weak organic acids which allow it to regulate pH and act as a transport medium for pollutants and nutrients from the terrestrial to the aquatic environment and as an important source for food for aquatic organisms. DNOM`s ability to absorb light darkens the colour of water resulting in a yellow-brownish colour. In natural waters receiving high concentrations of DNOM light is inhibited from reaching the deeper parts of the water column. Such conditions may severely affects the organisms living there by preventing photosynthesis, but also by affecting the waters temperature causing severe changes in both production and species diversity.

During the past 30 years there has been a widespread increase in colour of surface waters in Europe and North-America. In Southern Norway the concentration of DNOM has more than doubled in just a few years, while the amount of colour has increased even more. This indicates that DNOM is not only increasing in concentration, but is also changing its physical and chemical character. The increase and change in DNOM is hypothesized to be driven by a number of factors; reduction in the amount of acid rain, changes in anthropogenic land use and climate change.

The objective of this thesis was to test a hypothesis that an increase in precipitation will not only increase the transport of DNOM to surface waters, but also supply the waters with DNOM of larger molecular weight and greater aromaticity, which could account for the change in relative colour. Both objectives were achieved by conducting an episode study where samples of water were collected from a 1st order stream in a virgin boreal forest area. The samples were collected sequentially during a rainstorm and subjected to analysis to see how changes in hydrology from dry base flow through a runoff peak affected the amount and chemical character of DNOM. The measurement of total organic carbon (TOC) is used as a proxy for the DNOM. Another objective was to improve a method for measuring biodegradation using novel instrument to monitor oxygen consumption.

The results confirmed that concentrations of DNOM increase during episodes. On the other hand, the UV-ViS absorption and fluorescence excitation- emission matrix (EEM) spectra,

contradicted the original hypothesis by showing a decrease in molecular weight and aromaticity. This is likely due to large peat coverage in the watershed. DNOM from mineral soils is more aliphatic and of lower molecular weight than DNOM from peat soils. As the water levels increases the change in flow patterns through the catchment affects the overall contribution of DNOM from the different soil sources, with more water originating from the mineral soils. The biodegradation experiments did not revealed any significant differences in the DNOM; however by using glucose as a reference the results from extensive method development showed a clear improvement in signal output when comparing the original method to the improved method. However, more future experiments are required in order to verify if the improved method for biodegradation can produce reliable results.

Preface

The research presented in this thesis was carried out as a part of the project “Effects of climate change on boreal lake ecosystems: Productivity and community responses (ECCO)”, funded by the research council of Norway (NFR), Norklima program, Project number 224779.

I want to start by extending a huge thank you to my supervisor Rolf D. Vogt for the guidance and support these last years. I am particularly grateful for expressing a trust in my capabilities as a researcher and giving me the confidence to explore the world of science on my own. I also want to thank my co-supervisor Kari Austnes for showing me how to do proper field work along with all the tips and tricks on everything from sampling procedures to cooking. Also, thank you to my co-supervisor Cathrine Brecke Gundersen for introducing me to the world of microorganisms and the art of biodegradation.

Finally, I want to thank all the wonderful and hardworking people at the Environmental Science group. Thank you Elena Martínez Francés and Christian Wilhelm Mohr for all the wonderful discussions and arguments we have had. Working alongside you two has done more to expand my scientific thinking than any lectures or courses I have attended. Thank you Tomas Mikoviny and Christian for introducing me to the exquisite art of programming and helping me to get started with RStudio®. Thank you Claus Nilsson, Armin Wisthaler, Hans Martin Seip, Liang Zhu, Wen Tan, Yemane Kidanu Gebreslasse and Nina Reijrink for your support, discussions and criticism. Captivating conversations in the late evening will be some of my best memories. I wish you all the very best in life.

Table of Contents

1 Introduction

The overall structure of this thesis focuses on the different aspects of the study and nature of natural organic matter (NOM). Chapter 1 gives an introduction to what NOM is and its potential positive and negative effects on the environment. Chapter 2 starts by introducing the reader to the history of NOM-studies to explain the emergence of various classification systems of NOM, but also to illustrate the challenges and thereby the uncertainties related to its structural and chemical characterization. Chapter 2 continues by outlining some of the latest theories on the source and formation of NOM and how natural physicochemical processes continuously alter the NOM-pool residing in soil and water. This is considered important in order to see any relation between analytical results and the observed effect NOM has on the environment. Chapter 3 lists and explains the experimental design and analytical techniques applied to characterize samples of dissolved natural organic matter (DNOM) collected in the field. Chapter 4 presents the results from the various experiments and discusses them in relation to the theory and challenges presented in Chapter 1 and 2. A conclusion based on the results is presented in Chapter 5. Based on the experience obtained from this study, Chapter 6 presents thoughts and ideas on how future studies can be improved to achieve a better characterization of DNOM. The various calculations, graphs and tables resulting from the analysis is listed and explained in Appendix (Chapter 8).

1.1 Dissolved natural organic matter. Source, characteristics and environmental effects

DNOM is a term describing a heterogeneous mixture of organic macromolecules naturally formed in soils, sediments and natural waters by biochemical and chemical reactions during the decay and transformation of plant and microbial remains (a process called humification). DNOM originate from a great number of different sources and is therefore omnipresent in surface waters. The contribution and physicochemical characteristics of DNOM from these sources differs greatly in time and space. Spatial differences in biotic, edaphic and topographic factors, along with anthropogenic influence and temporal fluctuations in hydrology governed by weather are examples of what governs the characteristics of DNOM (Vogt et al. 2004). Each water sample is a mixture of organic molecules of different form, size and functional groups composition (Tipping et al. 2016) - causing the complex nature of DNOM. The physicochemical characteristics of DNOM dictate its mobility, transport, fate and impact. We need therefore to determine DNOMs physicochemical properties in different water sources so that we can set those properties in context with its different sources and the factor governing its mobility and transport. This is a prerequisite in order to predict how these

characteristics will be influenced by changes in the environment, such as global warming and changes in land-use and management practices.

DNOM has a profound influence on water chemistry in the boreal environment by acting as a transport medium for pollutants and nutrients from the terrestrial to the aquatic environment, as well as regulating pH and light attenuation in surface waters. DNOM is characterized by its many weak acid functional groups which generates a low pH in poorly buffered water courses and gives the molecules ability to form strong metal-complexations (Rahman et al. 2010) with Fe, Al and heavy metals (Hg, Pb, Cd), and to participate in redox-reactions. As a complex mix of organic compounds, DNOM has lipophilic sorption capabilities and thus enhances the transport of persistent organic pollutants (POPs). Moreover, DNOM plays an important role in transporting nutrients through the environment and serves as a source for food for many heterotrophic organisms (Amon and Benner 1996).
DNOM`s ability to absorb light darkens the colour of water and inhibits light from reaching the deeper sections of a lake. In doing so it is influencing the organisms living there.

A widespread increase in colour of surface waters in Europe and North-America was in 2003 reported by the Norwegian Institute for Water research (NIVA) (Skjelkvåle 2003). This finding was based on chemical analysis of 189 different lakes which pointed to a significant increase in the concentration of dissolved organic carbon (DOC; i.e. the main constituent of DNOM) in 60% of the studied lakes. The finding has been hypothesized to result from three different factors: 1) Reduction of acid deposition from long-range transported pollutants (Garmo et al. 2016). 2) Climate change, involving an increase in global temperature and longer growing season, as well as accumulating of reactive nitrogen. This stimulate production of more terrestrial biomass (greening) and subsequently more degradation products like DNOM in the runoff leading to the increase of discolouration (browning) of surface waters (Finstad et al. 2016). 3) In areas influenced by human activities such as agriculture and industry, changes in land-use such as grazing, also affect the amount of biomass and thus the properties of DNOM (Vogt et al. 2004).

1.2 The ECCO-project

In 2013 a research project was launched to study: “Effects of climate change on boreal lake ecosystems” (ECCO). This was a collaboration between University of Oslo, University of Uppsala, Finnish Environmental Institute and NIVA.

The aim of this three-year project was to determine the effects the loads of DNOM have on the productivity and community responses in lakes in Norway, Sweden and Finland. This was pursued by using existing models and datasets, and also by collecting new data. Additionally, the project aimed to increase the understanding of how boreal lake ecosystems respond to the different drivers hypothesized to drive the increasing DNOM loading (increasing temperature, nitrogen (N) accumulation, decrease in sulphur (S) deposition and greening).

1.3 Aim of master thesis

The aim of this master thesis was to determine how natural processes such as hydrological flow-paths and storage in different soils are affecting the amount and composition DNOM in head water stream. In soil water of mineral soils the DNOM concentration, molecular weight and hydrophobicity is highest in the organic forest floor and decreases down through the soil horizons (Cotrufo et al. 2015). The theory at the onset was that increased flow leads to more flow through the organic rich forest floor horizon directly into surface waters, bypassing the sorbing capacity of the deeper mineral soil horizons. The hypothesis to be tested is that an increase in precipitation due to climate change will thus result in an increase in flushing of DNOM into freshwater systems, and that this DNOM is expected to be higher in aromaticity, molecular weight and hydrophobicity. Water samples were collected through rainfall episode from a small stream in a relatively virgin boreal forest and brought back for analysis. By applying various chemical and spectroscopic techniques the DNOM was analysed to determine if there is any fluctuations in its characteristics during the episode.

Allochthounous DNOM is a vital source of food for microorganisms living in the water column. A specific attempt was therefore made to see if there were any changes in bioavailability of the DNOM during the runoff episode. This was done by applying and improving an existing method for determining bioavailability by measuring the consumption of oxygen as a proxy for bacterial growth in water samples.

2. Theory

2.1 A brief historic review of NOM research

Natural organic matter (NOM) is a very broad term incorporating all forms of natural occurring organic materials found in nature. The study of NOM dates back to the 18th century when some of the first studies of NOM were published (Stevenson 1994; Senesi et al. 2009). One publication by Achard in 1786 described a dark brown solution extracted from peat using alkali and precipitated with acid. He discovered that a higher content of organic matter was extracted from the lower, more humified layers of peat than the upper, less decomposed layers. This solution was at the time considered to be one particular type of compound and was later named "humus" (latin meaning soil). In 1839, the Swedish scientist Berzelius conducted further studies on humus and determined its ability to form metal complexes with polyvalent cations (Al, Fe, Cu, Pb, Mn, ect). With the emergence of new analytical methods it was by the end of the 19th century widely recognized that humus was in fact a complex mixture of organic compounds with weak acidic properties that was largely colloidal in nature (Stevenson 1994).

At the start of the 20th century focus shifted toward determining the molecular structure and chemical nature of humus. In 1908, Schreiner and Shorey began a three decade long study to determine the different compound that constituted humus (Stevenson 1994) and had already by the end of 1910 discovered over 24 different compounds such as organic acids, hydrocarbons, fats, sterols, aldehydes, carbohydrates and specific N-containing substances. In 1930, A. Shmook published a book on pedology explaining some of the characteristics of humus and how it was formed by microorganisms (Stevenson 1994). He proposed that the nitrogen found in humus was proteins derived from microorganisms and an important part of the humus structure. The other part of the structure was aromatic rings derived from plant material (Stevenson 1994 and references therein).

Due to the discovery of an increasing number of constituents in humus it became necessary to infer a classification system based on a fractionation related to their general chemical properties. The first classification was simply to separate humus into two groups. First were the non-humic compounds belonging to well-known classes of organic chemistry. Second was the humic substances (HS), consisting of High Molecular Weight (HMW; i.e. 500-10000 Daltons)(VanLoon and Duffy 2011) compounds with a characteristic dark colour (Lehmann and Kleber 2015). After HS were determined to be a complex and heterogeneous mixtures of polydispersed materials a further sub-classification was necessary. It was already established

by Achard that humus was soluble in alkali and precipitates in acid and studies performed by many of Schreiner and Shorey`s contemporaries (Stevenson 1994) found that different compounds were soluble at different pH. After some refinement it became the classification system still used today (Table 2.1).

Table 2.1: Classification of humic substances.

(Aiken et al, 1986;VanLoon and Duffy, 2011).

Compound group	Solubility characteristics
Humin, HU	In-soluble at all pH
Humic acid, HA	Soluble at pH > 2 Precipitate at pH < 2
Fulvic acid, FA	Soluble at all pH

Data generated by the large number of studies made it clear that humic substance consists of a highly varied continuum mix of different compounds for which no single model will suffice. However, a molecular model representing the generic structure of HA and FA was necessary to infer chemical reactions. From the 1930s, scientist began to propose various generic molecular structures to describe HA and FA. One of the first proposed structures of HA was published by W. Fuchs in the beginning of 1930s (Stevenson 1994; Al-Faiyz 2013) and illustrated a condensed ring-system with carboxylic (COOH-) and hydroxyl (OH-) groups attached (Figure 2.1).

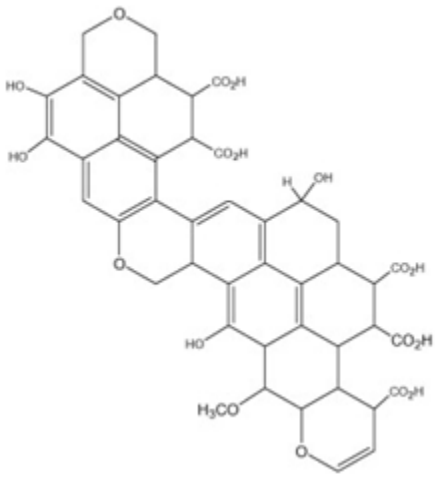

Figure 2.1: Proposed HA structure by W. Fuchs. Adapted from Al-Faiyz (2013).

However, widely accepted and cited by literature, this structure does not take into account alkyl chains, carbohydrates, proteins or nitrogen atoms. Introduction of X-ray diffraction analysis also revealed that Fuchs molecule was too condensed and a new model was required. Two new structures were proposed a few years later by Dragunov (Al-Faiyz 2013; Kononova 2013) (Figure 2.2) and Flaig (1960) (Figure 2.3).

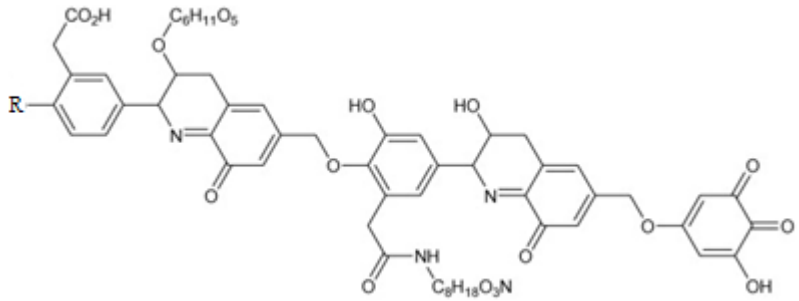

Figure 2.2: Structure of HA, by Dragunov. Adapted from Al-Faiyz (2013).

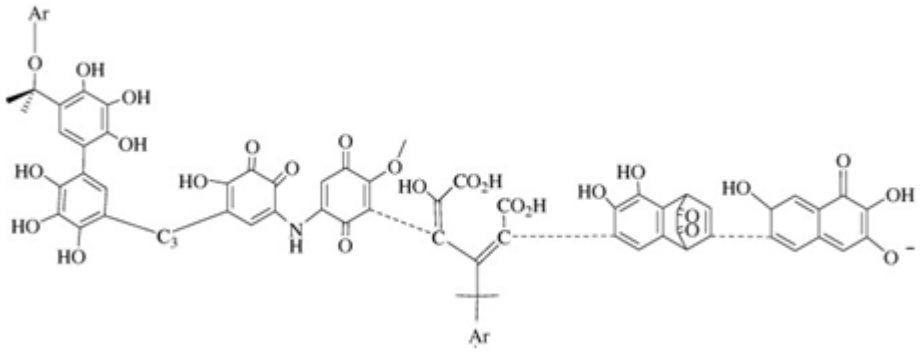

Figure 2.3: Structure of HA, by Flaig (1960). Adapted from Stevenson (1994)

Both models illustrated a more open structure in according with findings by X-ray diffraction and took into account the functional groups missing in the Fuchs model, but a fully acceptable model must also take into account a large number of COOH-groups to explain the acidic properties. In 1982, a hypothetical structure of HA was proposed by F. J. Stevenson (1994) (Figure. 2.4).

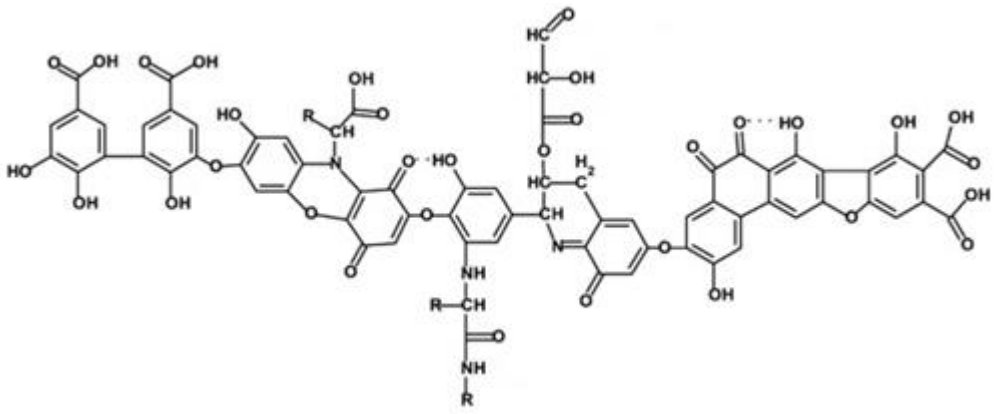

Figure 2.4: Hypothetical structure of HA by F. J. Stevenson. Adapted from Al-Faiyz (2013)

This has become the most common model cited in modern literature and will also be used as a reference for HA in this thesis. This model has an open structure in accordance with X-ray diffraction studies and contains functional groups most commonly associated with HA, including a larger number of COOH-groups. In addition to this model of HA, a second accepted model of FA was proposed a few years earlier in 1977 by J. A. E. Buffle (Stevenson 1994; Al-Faiyz 2013) (Figure 2.5). The average composition of HS is 45-60% carbon, 25-45% oxygen, 4-7% hydrogen, 2-5% nitrogen and 0.5-5% inorganic elements (VanLoon and Duffy 2011).

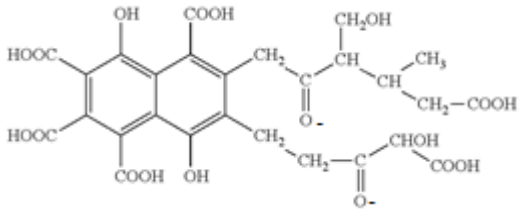

Figure 2.5: Structure of FA by J. A. E. Buffle. Adapted from Al-Faiyz (2013)

This model implies a smaller molecule with much higher oxygen content than HA, but they are largely accounted for in known functional groups such as COOH- and OH-groups while in HA oxygen is more incorporated in the nucleus. The model also implies a higher number of acidic groups compared to aromatic rings which explain its ability to remain in solution regardless of pH (Table 2.1). More recent experiments have also confirmed that FA contains a proportionally higher number of acid groups than HA (Perdue and Ritchie 2003).

2.2 Soil organic matter (SOM)

Soil organic matter (SOM) is a term referring to natural organic matter (NOM) found in soil. Many of the studies presented in Chapter 2.1 were actually performed on extracts of SOM. Recent studies reveal that there is a huge geographical and temporal variation in molecular

size, structure and elemental composition of SOM (Tipping et al. 2016). SOM affects many biogeochemical processes in soil due to the acidic properties and the ability to form metal complexes (VanLoon and Duffy 2011). SOM originate from all organisms in an area and is comprised of incomplete biotic and abiotic decomposition of their organic material as well as excretions from plants and animal. Plant remains are recognised to be the major source of SOM in forest areas (Nieder et al. 2008; Cotrufo et al. 2015). Moieties of SOM are known to be very recalcitrant and may persist in the environment for thousands of years (Schmidt et al. 2011; Lehmann and Kleber 2015; Barré et al. 2016).

The degradation pathways leading to SOM formation are referred to as the humification process (Cotrufo et al. 2013). The humification process was considered to be both a abiotic and biotic degradation of animal and plant remains, as well as an abiotic polymerization of low molecular weight (LMW) phenolic- and carboxylic molecules through concomitant ring cleavages forming aliphatic polymers (Hardie et al. 2009) and metal-LMW ring formation (Aiken et al. 2011). However, more recent studies questions the polymerization theory (Schmidt et al. 2011; Lehmann and Kleber 2015). This study emphasize that previous studies have used various extraction techniques to derive SOM from soil and later analysed and interpreted the results in the lab. However, this sample preparation has later shown to be inadequate in giving a quantitative representation of the size distribution of SOM. By observing SOM in situ using non-destructive extraction and analysis techniques it became possible to interpret SOM primarily as a collection of relative simple biomolecules (Figure 2.6). This weakens the theory of SOM formation by polymerization due to the lack of observed macromolecules in situ.

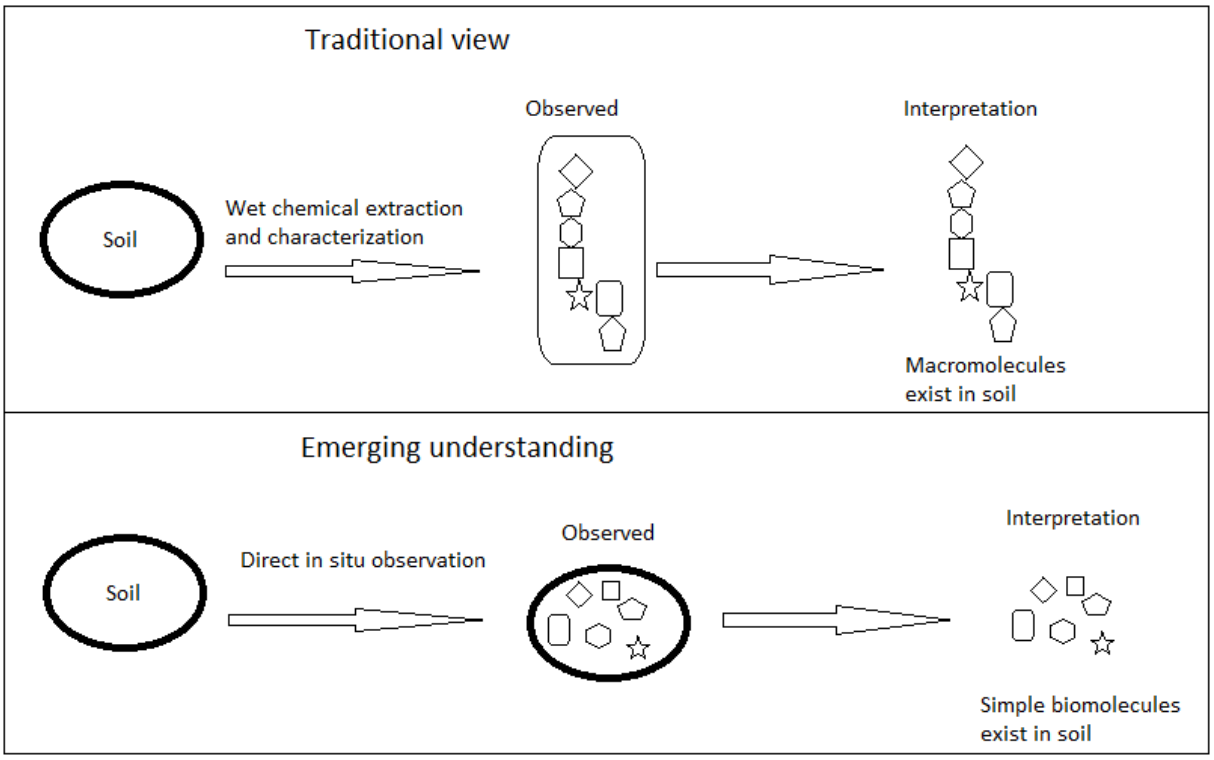

Figure 2.6: Illustrating how historic interpretations of SOM were influenced by method. In situ observations change the interpretation of the composition of SOM. Adapted from Schmidt et al. (2011). (Schmidt et al. 2011)

These findings are interesting but require more data to be verified by the scientific community. However, modern studies incorporating this new insight have given traction to two other models explaining the formation of SOM (Cotrufo et al. 2013; Cotrufo et al. 2015):

1. At the initial phase of plant decomposition the more labile compounds found in litter rapidly dissolves in water and leaches into the soil. The compounds are then readily available as food for microorganisms living there. This process has been described as a "microbial filter" (Figure 2.7) separating labile products from the more stable recalcitrant moieties (Wickland et al. 2007). The efficiency of the microbial filter depends on many factors such as amount of water available to dissolve the SOM and transport DNOM, temperature influencing the activity of microorganisms, substrate quantity and substrate quality such as the content of carbon and nitrogen (Wickland et al. 2007; Allison et al. 2010; Cotrufo et al. 2013; Kellerman et al. 2014).

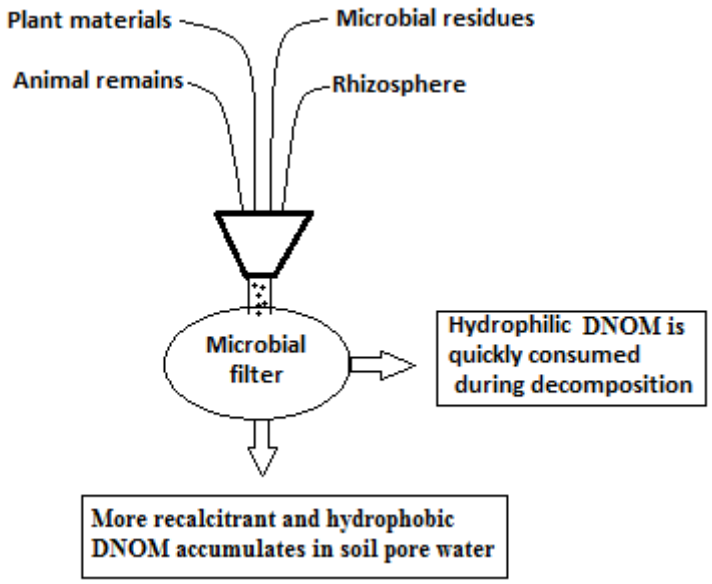

Figure 2.7: Illustrating the microbial filter separating the labile OM from the stabile OM. Adapted from Wickland et al. (2007).

2. The second model on the formation of SOM is the abiotic incorporation of the DNOM onto the soil structure (Figure 2.8). This takes place by an interaction between DNOM and the various components in the soil matrix. The adsorption may be directly to clays (phyllosilicates) or Al-, Fe-, Mn-oxides/hydroxides/sesquioxides - and using polyvalent cations such as Al^{3+}, $Fe^{2+/3+}$ and Ca^{2+} to name a few, as a charged bridge to bind negative charged DNOM to negative charged soil particles (Cotrufo et al. 2013). The binding of DNOM to soil stabilizes the organic compounds and makes part of SOM recalcitrant regardless of the chemical properties of the DNOM.

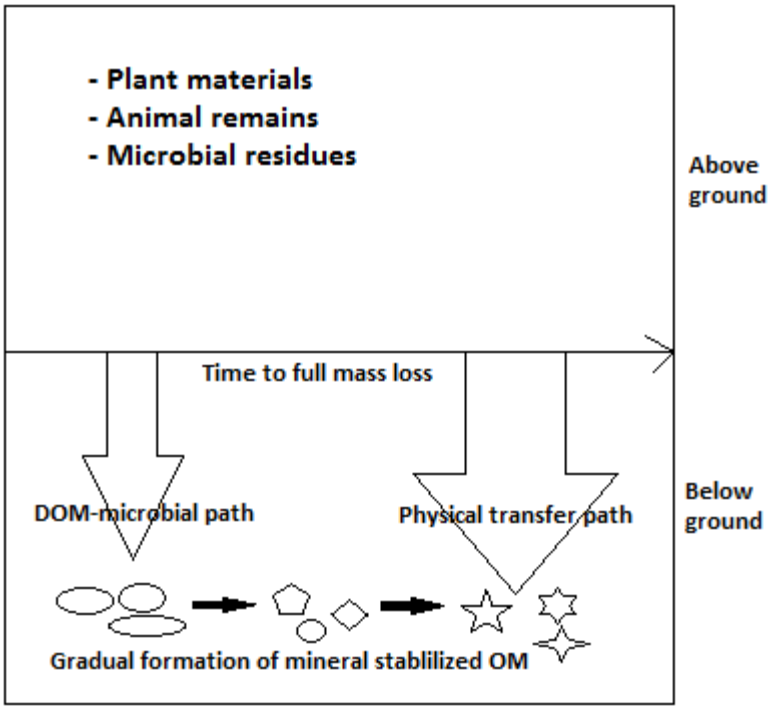

Figure 2.8: Illustrating the two theories of SOM formation: 1. Microbial filter to the left and 2. Abiotic incorporation of OM into the soil structure to the right. Adapted from Cotrufo et al (2015).

Assuming the second path of SOM formation, a consequence is longer residence time for both stabile and labile compounds in soil. Traditionally the term "recalcitrant" has been used to describe moieties with particular chemical properties that make them resistant against decomposition. However, based on the physical transfer path the term recalcitrant should actually refer to compounds stabilized by the environment regardless of their chemical properties (Schmidt et al. 2011). A large number of studies have showed that there is a distinct correlation between persistent OM and the lack of high-energetic C-H bonds in the molecular structure. This supports previous finding that the humification process creates more H-depleted OM that instead becomes enriched in oxygen due to the oxidation process (Barré et al. 2016).

2.3 Soil structure and composition

The International Organization for Standardization (ISO) lists 28 distinct soil types in the world and divides them further into 153 sub-divisions based on their structure, texture and chemical composition (International Standard 1998). Types of soil found in an area are determined mainly by the areas geological and climatic history, but are often influenced by human activity such as agriculture, industry and urban development. As a result soils develop

into a variety of different physical and chemical properties with depth. A description of these features is called a soil profile (VanLoon and Duffy 2011).

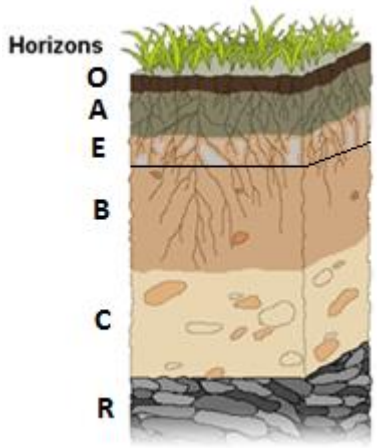

Figure 2.9: Illustrating the 5 main horizons that are generally found in a soil profile. Adapted from: Biggs and Nambiar (2016)

As illustrated in Figure 2.9 a typical soil profile consists of one or more of the following generic horizons (Maier et al. 2009):

O- The soils top layer consisting of organic materials such as litter and animal remains in various stages of decomposition.

A- Have a higher content of mineral materials such as clays, but also iron- (Fe) and aluminium- (Al) oxides compared to the O-horizon. OM has been decomposed beyond recognition and is constantly supplied from the O-horizon. The high content of OM, Fe and Al gives this layer a dark colour.

E- Zone of eluviation. OM bound to clays and metal oxides are removed from this horizon due to heavy leaching. The soil is often bleached and has a greyish to white colour.

B- Also named zone of illuviation. Clays, metal oxides and OM leached from the E-layer accumulates in the B-layer. The horizon is often brown in colour.

C- Has often a more coarse texture than the other horizons due to poorly weathered minerals from the underlying bedrock.

R- Solid bedrock and an important source of minerals to the soil although, not considered as part of the soil profile.

As litter and animal remains accumulate and starts to decompose in the O-horizon, OM dissolves in water as DNOM and percolate downwards. This leads to that the OM is slowly

relocated deeper into the soil. SOM in deeper soil horizons is mainly formed by abiotic incorporation of DNOM into the soil matrix (Schmidt et al. 2011; Cotrufo et al. 2015). The SOM is subjected to various forms of decomposition in the different soil horizons. In the upper part of the soil profile communities of microorganisms readily degrade the more labile fractions of the SOM, while in the lower parts the bioactivity is slower (Fierer et al. 2003) as there is less bioavailable material available. This entails that at any given time the SOM located in the upper part of the soil are chemically different from the SOM in the deeper layers.

2.4 Environmental impact of dissolved natural organic matter (DNOM)

Dissolved natural organic matter (DNOM) or dissolved organic matter (DOM) are two similar terms referring to the dissolved NOM described earlier that occurs ubiquitously in surface waters as well as in soil- and groundwater (Vogt et al. 2004; VanLoon and Duffy 2011).

Once dissolved, DNOM can have a profound impact on the water chemistry beyond lowering the pH. As mentioned earlier when describing humic substances, DNOM does not refer to single compounds but to a heterogeneous mixture of organic molecules too complex to be studied on the level of a single molecule. The observed properties of DNOM in the field or in the laboratory must therefore be considered as a weighted average for the whole mixture (Perdue and Ritchie 2003) or of a fraction of the material.

2.4.1 Acidic properties of DNOM

Because of the acidic properties OM may dissolve in water thus lowering the pH in the process (Oliver et al. 1983):

$$OM^{-}H^{+}_{(s)} + H_2O_{(l)} \leftrightarrow OM^{-}_{(aq)} + H_3O^{+}_{(aq)} \quad (2.1)$$

As illustrated in the generic models of HA and FA (Figure 2.4 and 2.5) the acidic properties of OM are largely associated with weak carboxylic- and phenolic acid functional groups. The former mainly have a pK_a-value between 2.5 and 5 depended on the molecular structure, while phenolic groups usually have a pK_a-range of 9 to 10 (VanLoon and Duffy 2011; Blackman and Gahan 2014). According to Henrys Law and given the average concentration of CO_2 in the atmosphere, pure water in equilibrium with atmospheric gases has a pH of about 5.6-5.7 (Appelo and Postma 2010; VanLoon and Duffy 2011). Under such circumstances OM are readily dissolved compared to waters with lower pH. However, the actual pH in various ground- and surface waters will vary considerably depended on soil composition. An example of this are soils containing a high concentration of acid cations such as Fe^{3+}, Al^{3+}, i.e. cations

with a high ionic index (charge-to-ionic-radius-ratio; Z^2/r). These ions can be exchanged for H^+ in the soil thus increasing the concentration of Al^{3+} and Fe^{3+} in the soil water while removing H^+. (Appelo and Postma 2010; VanLoon and Duffy 2011):

$$(Soil - M^{b+})_{(s)} + bH^+{}_{(aq)} \rightarrow (Soil - H_b)_{(s)} + M^{b+}_{(aq)} \quad (2.2)$$

Other examples are areas rich in carbonate minerals, such as limestone and dolomite, where the carbonate ($CaCO_3$) dissolves in water and make it more alkaline (Appelo and Postma 2010):

$$CO_{2(g)} + H_2O_{(l)} + CaCO_{3(s)} \rightarrow Ca^{2+}_{(aq)} + 2HCO^-_{3(aq)} \quad (2.3)$$

As the concentration of bicarbonate (HCO_3^-) increases it acts as a buffer by consuming H^+-ions thus elevating the pH:

$$HCO_3^-{}_{(aq)} + H^+{}_{(aq)} \rightarrow H_2CO_{3(aq)} \quad (2.4)$$

2.4.2 Chromophoric Dissolved Organic Matter (CDNOM)

An important property of DNOM is its ability to absorb light, thus darkening the colour of the water. Light is absorbed by the excitation of electrons surrounding the nuclei to a higher energy state. For most molecules the electrons of lowest energy surrounding the nuclei are those involved in single (σ-orbitals) and double (π-orbitals) bonding between atoms. Electrons not involved in bonding (n-orbitals) are at higher energy level while electrons involved in anti-bonding (σ^*- and π^*-orbitals) are at the highest energy levels. These energy levels are separated by gaps that need to be overcome in order for the electron to be excited. The larger the gap, the more energy are required. The nuclei determine the strength with which the electrons are bound and thus influence the energy spacing between their original and excited state (Lampmann et al. 2010). This means that the energy of a transition and thus the wavelength absorbed is determined by a group of atoms and their chemical environment (Senesi et al. 2009). The most probable transitions are $n \rightarrow \pi^*$ and $\pi \rightarrow \pi^*$ which requires low energy for their occurrence and thus occur readily in both the UV- and visual region of the electromagnetic spectrum (200-750 nm). As transitions require more energy they become increasingly rare at higher wavelengths (Senesi et al. 2009). The parts of a molecule that absorb radiation in the UV and visual spectrum are referred to as chromophores. The moieties of DNOM that have this ability are referred to as Chromophoric Dissolved Organic Matter (CDNOM) and can be a sizeable fraction of the mixture (Stedmon et al. 2000). As illustrated in Figure 2.4 and 2.5 the DNOM compounds contain many aromatic rings and aliphatic

groups constructed by conjugated double-bonds. It is these conjugated double bonds that exhibit chromophoric properties (Xiao et al. 2015). This allows DNOM to absorb light primarily in the UV-region with a gradual reduction of absorbency towards the red region (Stedmon et al. 2000). The longer the length of the conjugated chain the higher the absorbency is at higher wavelengths.

This effect has a major impact on an aquatic environment with high concentration of CDNOM. Its absorption of light reduces the sunlight's ability to penetrate through the water column thus leaving the lower depths deprived of photosynthetically active radiation, often abbreviated PAR. Phototrophic aquatic organisms are depended on PAR to maintain their lifecycle and will be unable to survive in lower parts of the water column. Similarly, predators depending on seeing their prey are unable to hunt in the dark environment. Forced upwards, the ecological niches of the euphotic zone is narrowed which can have a major impact on the amount and diversity of species in the aquatic ecosystem.

2.4.3 Metal complexation with DNOM

In the range of pH values commonly found in surface waters a substantial fraction of the weak acid functional groups on the DNOM are dissociated as indicated by the pKa-values given in Chapter 2.4.1. This leaves the DNOM compounds negatively charged and thus prone to complexation with metal cations, particularly forming chelates with trivalent cations such as $Al^{3+}$and Fe^{3+}. In a complex mixture of compounds such as those found in natural waters the various elements compete for available binding sites on DNOM. When analysing correlations between organic carbon and metals, those metals forming the most stable complex tend to have a high correlation with total organic carbon (TOC). Conditional stability diagrams show that trivalent cations with a high ionic index (Z^2/r) and transition metals with a high covalent index (X^2/r) are favourable (VanLoon and Duffy 2011) but this trend can be obscured if the concentration of one or more elements are higher than the average (Oliver et al. 1983), thus manage to outcompete the other elements for the most favourable binding sites. The overall abundance of inorganic anion ligands in water is also important as they will react with metals thus inhibiting metal-DNOM formation. Humic materials ability to bond to metals is therefore inversely related to the waters ionic strength (VanLoon and Duffy 2011).

A concern related to metal-DNOM formation is when organic matter forms complexes with toxic `soft` or `type B` metals with high covalent index, such as Pb, Hg and Cd. Since the start of the industrial revolution there has been report of large atmospheric deposition of heavy metals in the environment (Fitzgerald et al. 1998). In Norway long-range transported

air pollution has led to the accumulation of these toxic metals in the organic forest floor horizon. Bound to the organic matter they remain largely inert and are stored making little impact on the environment, but when forming covalent bonds with DNOM they may be suspended in the water column and subjected to transport and chemical reaction (Jordan et al. 1997; Haitzer et al. 2002). The increase of dissolved heavy metals may have a toxic effect on the aquatic life, pertly through methylation processes, and could affect the entire ecosystem, including humans who may depend on the aquatic environment for food, industry or recreation (Fitzgerald et al. 1998; Zheng et al. 2012).

2.5 The hydrological cycle and climate change

Water covers 73% of the earth's surface with the oceans making up about 97% of the total mass of earths water (VanLoon and Duffy 2011). The hydrological cycle is the cycling of the world's freshwater and encompasses all forms of water above ground and much of the water below ground. An important driver for the hydrological cycle is atmospheric temperature which causes evaporation from the ground surface to the atmosphere. As the vapour reaches lower temperatures in the higher atmosphere or further north, vapour condensates into clouds and precipitates back to the earth surface. Due to the importance of temperature, a change in the annual precipitation is considered a robust indication of global warming (Hov et al. 2013). However due to the large uncertainties linked to the measurement of precipitation and drought the numbers presented must be considered only as indicators of change and evaluated with care (Seip 2016).

Precipitation for northern Europe has on average increased between 10 and 40% during the 20th century while in some parts of southern Europe it has decreased by 20% (Dore 2005). In Russia, Canada, Norway and Poland there has been a 5 % increase in the amount of mean summer precipitation during the last century. Moreover, the probability for extreme rain-events has increased with more than 20% (Groisman et al. 1999). In Norway there are huge geographic differences in annual precipitation (200-2000 mm) due to topography (Groisman et al. 1999) but the overall trend points to an 18 % increase in annual precipitation for the whole country between 1900 and 2015 (Hanssen-Bauer et al. 2015). For the far northern regions, such as Svalbard there has been reported a 30% increase in annual precipitation from 1912 to 1996. This is believed to be caused by change in atmosphere circulation patterns due to increased greenhouse effect (Hanssen and Forland 1998). An annual temperature increase has also been observed along the east coast of Norway starting from the middle of the 1980s (Jensen et al. 2017).

2.6 Hydrogeology. Transport and hysteresis

Hydrogeology is a discipline that encompasses a broad and interdisciplinary study of water in the earth's crust (Hiscock 2011). As water precipitates on to land surface, most of it will percolate down into the soil, saturating the different soil horizons (Figure 2.10). The waters ability to move through the soil is measured as the hydraulic conductivity, K and is highly depended on the porosity and permeability of the soil matrix. In general, unconsolidated deposits such as those found in glacial bottom moraines tend to have a relative high K, and quickly absorbs rainwater thus preventing overland flow (Hiscock 2011). As the soil becomes saturated during rainfall event, water begins to move laterally. The movement of water in the soil, both vertically and horizontally can be described by Darcy`s law:

$$Q = -KA\frac{(h_1-h_2)}{L} \tag{2.5}$$

Where Q is total flow, K denotes hydraulic conductivity, A is the cross-section area of flow, (h_1-h_2) is the difference in height between two geographical points in the terrain and L stands for the distance between those two points. $\frac{h_1-h_2}{L}$ is also referred to as the hydraulic gradient and can be re-written as $\frac{dh}{dl}$ which gives the equation:

$$Q = -KA\frac{dh}{dl} \tag{2.6}$$

The negative sign indicates that the direction of flow is dictated by decreasing hydraulic gradient.

In situations with little rain the soil profile is unsaturated. The water then percolates through macropores through the soil profile and accumulates as ground water in the deeper unconsolidated deposits in the valley floor (Appelo and Postma 2010). This slow seepage of matrix flow through the ground water gives rise to base flow conditions. This water has had ample contact with the soil allowing for enhanced weathering and for practically all the DNOM to be lost through sorption. There is thus only a restricted transport of organic compounds to the stream from the lower part of the soil profile only – typically less than 2 mg C/L of DOC. As the amount of rain increases, the water levels in the soil rise and saturate the upper horizons. This causes interflow conditions (sub-lateral flow) and allows for a broader vertical and horizontal mixing of chemical compounds as well as of different microorganisms thriving near the ground surface (Fierer et al. 2003). Moreover, this sub-lateral flow allows for water passing through the organic rich forest floor O-horizon to drain directly into the stream, thereby by-passing the sorption capacity of the deeper mineral soils. The more

hydrophobic moieties of DNOM released from the SOM may then enter the stream as it is not sorbed to the mineral soil. Overland flow occurs if the intensity of rain surpasses the soil capacity to absorb or the amount of rain is so high that the soil becomes completely saturated with water. The soil profile in topographic depressions is the first to become water logged. As the rainfall continues the zone of saturation moves up along topographic gradients until all the soils are saturated with water (Figure 2.10). Then the water is no longer transported through the soil, but instead serves to dilute the chemical constituents in the streams and rivers (Hiscock 2011).

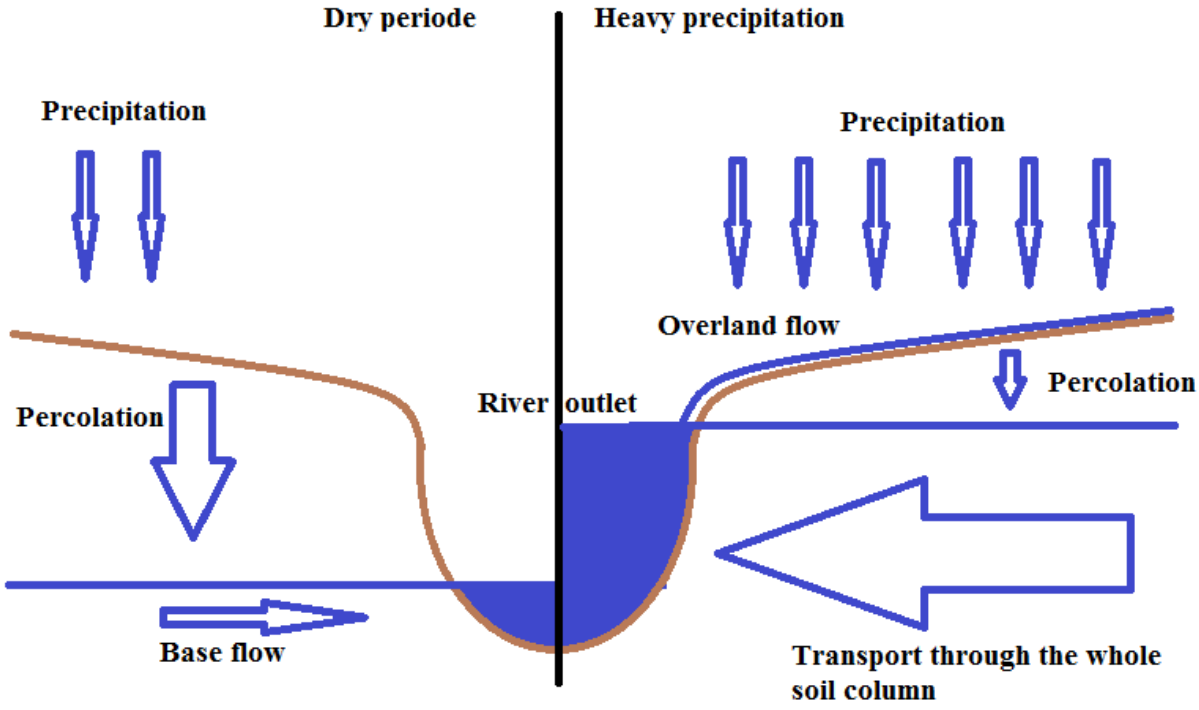

Figure 2.10: A schematic presentation of the different flow regimes induced by an increase in precipitation.

As the water moves sub-laterally through the soil it will eventually start to accumulate in topographic depressions (Figure 2.10). Rivers fed with water from the surrounding area, called a catchment, may serve as a "chemical fingerprint" for that catchment. It is possible to get an impression of the ongoing hydro-biogeochemical processes taking place in the watershed by sequentially collecting water from its rivers over a rainfall episode (from dry to wet – to dry) and analyse its composition (Austnes et al. 2010; Moravcová et al. 2010). However, the various concurrent geochemical processes in a catchment influence the water quality differently. At base flow the compositional changes in a stream occur slowly. This indicates a single large source of ground water slowly seeping out. Due to its long residence

time and good contact with the soil the base flow water is typically relatively richer in weathering products (silica and base cations), low in DNOM and with a rather high pH. When the water flow is increasing more water is entering the stream that has had shorter residence time and only been in contact with the shallow soil horizons. This water will be poorer in Si, richer in DNOM and with a lower pH. This causes the concentration of Si and base cations to decrease, while DOC and H^+ increases with increasing flow. When the soils become saturated and overland flow predominates the water dilutes all constituents causing all concentrations to decline. Higher concentration (c) of constituents in the rivers during increasing discharge (q) than during the same runoff intensity at decreasing runoff (Moravcová et al. 2010) is a phenomenon known as hysteresis and can be studied by plotting the c-q relationship in a diagram.

Hysteresis can be observed when a physical system (water catchment) is influenced by both an external source (precipitation) and by the systems history (accumulation and storage of elements and compounds in the soil) (Hornberger et al. 2001; Moravcová et al. 2010; Fovet et al. 2015). During a rainstorm, the discharge in a river will respond faster to the onset of heavy rainfall, but respond slower to the decline in rainfall. As the water start to percolate through the macropores of the soil it dissolves and flushes the soluble chemical compounds that have accumulated in the soil horizons since the last rainfall episode. These constituents are flushed out into the river. The water chemistry in the stream will therefore depend on the accumulated amount of soluble compounds in the different soil horizons and the predominant water flow-paths (described above) through the watershed into the stream during the different hydrological regimes over a rainfall episode. Temporal changes as the discharge increase or decrease lead therefore to an increase or decrease in concentration of different chemical constituents. By plotting the c-q relationship in a diagram we can see the positive or negative response of the different water chemical constituents to an increase in flow depending on what compartment of the catchment (i.e. end-member) is contributing water to the runoff. This is reflecting the changes in predominant water flow-paths. By also drawing arrows connecting each point in the diagram in accordance with the time the sample was collected, a hysteresis trajectory emerge showing a specific loop pattern (Hornberger et al. 2001; Moravcová et al. 2010). It is possible to identify the various geochemical processes in the area by analysing the elements hysteresis trajectories creating the different loop patterns (Moravcová et al. 2010). In general there are three different loop patterns:

Clockwise loops, CW (Figure 2.11). Seen when the amount of a compound stored in soil is small or is slowly accumulating. In such cases, as the river discharge is increasing, the soil is emptied for that particular compound giving the highest concentration in the rising limb of the hydrograph than in the lowering limb (Hornberger et al. 2001).

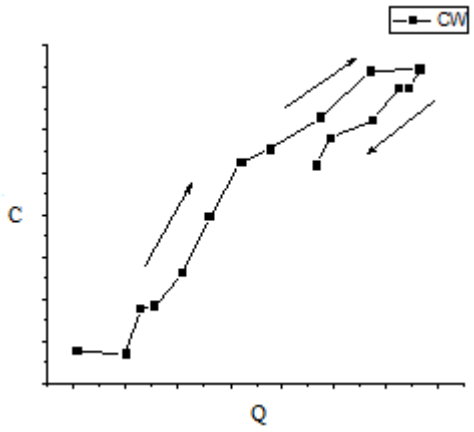

Figure 2.11: An example of a clockwise hysteresis loop.

Counter clockwise loops, CCW (Figure 2.12). This phenomenon is seen when the q- peak arrives before the c- peak, giving a c/q-ratio that is lower on the rising limb on the hydrograph than on the falling limb (Williams 1989). As the soil is flushed, the storage is too great for the soil to be emptied or the compound is accumulated rapidly, replenishing the system. In such cases the concentration is steadily increasing in the river as more and more are flushed from the soil. As the rainfall stops, the river only receives water from soil seepage saturated by the compound. The river receives the same amount of the chemical while the discharge drops, giving a higher concentration on the descending limb of the hydrograph than the rising limb (Hornberger et al. 2001).

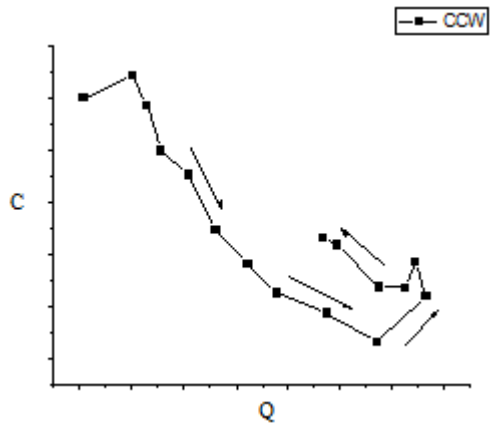

Figure 2.12: An example of a counter clockwise hysteresis loop.

Figure eight loops (Figure 2.13). Often referred to as ambiguous, they normally do not give clear information of any specific process (Hornberger et al. 2001) . These loops are often seen when there are several sources for a compound providing the river with overlapping waves of water containing high concentrations (Tananaev 2015).

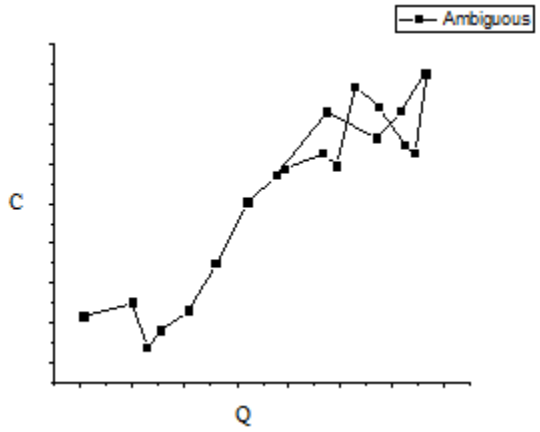

Figure 2.13: An example of an ambiguous hysteresis loop.

2.7 Diffuse double layer and acid rain

The DNOM suspended in the water column has a net negative charge (Equation 2.1). A negatively charge molecule has the potential to attract positively charged ions. As the positive ions are attracted to the surface they form a layer surrounding the molecule thus creating a diffuse double layer (DDL) of positively charged outer- and negatively charged inner layer extending out some distance from the surface of the molecule, gradual loosing charge as the distance increases. A property of DDL is that it repels other compounds thus inhibiting the molecules to get close enough to aggregate into larger, settle able units. As a consequence the DNOM remains suspended in the water column. The thickness of DDL is defined as the distance from the surface to where the charge is reduced to 1/e (0.37) of the charge on the surface of the molecule (Appelo and Postma 2010; VanLoon and Duffy 2011). In water with a low ionic strength the low concentration of ions means the DDL extend further out from the surface before it has attracted enough ions to reach the value of 1/e, thus creating a thicker DDL. However, when the ion strength is high, more ions are available to be attracted to the surface which means the DDL reaches the value of 1/e before it reaches significant thickness. This result in a thin DDL that is less able to repel other compounds suspended in the water thus allowing for compounds to aggregate and precipitate out from solution.

One of the major environmental problems in the 1970-90ties was acid rain (VanLoon and Duffy 2011). Long-range transport of anthropogenic emissions of sulphur and nitrogen to the atmosphere lead to the formation of sulphuric – and nitric acids when mixed with rain water and consequentially lowered the pH (Appelo and Postma 2010). As a consequence precipitation caused an increased acidification of streams and lakes, especially in northern Europe and North-America. The increased concentration of H^+-ions and sulphate in freshwater lakes and streams had two distinct effects on DNOM. 1) Increase in the waters ion strength which affected the thickness of DDL surrounding the DNOM molecules. 2) An increase in waters acidity leads to an increase in the dissolution of trivalent cations from the soil such as Fe^{3+} and Al^{3+} (Chapter 2.5.2). As a result DNOM became less soluble which reduced the concentration of total organic carbon (TOC) and colour in freshwater lakes and streams. However, due to public pressure the emissions acid oxides have been reduced. By 1986 a weak increase in pH and a decrease in sulphate in freshwater lakes were observed all over Norway. In correlation with the decrease in sulphate were numerous observations of a change in colour and increasing reports of elevated concentrations of TOC (Skjelkvåle 2003; Fasching et al. 2015; Finstad et al. 2016; Garmo et al. 2016). Given how the solubility of DNOM is influenced by the waters ions strength a question arises if it is possible to separate the effects of reduced acid rain from the effects of changes in flow paths due to changes in climate.

2.8 Biodegradation. A theoretical framework

The interaction between DNOM and microorganisms has been a well-known topic amongst scientists since the early days of DNOM- studies (Stevenson 1994), but research has yet to provide a full understanding (Hessen and Tranvik 1998; Cotner et al. 2010) nor does it seems to be any standard method for doing research.

Microorganisms that utilize organic carbon as a substrate for biosynthesis are called heterotrophs (Maier et al. 2009). They have the ability to either digest labile DNOM directly or transform recalcitrant DNOM to more labile forms (Hessen and Tranvik 1998). As DNOM is consumed by smaller organisms, they themselves become food for other larger organisms. Thus, DNOM becomes a part of a larger food-chain which sustains organisms on many trophic levels. As the microorganisms and larger organisms die, they themselves decompose and slowly turn into DNOM which becomes available for microorganisms. This process of DNOM sustained organisms who in turn becomes DNOM as they die is referred to as the microbial loop (Azam et al. 1983). In dystrophic lakes, DNOM seems to play a key role in bacterial activities which indicate that DNOM could in some cases be vital in sustaining an aquatic ecosystem.

In literature, a mathematical description of biodegradation rate is often given using the Monod equation (Neidhardt et al. 1990; Appelo and Postma 2010; Maier 2010).

$$\frac{dS}{dt} = \text{Growth rate} = \text{Kmax} * \frac{S}{S+K1/2} \quad (2.7)$$

Where S denotes substrate concentration in mg/L, dt is the incubation time in seconds, Kmax is maximal growth rate and K1/2 denotes the half saturation constant and represents the bacterium's affinity to the substrate being consumed. Thus, K1/2 depends on both type of substrate and species of bacteria.

A graphical representation of Equation 2.7 is illustrated in Figure 2.14.

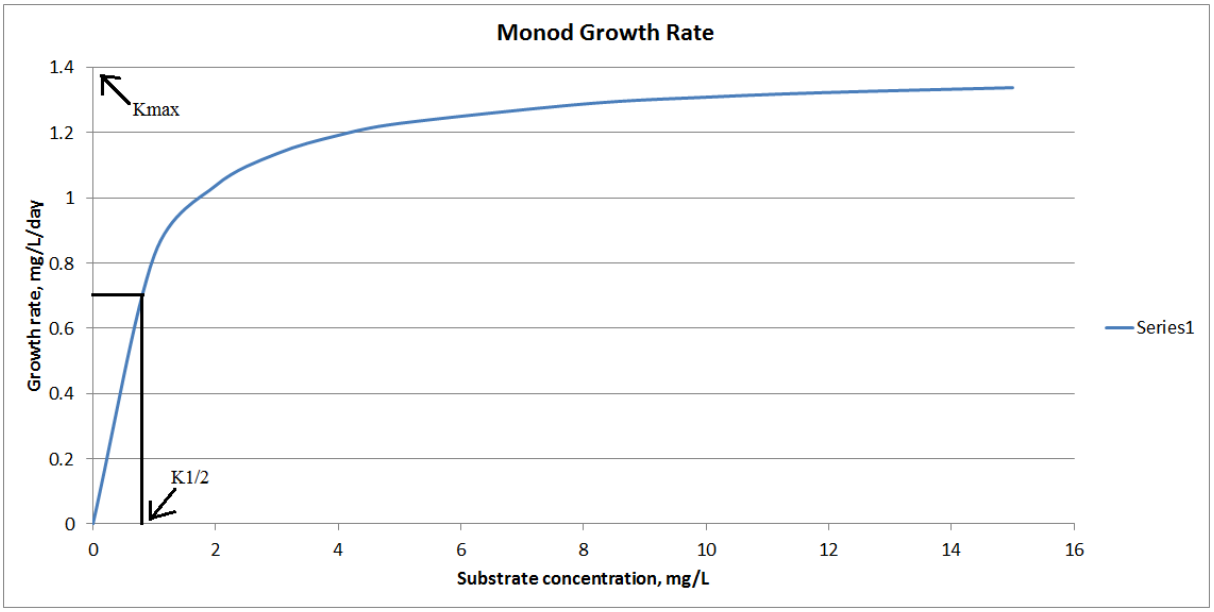

Figure 2.14: Illustrates the bacterial growth rate curve based on Equation 2.7.

As illustrated in Figure 2.14, when the substrate concentration is high it induces a high bacterial growth rate and sub-sequentially; when the substrate concentration is low it causes a low growth rate. If the observed increase in colouration of freshwater is due to increased concentration of bioavailable DNOM compounds it could lead to improved living conditions for heterotrophic bacteria.

However microorganisms cannot survive on an organic carbon source alone, but require a range of different nutrients to sustain growth. Inorganic elements such as nitrogen (N) and phosphorus (P) have proven to be particularly vital if bacteria are to generate biomass (Correll 1999; Elser et al. 2007; Hall et al. 2008). The mean molar biomass composition in bacteria taken from ocean samples is106C:16N:1P (Arrigo 2005). This has also been shown to be generally the case for freshwater bacteria (Cotner et al. 2010). This composition has become known as the Redfield ratio based on the work of Alfred C. Redfield (Redfield 1934) who first described such a relationship and gave an indication of what the substrate must contain of organic and inorganic nutrients in order to sustain growth. Given the average molar composition of humic substances (Chapter 2.1) it could potentially provide well as a substrate for bacteria. Studies have shown that there is a strong correlation between bacteria growth and the degree to which the substrate is reduced or oxidized (Sun et al. 1997):

$$\text{Growth} = 38.4 + 10.6\frac{H}{C} - 70.9\frac{O}{C} + 183.2\frac{N}{C} \quad (2.8)$$

Where $\frac{H}{C}$, $\frac{O}{C}$ and $\frac{N}{C}$ are element concentration ratios.

As illustrated by Equation 2.8 the higher the oxygen content the more difficult it is for the bacteria to utilize the substrate for growth (Vallino et al. 1996). Since higher oxygen content is associated with older and more degraded DNOM (Hessen and Tranvik 1998) it is easy to deduce that bacteria will prefer freshly produced DNOM, but resent experiments have also found evidence of the contrary (Kellerman et al, 2015).

The aerobic microbial oxidation of substrate of substrate by bacteria can be described using Equation 2.9 below (Maier 2010):

$$a(C_6H_{12}O_6) + b(NH_3) + c(O_2) \rightarrow d(C_5H_7NO_2) + e(CO_2) + f(H_2O) \quad (2.9)$$

where a, b, c, d, e, and f represents mole numbers of substrate, nitrogen source, oxygen, cell mass, carbon dioxide and water respectively.. In Equation 2.9 the substrate is pure glucose ($C_6H_{12}O_6$) and the formula for cell mass ($C_5H_7NO_2$) does not represent a particular molecular structure but serves as a stoichiometric representation of a bacterial cell. Phosphorus is also vital for bacterial growth, however the concentration in bacterial cells is very low (Redfield ratio) and is thus exempted from Equation 2.9. The mole numbers varies from substrate to substrate, but can be determined by measuring the flux of one or more of the compounds in Equation 2.9 during a biodegradation experiment using batch cultures (Maier 2010). The letter d represents cell mass and is determined by the cell yield (Neidhardt et al. 1990):

$$\text{Cell yield, } Y = \frac{number\ of\ cells\ produced}{Amount\ of\ substrate\ consumed} \quad (2.10)$$

This means that the more efficiently the substrate is consumed the more bacterial cells are produced. The cell yield is determined experimentally for each compound and is depended on the structure of the substrate. The cell yield for aliphatic compounds such as octadecane ($C_{18}H_{38}$), which contains only aliphatic carbon and hydrogen, is around 1.49. A more recalcitrant compound, such as pentachlorophenol (C_6HCl_5O) with a high content of halogens has a cell yield of 0.05. Glucose, a compound considered as highly bioavailable has a cell yield of 0.4 (Maier 2010).

Balancing Equation 2.9 for different values of d reveals that at higher values of d the O_2 consumption and the production of CO_2 are reduced while the consumption of NH_3 increases. If the substrate is more recalcitrant (i.e. giving a low value for d) the opposite is the case. The bacteria are then unable to incorporate the organic carbon into their cell structure and instead the carbon is used to produce CO_2. The overall consumption of the substrate remains the same (calculations presented in Appendix, Chapter 8.1). This suggests that the structural character of organic matter being decomposed by bacteria may have a significant influence on the gas

exchange between soil, water and the atmosphere (Dijkstra and Cheng 2007). The application of the Monod equation and cell yield constants has received some criticism for being inadequate in describing how DNOM quality affects bacterial growth (Vallino et al. 1996). However, with the emergence of new technologies it is now possible to monitor more precisely the consumption of oxygen that occurs during biodegradation. This may be used as a proxy for bioactivity and subsequently the consumption of substrate.

The consumption of substrate is intimately linked to the growth of the bacteria culture. The different growth phases of a bacteria culture after being exposed to bioavailable substrate is shown in Figure 2.15:

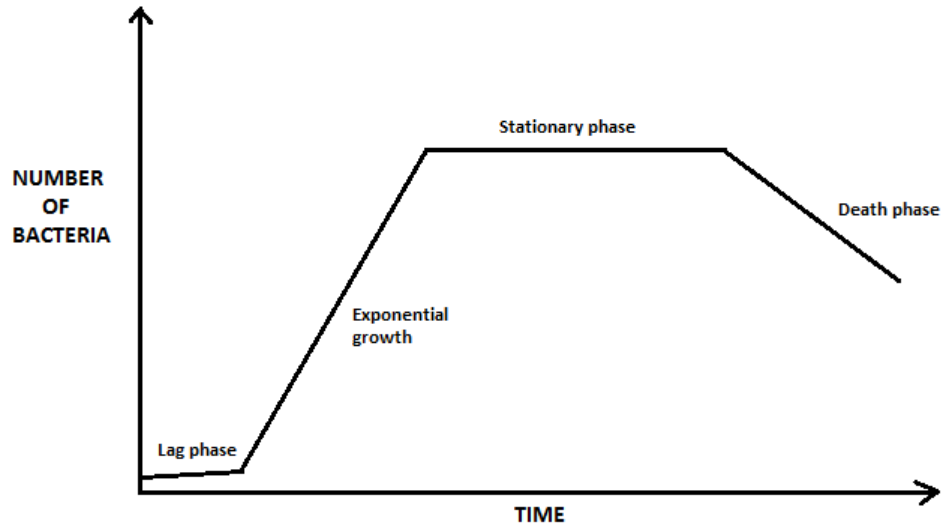

Figure 2.15: A typical growth curve for a bacterial population. Reconstructed and adapted from (Maier 2010)**.**

Usually there is an initial lag phase after a bacteria culture is exposed to substrate. In monocultures the lag phase is defined as the time it takes for the number of bacteria to double from its initial population. However, in the natural environment the initial population that can utilize the substrate is often very small thus neither the initial disappearance of substrate nor a significant increase in cell number are observed for several generations. This can lead to lag times lasting from several days to even years. The length of the lag phase may vary depended on how different their new surroundings are to their previous. Large differences in pH, temperature, type of substrate or the availability of inorganic nutrients can give quite lengthy lag phases where bacterial growth is minimal. But as bacteria is added to a substrate medium they start to adjust to their new surroundings, an phenomenon known as adaptation. As the number of bacteria increases the lag phase is usually overcome when the culture reaches about 10^6 bacteria pr. mL sample (Maier 2010). At this stage the bacteria have adapted to the

substrate and are capable of multiplying at an exponential rate and substrate are consumed accordingly.

The rate and length of the exponential phase are depended on the available substrate and other nutrients such as O_2, N and P. Studies have also shown that the bacteria will consume the most labile parts of the substrate first before they start to consume other more recalcitrant moieties. When the labile parts are consumed, they enter a new lag phase while they once again adapts before enter into a new exponential growth. This is called a diauxic growth rate and gives a bi-phasic growth curve (Figure 2.16) (Madigan and Martinko 2006):

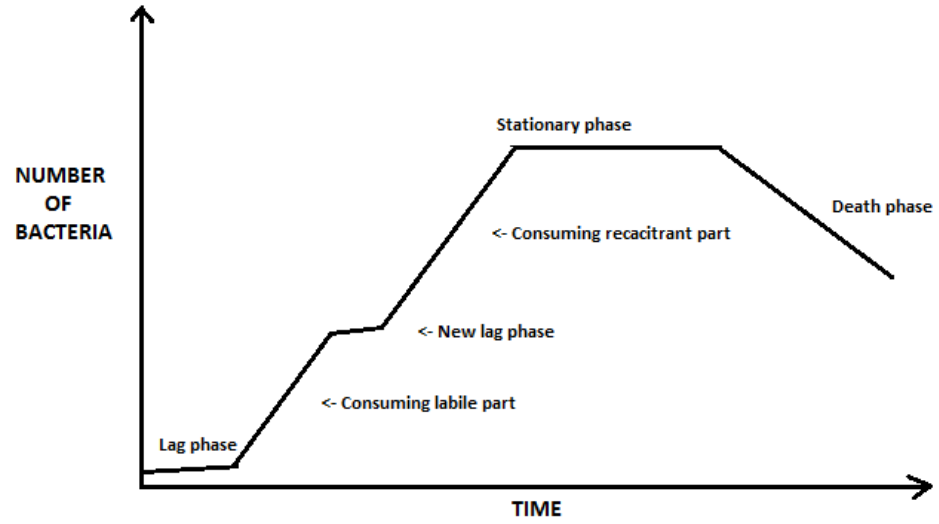

Figure 2.16: Illustrating a bi-phasic growth curve. Reconstructed and adapted from (Madigan and Martinko 2006)**.**

As the amount of bacteria reaches a certain number nutrients become scarce and competition increases. This is called the stationary phase where there is no net increase or decrease in bacteria. Nutrients are consumed at a steady rate until depletion. As the amount of nutrients diminishes to a level that cannot sustain the existing number of cells, the bacteria culture enters the death phase where there is a net decrease of cells. Data generated by biodegradation experiments can be related to Figure 2.15 and 2.16 to understand microbial processes in the samples.

2.8.1 Aquatic priming effect

In soil studies, a process referred to as priming effect (PE) has been observed (Dijkstra and Cheng 2007). PE is a mechanism where a pool of recalcitrant OM becomes more or less biodegradable with the addition of labile OM. The exact mechanism behind PE is not fully understood but since PE has never been observed in sterile samples it is believed to be microbial mediated (Catalán et al. 2015). PE could be of particular interest in episode studies

since the hydrological processes influencing an area will mix together different pools of DNOM that are normally separated in the soil horizons. However, while PE has been reported for DNOM in soil pore water, recent studies related to surface water presents a more ambiguous picture (Guenet et al. 2010; Danger et al. 2013; Guenet et al. 2014; Catalán et al. 2015; Bengtsson et al. 2015a). One argument against PE in aquatic systems is the effect presented in Figure 2.16; Due to the mixed nature of DNOM the microorganisms will simply consume the more labile fractions first before turning towards the more recalcitrant moieties (Bengtsson et al. 2015b). The number of microorganism's increases while the more labile fractions are consumed, thus presents the appearance of increased degradation. It would be interesting to see if biodegradation experiments performed on DNOM-samples from an episode present a classical Monod response as illustrated in Figure 2.16 or just an overall higher degradation rate which could indicate PE.

2.8.2 Analytical methods

There exists several different methods for determination of the amount of biodegradable dissolved organic matter (BDNOM) (Marschner and Kalbitz 2003; Grinhut et al. 2011; Fasching et al. 2015). This adds on to the complexity of this issue (Amon and Benner 1996). Determination of BDNOM has traditionally been measured based on the change in DNOM concentration in the sample (Badis et al. 2009), increasing number of bacteria (Vallino et al. 1996), changes in spectroscopic characteristics (Badis et al. 2009; Kothawala et al. 2012), the production of CO_2 (Wickland et al. 2007) or the consumption of O_2 (Gundersen et al. 2014). Each method has significant strengths and weaknesses. Measuring the concentration of DNOM and its spectroscopic characteristics is a very direct way of not only determining the bioavailability, but also which part of the DNOM is consumed by assessing the changes in the UV-/Visual absorption or fluorescent radiation. However, especially regarding recalcitrant materials the measure of changes in DNOM concentration or spectroscopic characteristics will require an experiment of significant duration as the bioactivity is often too low in natural samples to induce any measureable changes in a short time span (< 20 days).

Counting the increasing number of bacteria is perhaps the most effective way to measure the bioavailability of DNOM as the results can be directly correlated with Equation 2.10 and sub sequentially Equation 2.9, 2.8 and 2.7, thus allowing for accurate determination of the bioavailability. However, this requires access to specialized training and equipment. The measurement of CO2-production or O_2 consumption can be correlated with Equation 2.9 and used as a proxy for bioactivity, however measuring CO_2 requires the user to regularly open

the container in which the sample are degraded thus exposing the sample to the environment. Only the measurement of O_2 can be done in a closed environment with the use of specialised equipment. In this experiment a system developed by PreSens for measuring O_2-consumption were chosen. This allowed for a continued, real time measurements and assessment of the bioactivity in the samples.

2.9 Structural characterization of DNOM by spectroscopy

As explained in section 2.5.2 DNOM exhibit certain optical properties related to parts of the molecular structure referred to as chromophores. By using spectroscopic techniques to measure the absorbance or emission of radiation by these moieties it is possible to determine the amount and density of these molecular structures in the DNOM. As these properties may have an environmental impact, they also allows for the application of various spectroscopic techniques to determine the functional characteristics of the DNOM in a sample.

2.9.1 UV/ViS absorbency

Due to the complex mixture of different organic molecules, a DNOM sample contain a large pool of various chromophores exhibiting overlapping light absorbing properties covering both visual and UV light over a broad spectrum of wavelengths (Korshin et al. 1997; Peuravuori and Pihlaja 1997; Chen et al. 2002). This generates a continuing absorbance spectrum with few if any distinct peaks (Senesi et al. 2009; Leeben et al. 2010). As the spectrum is a continuum across the different wavelengths, calculating specific absorbance ratios (SAR) and spectral slope ratios (Sr) are often preferred to quantify the data (De Haan and De Boer 1987; Stedmon et al. 2000; Twardowski et al. 2004; Helms et al. 2008b). Studies have shown that certain DNOM properties influence different parts of the UV-/ViS-spectrum. Low molecular weight (LMW) organic compounds absorb at a lower wavelength than high molecular weight (HMW) organic compounds. By scanning the absorbency of radiation in the range of 200-800nm (i.e. UV-/ViS spectrum) by a DNOM sample a distinction can be made of the relative amount of each size fraction in the sample (Senesi et al. 2009; Lampmann et al. 2010). A relatively high absorbance in the lower wavelengths of the spectrum indicates a higher amount of LMW organics compared to HMW. At higher wavelengths the HMW molecules containing a larger number of conjugated double bounds, shifts the absorbance towards the longer wavelengths. Analogously, the addition of aromatic rings in the chemical structure causes the same shift. This is an effect called a bathochromic shift (Senesi et al.

2009; Lampmann et al. 2010). By using the ratio of the absorbance at 250nm and 365nm, referred to as E_2:E_3, it is thus possible to determine the relative size and the degree of aromaticity of the molecules in a sample. As the size and number of aromatic rings increases, E_2:E_3 decreases because the absorbance shifts towards longer wavelengths (De Haan and De Boer 1987; Peuravuori and Pihlaja 1997). The SAR-values can be obtained by calculating the ratio of 254/400nm (SAR_{UV}) and 400/600nm (SAR_{ViS}). Low SAR correlates with a high MW (Hautala et al. 2000), but as oxygen content increases SAR will also increase due to more $n \rightarrow \pi^*$ and $\pi \rightarrow \pi^*$ transitions induced by C-O bonds (Chen et al. 1977). A shoulder on the declining peak in the UV range is often observed at 254nm. This is related to conjugated double bonds of C=C and C=O (Abbt-Braun and Frimmel 1999) which are characteristic for aromatic compounds. By dividing the absorbency found at this wavelength with the concentration of DOC in the sample the specific UV absorbency index (sUVa) is obtained. This index correlates well with percent of aromaticity of the DNOM sample (Weishaar et al. 2003).

It has also been recommended to calculate the ratio between different spectroscopic slopes using the ratio of 275-295nm and 350-400nm, referred as S_R. This ratio has been correlated with MW and to photochemical induced shifts in MW, and can thus be used to classify the water as it facilitates comparisons between dissimilar water types such as CDNOM-rich forest waters recognised by low values of S_R and CDNOM-poor coastal waters usually having a high S_R-value (Helms et al. 2008b).

2.9.2 Fluorescence spectroscopy

As a contrary to UV/ViS- spectroscopy techniques that measure the absorbance of light as it travels through the sample, fluorescence spectroscopy analyse the fluorescent light emitted from the sample as each molecule is excited by an external light source. The molecules are excited using one wavelength at the time in a consecutive order and then the instrument scans for fluorescence at all wavelengths. This creates a three dimensional excitation-emission matrix (EEM) with excitation wavelengths and emission wavelengths on the x-and y-axis and the fluorescent intensity at those wavelengths on the z-axis. The obtained spectra are often represented in the form of a coloured contour map (Chapter 8.3.2). As with UV-ViS-absorbency, information about the structural characteristics can be obtained by assessing the intensities at certain wavelengths and correlate this with known spectroscopic properties of

organic compounds. Figure 2.17 illustrates where the fluorescence from different compound classes generally found in DNOM are distributed in an EEM spectra.

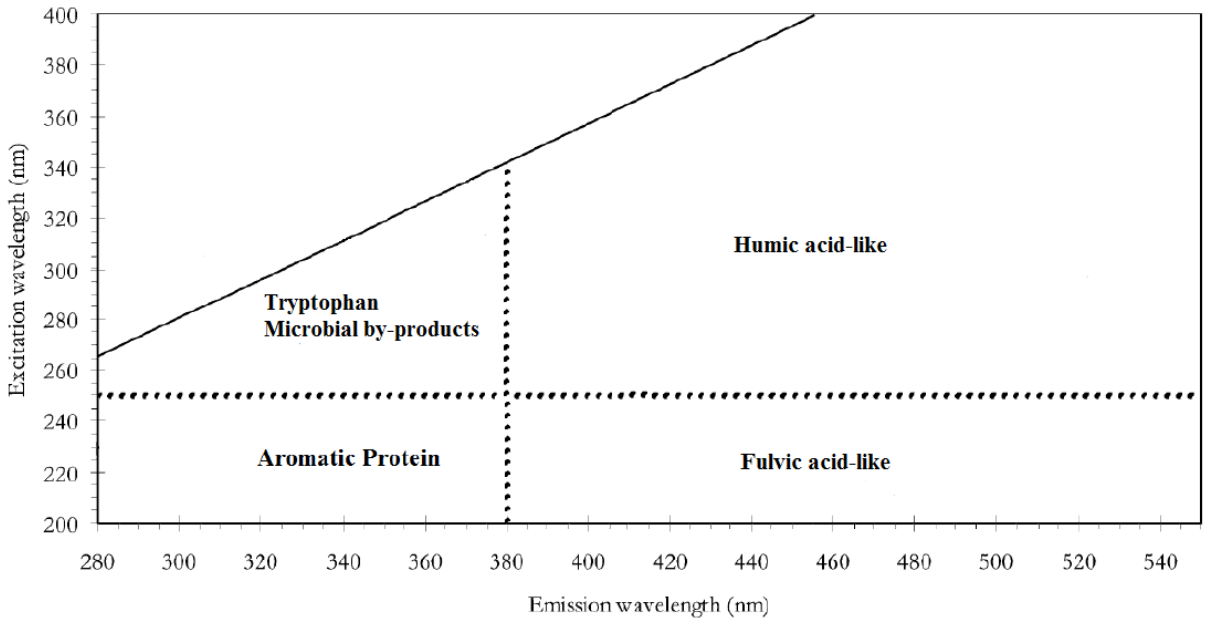

Figure 2.17: An illustration of how the different compound classes often found in DNOM are distributed in an EEM spectra. Adapted from Chen et al. (2003) and modified using information from Baker (2001).

By studying the relative intensity and position of the fluorescent peaks found in each section in the EEM spectrum it is possible to determine the relative amount of each class of compound in the sample (Chen et al. 2003).

Another widely used method for quantifying fluorescence spectra is the determination of the fluorescent index (FI). FI can be determined as the ratio between the emission intensity at 470nm and 520nm excited at 370nm (Cory and Mcknight 2005) and is strongly correlated with various sources of DNOM. FI can be used to determine if the humic matter in the sample are derived in situ by microbial activity or supplied from the terrestrial environment. Another useful value can be obtained from the EEM spectra by calculating the ratio between the intensity at 380nm divided by the maximum intensity observed between 420-435nm, excited at 310nm. This is called the freshness index because it indicates how decomposed or newly derived the humic matter is in the sample. Written as β:α, where β represents the recently derived DNOM and α the more decomposed DNOM. A high freshness index indicates newly derived DNOM that has not yet been decomposed by microorganisms or other abiotic processes (Fellman et al. 2010).

3. Materials and methods.

3.1 Field site description: Langtjern

Langtjern is a boreal lake catchment located in a remote area in the southern of Norway (Figure 3.1). Due to the remote location it has been left largely unaffected by human activities (with the exception of long-range air pollutants and climate change) for more than 200 years and is thus a suitable location for investigating natural changes in the environment. The area was established as a climate station by NIVA in 2010, and has also been used for monitoring the effect of acid rain on water chemistry and biota since the 1970s (de Wit 2015).

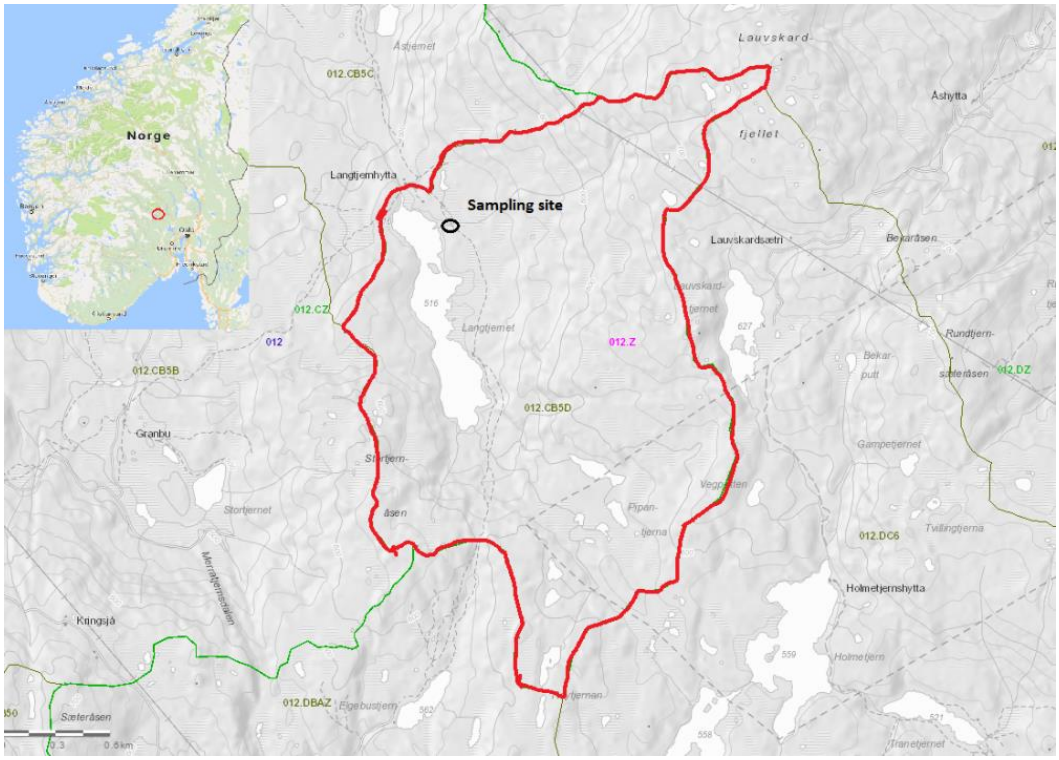

Figure 3.1: The location (top left) and boarder of the Langtjern drainage basin (red line) and the sampling site (black circle). Source: NVE (2017).

3.1.1 Sampling site description

The lake catchment covers an area of 4.69 km^2 and is situated between 516 - 760 meters above sea level (m.a.s.l). Langtjern watershed has a surface area of 0.227 km^2, has an average depth of 2 meters and is partly supplied by a small river located at the sampling site (Figure 3.1) to the north-east of the lake. The surface area surrounding the lake is largely covered by trees (63%) such as birch, pine and spruce while the remaining open areas consists of bogs (16%) with histosols and exposed bedrock (16%) (Henriksen and Grande 2002). The bedrock is largely of granites and gneisses. On the slopes a well-drained thin layer (typically less than 50 cm) of unconsolidated morraine or glaciofluvial deposits have developed into cambisol

and podsol soil profiles. The surface area displays a wavy pattern of small hilltops and depressions characteristic of glacial erosion. Along stream banks and bogs the soil profiles consists of water saturated histosols (Vogt 2005).

The stream at the sampling site has been equipped by NIVA with sensors to monitor parameters such as temperature, water level and CDOM. The data are recorded every two hours through the whole year and made publically available at the online Aquamonitor website: www.aquamonitor.no/langtjern/.

The frequent and long term recording of data from this river makes it an ideal sampling site for an episode study in that it makes it possible to correlate laboratory findings with data recorded by the sensors at the time of sampling. The river is also equipped with a V-notch weir which is used as a reference point for the water level. This helps to determine how the water level is calculated.

3.1.2 Water sampling

Water samples from the stream were collected using an ISCO water sampler; (US model 2900).The sampler collected 1 L of water split into two bottles (0.5 L each, 24 bottles in total) every hour for the duration of the episode. The sampling time were synchronized with the timer on the sensor installed in the river to ensure consistency with sensor data. Every 12th hour the sampler was emptied by the author and a fellow researcher from NIVA and the water samples were store in HDPE bottles in the dark on site until the end of the episode. The samples were later divided between NIVA (250mL) and UiO (500mL).

3.1.3 Sample selection and conductivity field measurements

The rainfall episode lasted for two days. This resulted in a large amount of water samples being collected. Due to practical reasons, a total of 26 different samples were kept while the rest was discharged at site. Selection of samples were made based on precipitation intensity at the time of sampling (high intensity was favoured) and conductivity of the samples. A large span in conductivity value was targeted as well as tracing the temporal changes in conductivity.

3.2 Sample pre-treatment

Upon arrival at the University of Oslo (UiO), the samples were stored in the dark at approximately 4°C. This was done to slow down any chemical and/or biological degradation of the DNOM.

3.2.1 Filtration

On the following day of arrival the samples were brought to the laboratory and left there in the dark until they reached room temperature (approximately 21°C). The samples were then filtered through 0.2µm membrane filter (cellulose acetate, Sartorius) using a water vacuum pump. This was done both to separate the particulate matter (PM) from the DNOM(< 0.45µm) and to sterilize the samples by filtrating out bacteria (>0.2µm) (Madigan and Martinko 2006; Maier 2010) . The filters were pre-rinsed with 150mL (Type 1) water to remove any traces of carbon on the filters (Khan and Subramania-Pillai 2006) . Loss of organic matter from the samples was observed during filtration as staining of the filter papers and reduced colour in the filtrate compared to the raw water sample. This is to be expected due to the very fine filters used. Frequent clogging of the filter papers was experienced which led to a prolonged filtration process lasting 2 hours pr. 500 mL sample.

After filtration a small volume (5 mL) of each sample was immediately analyzed for UV-Vis absorbency (se section 3.5.1). This was done to determine the structural character of each sample. The rest of the samples volumes were transferred to amber glass bottles and stored at 4°C until analysis.

3.3 Water characterization

The water characterizing analyses were conducted both at NIVA and the UiO.

3.3.1 Conductivity

Field measurements of conductivity and temperature were conducted using a Mettle-Toledo AG FiveGo^{TM} conductivity- and temperature sensor. The instrument was calibrated before departure from the University using a standard 85µS cm^{-1} calibration colution.

Conductivity was measured in the lab by NIVA according to ISO 7888 with a WtW inoLab Level 3 Conductivity meter using a WTW TetraCon 325 cuvette with a 10mm pathlength.

3.3.2 pH

pH measurements were conducted potentiometrically by NIVA using a GK 2401 C combined glass- and calomel electrode according to NS 4720. For measurements a Metrohm Titrino 799 GPT titrator were used with an GK 2401 C Radiometer electrode connected to a 789 Robot autosampler. All measurements were conducted at 25°C. A Metrohm temperature probe were used to correct for any temperature fluctuation during measurements.

3.3.3 Alkalinity

Total alkalinity was determined potentiometric by NIVA with a Metrohm Titrino 700 GPT automatic titrator and HCl. Sample aliquots of 50mL were titrated to pH 4.5 and measurements were conducted using a GK 2401combined glass electrode from Radiometer connected to a 789 Robot autosampler.

3.3.4 Colour

The samples colour (mg/L Pt) was determined by NIVA and is measured on samples filtrated at 0.45µm according to NS 4787. The absorbance is measured at 410 nm with a Perkin-Elmer Lambda 40P UV/VIS Spectrophotometer in a 5 cm special glass cuvette, using deionized water as reference. The results is given as unit less numbers but is compared to a calibration solution of potassium hexachloroplatinate and cobalt chloride which is measured as mg/L Pt.

3.4 Elemental composition

3.4.1 Anions

Major anions consisting of chloride (Cl^-), sulphate (SO_4^{2-}), nitrate (NO_3^-), fluoride (F^-), bromide (Br^-) and phosphate (PO_4^{3-}) were determined in accordance with Standard Method for the Examination of Water and Wastewater, Method 4110B. A Dionex ICS-2000 ion chromatographic system at the Department of Geosciences, UiO was used for the analysis. This is a two channel ion chromatography system capable of analysing both anions and cations. Samples were injected sequentially with a Dionex AS40 autosampler and separated using a Dionex AS18 column. The anions were separated based on their ion character which is a summary of their ion charge and hydration radius. The anions were detected using a Dionex Conductivity DS6 cell Detector. The signal-to-noise-ratio was improved using a Dionex ASRS300 4mm Anion self-regenerating suppressor to remove potassium from the eluent and replace it with H^+ thus converting KOH that has a high conductivity to H_2O with a low conductivity. This lowers the background noise created by the eluent. Finally, a computer running chromatography software produced a chromatogram and quantifies the data by converting each peak area in the chromatogram to a sample concentration.

The charge contributions from organic acids (DOC-[A^-]) were determined using a model developed by (Oliver et al. 1983).

3.4.2 Cations

Analyses of major cations (sodium (Na), potassium (K), calcium (Ca) and magnesium (Mg)) were conducted on two separate occasions. First analysis was conducted at the Department of Geosciences in together with analysis of major anions (Section 3.4.1). The samples were injected using a Dionex AS40 autosampler and separated in Dionex IonPac CS16 Analytical self-regenerating column using methane sulfonic acid as an eluent. A Dionex CSRS300 self-regeneration suppressor was used to improve signal-to-noise-ratio by removing methane sulfonic anion from the solution and replace it with OH^-. This converts the eluent to H_2O with a low conductivity, thus lowers the background noise. The cations were detected with a Dionex Conductivity DS6 cell Detector.

Second analysis was performed at the Department of Chemistry using a Varian VISTA Inductively Coupled Plasma Optical Emission Spectrometer (ICP-OES) to determine total aluminum (Al), Iron (Fe), manganese (Mn), Na, Ca, K and Mg. Sample aliquots of 20mL were preserved prior to analysis by adding 0.2 mL of a solution containing 32.5% nitric acid (HNO_3) and 4.6% cesium (Cs) as an ionization buffer to a final concentration of

approximately 3.3% HNO_3 and 463 mg/L Cs. The instrument is equipped with an echelle polychromator for wavelength selection and a Charged Coupled Device (CCD) detector to detect light emanating from atoms and ions excited at 6000-10000 kelvin. Samples were analyzed axially to maximize sensitivity.

The H^+ -concentration were calculated from pH.

3.4.3 Iron

Samples were conserved by lowering the pH (< 2) prior to analysis with nitric acid (HNO_3) and analyzed with a ICP-Mass spectrometer (MS) (Perkin-Elmer Sciex ELAN 6000) by NIVA. Samples were introduced sequentially with a P-E AS-90 autosampler and a peristaltic pump to a nebulizer where it is transformed into an aerosol. The aerosol is then atomized and ionized in argon plasma and transported to a low pressure compartment were the argon gas is removed. The charged ions are retained with an electric current and transported through an ion lens, focusing the current into an ion beam before it reaches the quadrupole mass spectrometry. Here the iron is separated from the other ions based on its charge-to-mass-ration and detected using a discrete electron multiplier detector.

3.4.4 Silica

Determination of silica (SiO_2) was conducted by NIVA by mixing each sample in a solution of HCl and molybdate (MoO_2^{-4}) (Grasshoff et al. 1985). Under acid conditions silica reacts with molybdate to form silicomolybdic acid, SMA (H_4SiO_4*$12MoO_3$). SMA is then reduced using ascorbic acid to give the solution a blue colour (molybden blue). The degree of blue colour is proportional to the amount of molybdate reactive silica and is measured spectroscopically by the absorbance at 830 nm. The analyzation was performed using a Skalar autoanalyzer (model not available).

3.4.5 Total Organic Carbon (TOC)

TOC were analyzed both at UiO and NIVA on samples filtrated at 0.2µm and 0.45µm respectably.

At NIVA samples were analysed according to ISO 8245 using a Tekmar Dohrmann (Apollo 9000 HS) carbon analyser and a method of non-purgeable organic carbon (NPOC). Samples are acidified by added phosphoric acid (H_3PO_4) and then purged with high purity air for 4 minutes to remove traces of CO_2. The organic carbon left in the sample is then decomposed to CO_2 using a platina catalyst at 680°C. The CO_2 is then transported to the detector using

synthetic air as the carrier gas and finally determined by a non-dispersive infrared (NDIR) detector.

At UiO TOC was determined using a Shimadzu TOC-V_{CPH} Total Organic Analyser. The same method of NPOC was applied. The final determination of CO_2 was conducted with a similar NDIR detector using argon instead of air as the carrier gas.

3.5 Structural characterization

The structural characterization of dissolved organic matter (DNOM) was conducted using spectroscopic analysis and performed primarily on samples filtrated at 0.2µm. Some analysis was also performed on aliquots filtrated on 0.45µm to correlate with existing datasets.

3.5.1 UV-/ViS absorbency

Each sample was analysed at UiO by recording full spectrum absorbency immediately after filtration on 0.2µm. The spectrum was recorded on a Shimadzu UV-1800 UV-Visible Spectrophotometer. The instrument is background corrected prior to analysis using cuvettes containing Type 1 water. During the scan one cuvette with Type 1 water is kept as a reference. The instrument starts measuring absorbency at 800nm using a tungsten hydrogen lamp and then scan the sample sequentially through each single wavelength. At 341 nm the instrument changes the light source automatically to a Deuterium lamp and then continues the scan to 200nm. Data are then extracted from the instrument via USB as csv-files and treated in Microsoft Excel.

At NIVA sample aliquots filtrated at 0.45µm were measured using a Perkin-Elmer Lambda 40P UV/VIS Spectrophotometer. Absorption was measured at every wavelength between 200 and 700nm.

Values of absorbency at λ = 254nm and λ = 400nm were used to calculate specific UV absorbency, sUVa (Abs_{254nm}/[TOC]*100) and specific visual absorbency, sVISa (Abs_{400nm}/[TOC]*1000) respectively. The same wavelengths were also used to calculate the specific absorbance ratio, SAR (Abs_{254nm}/Abs_{400nm}). The absorbency ratio known as E_2/E_3 were determined by dividing the absorbance at λ = 250nm with the absorbance at λ = 365nm. The E_2/E_3-ratio was then incorporated into models to determine the numbered average molecular weight of DNOM and the degree of aromaticity (Peuravuori and Pihlaja 1997);

$$Log_{\text{numbered-averaged MW}} = 5.341\text{-}0.401E_2/E_3 \quad (3.1)$$

$$\text{Aromaticity} = 52.509\text{-}6.780E_2/E_3 \quad (3.2)$$

Slope ratio, S_R were determined by dividing the slope in the absorbance region of λ = 275-295nm with the slope of λ = 350-400nm.

3.5.2 Fluorescence

Measurements of EEM spectra of the DNOM were performed at in cooperation with a fellow researcher NIVA on samples filtrated at 0.2µm at UiO. The analysis was conducted using a Cary Eclipse Fluorescence Spectrophotometer from Agilent Technologies. Due to the complex nature of DNOM and the large number of samples it became necessary to use instrument parameters that struck a balance between scanning time and resolution. Instrument parameters are presented in appendix.

3.5.3 Rate of biodegradation

The rate of biodegradation, known as the respiration rate (RR), in each sample was determined by calculation the reduction of oxygen during exponential oxygen consumption rate divided by the incubation time (Amon and Benner, 1996).

$$RR = \frac{O_{2(i)} - O_{2(f)}}{\Delta t} \quad (3.3)$$

Were $O_{2(i)}$ is the initial oxygen concentrations in the samples at the start of exponential oxygen consumption, $O_{2(f)}$ is the oxygen concentration at the end of the incubation and Δt is the time (h) between $O_{2(i)}$ and $O_{2(f)}$. The start of exponential consumption is defined as the point at which the measured values are more than three times standard deviation lower than the initial measurements during lag time. During method development, for the first approach to biodegradation a clear transition from no consumption to exponential consumption could not be made. Therefore the RR was calculated from the time of stable temperature to the end of the incubation.

3.6 Biodegradation experiment

The lack of an established method at UiO for conducting biodegradation assessments of DNOM necessitated a shift in focus from determining the bioavailability of DNOM to develop a method that produces reliable biodegradation data for future experiments. The method development consisted of four stages:

- Induce bacterial growth in the samples by inoculation
- Improve signal-to-noise ratio
- Extracting and interpreting the data
- Correlate method and results with literature for verification

Biodegradation experiments were conducted using two different approaches. The first experiment focused on absolute degradation while trying to mimic conditions found in the natural environment at the time and place of sampling. Degradation was performed on each sample at low temperatures and adding few nutrients to stimulate bacterial growth. As the knowledge and understanding for bacterial growth increased, a second experiment were conducted, focusing on the relative difference of degradation rate between the samples. Degradation during the second experiment was performed at a higher temperature while adding more nutrients to stimulate for higher growth rate, thus improving signal-to-noise ratio. Minor changes to the instrument set-up were also necessary to improve the results and will be explained in this section.

3.6.1 SensorDish® Reader

The SensorDish® Reader (SDR) is an analytical tool developed for easy and convenient measurement of oxygen levels in liquids. The system consists in principal of three main components: The SensorVials containing the samples, the SensorDish Readers and a computer with designated software for data processing and operating the system.

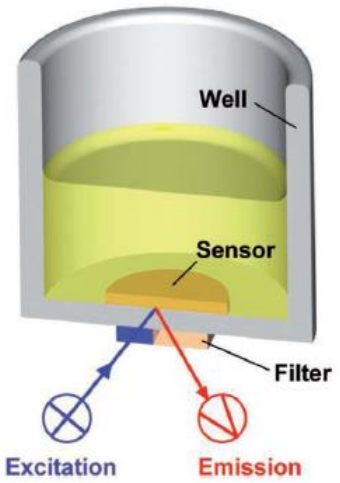

Figure 3.2: Illustrate the PSt5-sensor used to measure oxygen. Used with permission (PreSens 2016).

The SensorVials consists of 5mL vials made of borosilicate glass. The vials are closed with screwcaps and a rubberized septum to ensure it is properly sealed

from the outside air. At the bottom of each vial is a 5mm sensor spot type with the designation SP-PSt5 (Figure 3.2).

This spot is made of a hydrophobic silicone, doped with rubidium and contains a luminescent dye that becomes excited by a blue light emanating from the SDR-plate. Once excited the sensor spot will emit a luminescent light detected by the SDR. Its luminescent lifetime depends on the oxygen partial pressure in the sample. Here the oxygen acts as a quencher, reducing the luminescent lifetime. This relationship can be calculated by the computer by converting the sensor response to an oxygen value using a variant of the Stern-Volmer equation (PreSens 2017):

$$\frac{I_0}{I} = 1 + Ksv * [O_2] \quad (3.4)$$

I_0 denotes luminescent lifetime with no oxygen, I is actual luminescent lifetime of sample, Ksv denotes quenching rate and $[O_2]$ is the oxygen (quencher) concentration.

The computer uses SDR_v38 software to convert the data and to control the system during the experiment. During the experiment the software received an update to SDR_v4. Before each run, a few parameters need to be set. The SensorVials are calibrated by PreSens before shipping and given a specific batch number. A software package matching the batch number are downloaded from the PreSens webpage and uploaded into the software. Finally, before start the measurement temperature must be entered into the software. This ensures an accurate interpretation and conversion of the sensor read-outs. Stable temperature during measurements is crucial for both accuracy and data interpretation. According to Dr. Sarina Arain, product manager at Presens (personal email received 30.09.2016) a 3% measurement error must be expected if the temperature fluctuates with more than 1°C. At stable temperature the instrument technical data reports of a resolution of +/- 0.4% O_2 with a precision of +/- 1% O_2.

3.6.2 Inoculum

Inoculum is the term used for a culture of bacteria added to another solution to initiate biological activity.

All fresh samples were filtered through a 0.2µm filters to remove microorganisms. The moment when inoculum was added gave the experiment a “time zero”. To produce an effective inoculum several approaches were tested using glucose solution of 10 mg C/L as substrate due to its high and predictable bioavailability (Maier 2010). The test of the various

approaches is presented in Table 3 and the results are presented in Figure 20.Filter papers were added to help the bacteria develop a biofilm which in theory could accelerate the generation of new bacteria. The experiments lasted for approximately 110 hours and were conducted in room temperature. The oxygen consumption rate measured between 10 and 110 hours when the temperature was most stable were used for calculations. Inoculum 2 and 4 yielded close to half the response compared to Inoculum 1 and was discarded. Inoculum 1 was slightly better compared with Inoculum 3, though this could be a coincidence given the similar results. However due to the higher response, low standard deviation and the convenience of not having to use filter paper the method used to make Inoculum 1 was chosen for future experiments.

Table 1.1: Different experimental designs for production of inoculum that were testes: Filter water to remove microorganisms except bacteria. Phosphate added to stimulate bacterial growth. Filter paper put in the water to act as a solid surface for which the bacteria can form biofilm. Results show the average oxygen consumption in the water after added the inoculum

Inoculum	1	2	3	4	0
Sample water	Filtered, 2.0µm	Filtered, 2.0µm	Filtered, 0.2µm	Un-filtered	Blank
Nutrients	Phosphate	No	Phosphate	Phosphate	Phosphate
Filter Paper	No	Yes	Yes	No	-
Results	0.87 ± 0.04 µmol/h.	0.37 ± 0.04 µmol/h	0.69 ± 0.05 µmol/h	0.42 ± 0.05 µmol/h	0.02 ± 0.05 µmol/h
Replicates	4	4	4	4	4

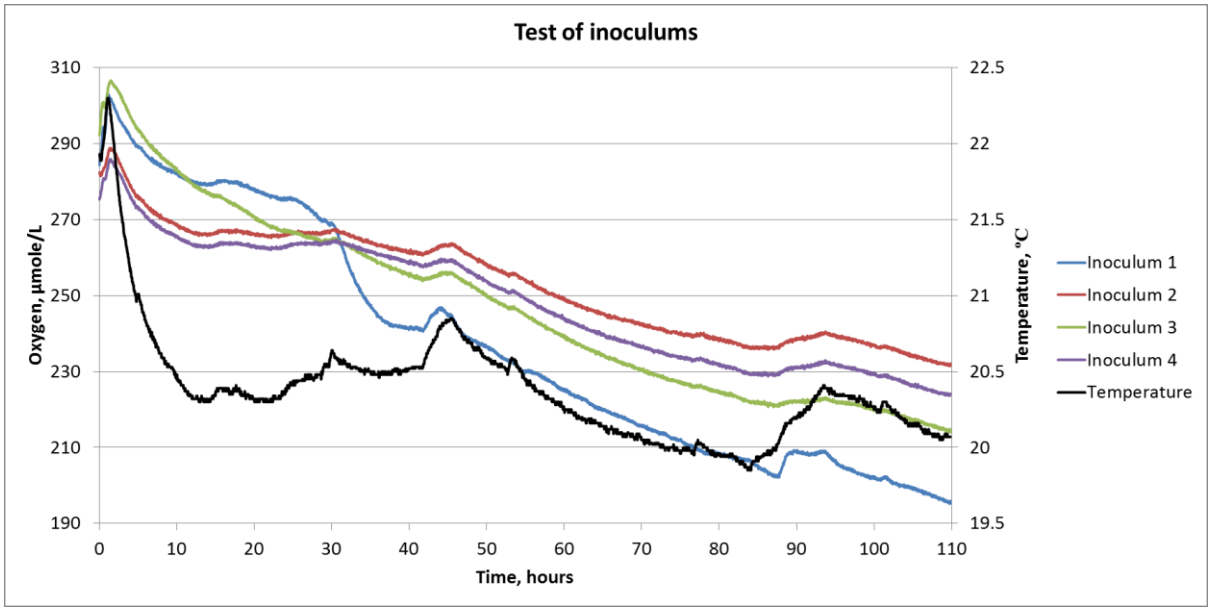

Figure 3.3: Illustrates the oxygen consumption in glucose solutions after adding different types of inoculums.

Based on the results shown in Figure 3.3 the Method 1, outlined in Table 3.1, was selected for the production of inoculum. The inoculum was thus prepared as follows:

A sample of raw water from Langtjern was filtered through 2.0 µm membrane filter (polycarbonate, Isopore) to allow for bacteria to pass the filter (Maier et al, 2009) while removing predatory animals and microorganisms larger than 2.0 µm that could feed on the bacteria. This is to ensure that bacteria are the dominant organism in the inoculum. Then, 100 mL of the filtrate was transferred to a 250 mL Erlenmeyer flask. To ensure optimal conditions for exponential growth, Phosphate (PO_4^{3-}) and Nitrate (NO_3^-) in the form of K_2HPO_4 and NH_4NO_3, respectively were added to a final concentration of 0.1 mM, and a headspace of 150 mL was set to ensure that the bacteria had enough oxygen. The inoculum was incubated at room temperature for two days on a shaking table at medium shaking speed to ensure the inoculum was properly saturated with oxygen. To avoid growth of algae the solution was covered with aluminium foil to remove light.

To ensure that ample bacteria were added to the samples to induce rapid degradation a volume of 2 mL were added during the first experiment. In the second experiment this volume was reduced to 250 µL in order to avoid excessive addition of organic carbon.

3.6.3 Nutrient solution

Adding nutrients such as phosphate and nitrate stimulate bacterial growth during biodegradation, thus improving signal-to-noise ratio when measuring oxygen consumption (Hall et al. 2008).

PO_4^{3-} and NO_3^- are considered important nutrients for bacterial growth (Correll 1999; Elser et al. 2007). However in freshwater ecosystems PO_4^{3-} is usually the limiting nutrient (Correll 1999). The decision was made to only add 0.1 mM of PO_4^{3-} to the samples to stimulate for exponential growth.

However, results from anion analysis revealed that neither PO_4^{3-} nor NO_3^- were present at detectable levels in the samples. As NO_3^- is essential for constructing bacterial cells had to be added to the samples in addition to PO_4^{3-}. Previous studies have shown that bacterial response is equally depended on nitrate as they are on phosphorous (Elser et al. 2007; Hall et al. 2008). It was therefore decided to add equal amounts of NO_3^- and PO_4^{3-} to both the samples and references.

The stock solutions of nutrients were prepared in the following way:

Dipotassium hydrogen phosphate (K_2HPO_4) and ammonium nitrate (NH_3NO_4) was dried in the oven at 105^oC for 24 hours to remove any trace of water and then left for cooling in a exicator for an hour before weighing out the correct amount using a Ohaus Discovery semi-

micro and analytical balance. For the first experiment a solution containing 10 mM (Kiikkilä et al. 2011) of phosphate was prepared by dissolving 2.282 g K_2HPO_4 in 1L of Type 1 water. For the second experiment a solution containing 10 mM of phosphate and 10 mM of nitrate was prepared by dissolving 2.282 g K_2HPO_4 and 0.8 g NH_3NO_4 in 1 L of Type 1 water. The solutions was then stored in a cold room until needed.

3.6.4 Reference material

With the establishment of the inoculums effect on glucose (Table 3.1 and Figure 3.3), a solution containing 10 mg C/L glucose became the reference of choice for future experiments in order to verify the presence of bacteria. Another advantage of using glucose as a reference is its well documented chemical properties (Blackman and Gahan 2014) and biological uptake (Neidhardt et al. 1990; Maier 2010; Brooker et al. 2011) which allows for a more quantitative analysis of bacterial response (Chapter 2.9).

An amount of anhydrous D(+)-Glucose was first dried in an exicator for 24 hours before weighing the correct amount. The reference for the first experiment were prepared by weighing 0.05 g glucose using a Ohaus Discovery semi-micro and analytical balance and dissolve it in 2 L type 1 water to a concentration of 10 mg $\frac{C}{L}$. For the second experiment the concentration of glucose was doubled to 20 mg $\frac{C}{L}$ to better match the average concentration of carbon in the samples.

3.6.5 Blanks

To compensate for instrumental drift two types of blanks were applied. First a theoretical blank were calculated by using the temperature fluctuations during measurements and Henry`s law.

$$K_H = \frac{p_{O_{2(g)}}}{C_{O_{2(aq)}}} * \frac{L_{water} * atm}{mol_{gas}} \qquad (3.5)$$

Were K_H is the Henrys law constant at a given temperature, $p_{O_{2(g)}}$ denotes the partial pressure of oxygen in the atmosphere and $C_{O_{2(aq)}}$ is the concentration of oxygen in water (Atkins and De Paula 2010).

The table value of K_H at standard conditions can be calculated for every given temperature using the following equation:

$$K_{H(t)} = K_{H(298.15K)} e^{(-C*\left(\frac{1}{273.15+t} - \frac{1}{298.15}\right))} \quad (3.6)$$

$K_{H(t)}$ is the Henrys constant at temperature t, $K_{H(289.15K)}$ denotes the Henrys constant at 25°C, -C is a constant in Kelvin (NIST 2016).

By applying Equation 3.5 to Equation 3.6 and then re-arranging Equation 3.5 to Equation 3.7, the concentration ($\frac{mol}{L}$) of oxygen in water at any given temperature can be calculated:

$$C_{O_{2(aq)}} = \frac{p_{O_{2(g)}}}{K_{H(t)}} \quad (3.7)$$

The second blank was made using vials containing Type 1 water as real blanks. For the first experiment the blanks were added nutrients and inoculum to account for O_2 consumption caused by bacteria feeding on the inoculum. However, as the bacterial activity in those blanks resulted in loss of oxygen, those blanks could not account for instrumental drift or used to evaluate if there is any leakage of oxygen into or from the vials. Therefore, for the second experiment only pure Type 1 water were used.

3.6.6 Sample preparation

The set of samples were prepared in 25 mL volumetric flasks by adding 250 µL of nutrient solution to each flask using an automatic pipette. A small aliquot of sample were then added to each flask to dilute the nutrients before adding inoculum. This was done as a precaution to avoid adding bacteria to a solution containing too much salt (nutrients) in fear of killing them, but also to ensure that an accurate volume of inoculum, nutrients and sample were mixed together. The flasks were then topped to the mark with sample and shaken by hand for 30 seconds to ensure proper mixing. Aliquots of 5.2 mL were extracted from each flask using an automatic pipette and transferred to 5 mL sensor vials. The surplus volume in each aliquot ensured no headspace was formed inside the vials during sealing. The vials were then sealed using designated screw caps and parafilm (Figure 3.4).

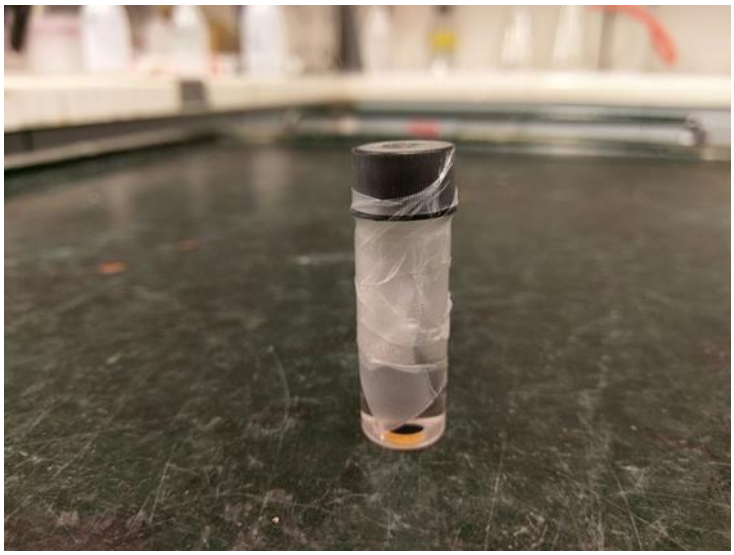

Figure 3.4: Proper sealing requires both the designated screw cap and a layer of parafilm to prevent leakage of oxygen in or out of the vial during measurements.

The vials were then systematically arranged on the SDR in a 4x6 grid before measurement (Figure 3.5).

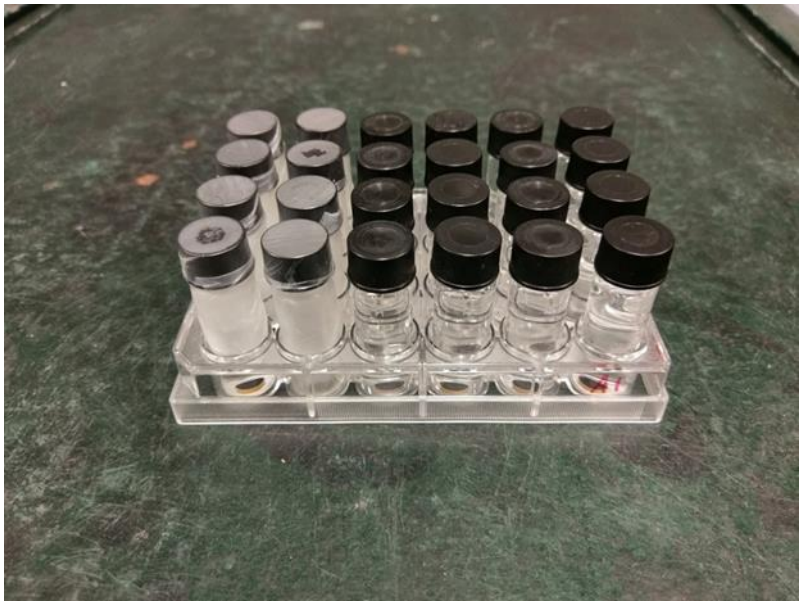

Figure 3.5: Illustration of how the vials were arranged on the SDR. All vials were sealed with parafilm before measurements.

3.6.7 Sealing test

Accurate measurements of the oxygen concentration in the samples depend to a large extent on proper sealing to avoid any gas diffusion. After the first biodegradation experiment had been conducted the PreSens provided a new type of screw caps for testing. According to Dr. Sarina Arain, product manager at Presens (personal email received 30.09.2016), these new caps have shown to improve the sealing. Results from tests performed at Presens are presented in Figure 3.6. A second test was performed at UiO comparing old caps with new caps and the effect of using parafilm as a precaution against leakage. Two samples of Type 1 water were prepared in 250 mL Erlenmeyer flasks. One sample was left in equilibrium with atmospheric O_2 while the other had the O_2 content purged from the water using nitrogen gas. The samples were then distributed on to the SDR as outlined in Table 3.2.

Table 3.2: Outlining how the vials were arranged on the SDR during test of sealing method. Each row contains 4 replicates of the same sample. By comparing the results from the different rows it is possible to see how the new caps compares to the old caps, but also to see the effect of using parafilm as a precaution against gas diffusion.

Row	A	B	C	D
1	Old Cap O_2-saturated	Old Cap O_2-saturated	Old Cap O_2-saturated	Old Cap O_2-saturated
2	New Cap O_2-saturated	New Cap O_2-saturated	New Cap O_2-saturated	New Cap O_2-saturated
3	Old Cap O_2-purged	Old Cap O_2-purged	Old Cap O_2-purged	Old Cap O_2-purged
4	New Cap	New Cap	New Cap	New Cap

	O_2-purged	O_2-purged	O_2-purged	O_2-purged
5	Old Cap + Parafilm O_2-saturated	Old Cap + Parafilm O_2-saturated	Old Cap + Parafilm O_2-saturated	Old Cap + Parafilm O_2-saturated
6	Old Cap + Parafilm O_2-purged	Old Cap + Parafilm O_2-purged	Old Cap + Parafilm O_2-purged	Old Cap + Parafilm O_2-purged

The results of this test are presented in the Table 3.3 below. Before calculating the average of each row, the values were standardised by calculating the Z-score:

$$Z = \frac{X - \bar{X}}{SD} \tag{3.8}$$

Z is the standardised value, X denotes the measured value, $\bar{X}$ denotes the average value of all the measurements and SD is the standard deviation of the population of measurements (Moore et al. 2012). Standardisation is a linear transformation that transforms the data to fit a standard scale of z-score with a mean of 0 and a standard deviation of 1. With all the values centred on x = 0 helped to clarify which sample had a net increase or net decrease in oxygen content during the measurements.

Table 3.3: The results from the sealing test presented as Z-scores. The values measured after 5 hours when the temperature had stabilised and again after 40 hours at the end of the measurements.

Row	Z-score (5h)	Z-score (40h)	ΔZ	Standard Deviation
1	8.56	-11.1	-19.66	0.15
2	0.64	-4.25	-4.89	0.59
3	-50.88	48.80	99.68	0.10
4	-56.32	58.57	114.89	0.13
5	5.08	-6.74	-11.82	0.85
6	-5.58	4.69	10.27	0.42

By comparing the results from Row 1 to Row 5 and the results from Row 3 to Row 6 presented in Table 3.3 demonstrate that using parafilm as a precaution against gas diffusion gives an improvement in signal-to-noise ratio with ΔZ-values closer to zero (little net gain or loss of oxygen during measurements). Using the new caps compared to the old gave mixed results with a clear improvement with oxygen saturated water (Row 1 vs Row 2) and somewhat poor results for the water sample purged of oxygen (Row 3 vs Row 4). A similar test was conducted by PreSens of the new caps before they were delivered to UiO and the results that were kindly provided (Figure 3.6) illustrates that the new caps provides the vial with significant better sealing.

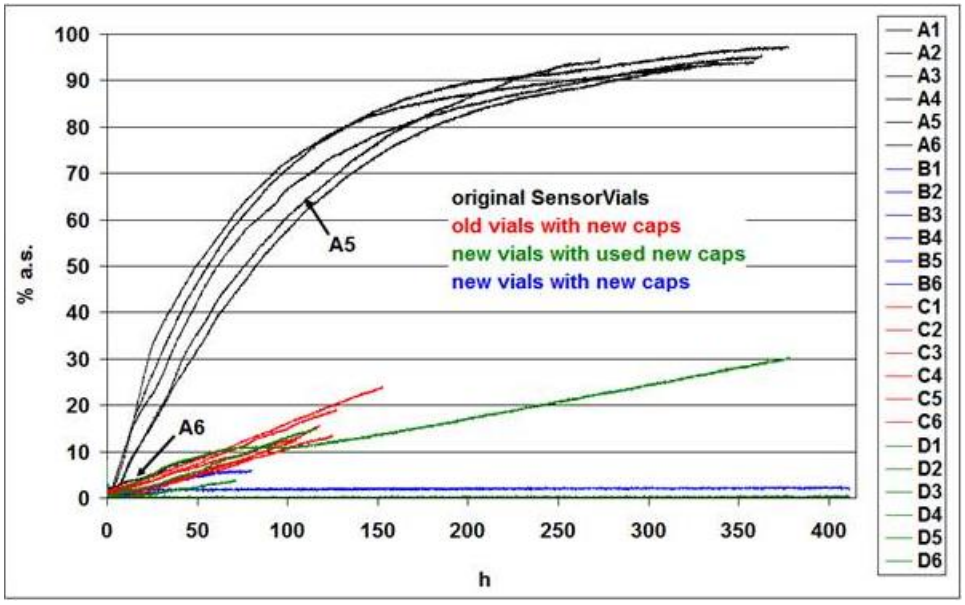

Figure 3.6: Test results comparing old and new caps. On the x-axis h is an abbreviation to hours and on the y-axis % a.s. denotes the present air saturation (alternative measurement unit in the Presens software) Courtesy of Dr. Sarina Arain, PreSens GmbH, Germany. Used with permission.

3.6.8 Temperature control

Once properly sealed the samples were put inside an incubator with temperature set to 18°C to ensure stable temperature during measurements. The PreSens instrument measures and log the temperature in the samples and uses this to calculate the concentration of oxygen. This makes the experiments particular sensitive to temperature fluctuations (Figure 3.7) and necessitates the use of an incubator. For the first experiment two different incubators were used. For the first half of the samples the biodegradation were conducted inside a Samsung Compression Refrigerator with a glass panel door (Figure 3.8). For second half of the samples a Termaks KBP-6395F Environmental Chamber with an isolated metal door were used with temperature set to 18^{o}C (Figure 3.9).

There were some technical difficulties with both incubators. The Samsung refrigerator was unable to maintain a stable temperature at its maximum settings of 18°C (Figure 3.8). Fluctuations in temperature caused similar variations in signal output, thus making it more difficult to separate oxygen consumption due to bacterial activity from noise caused by the fluctuation. The experiment where therefore moved to be conducted inside the Termaks incubator. Termaks had previously experienced several technical breakdowns which lead to the removal of the cooling element used to lower the temperature inside. As a result the incubator were placed inside a cool room (t < 15°C) to allow for measurements at temperatures below that of normal room temperature. However, the incubator was unable to maintain a stable temperature at the correct settings (Figure 3.9). As a result a third incubator

(INCU-Line IL 56 Prime) was acquired (Figure 3.10). The temperature set for the experiment was also changed to 25ºC as this is the temperature at standard conditions for determining physicochemical constants for various compounds. By performing the experiment under standard conditions it is possible to use the results as a reference for later experiments performed under non-standard conditions for example when mimicking natural conditions.

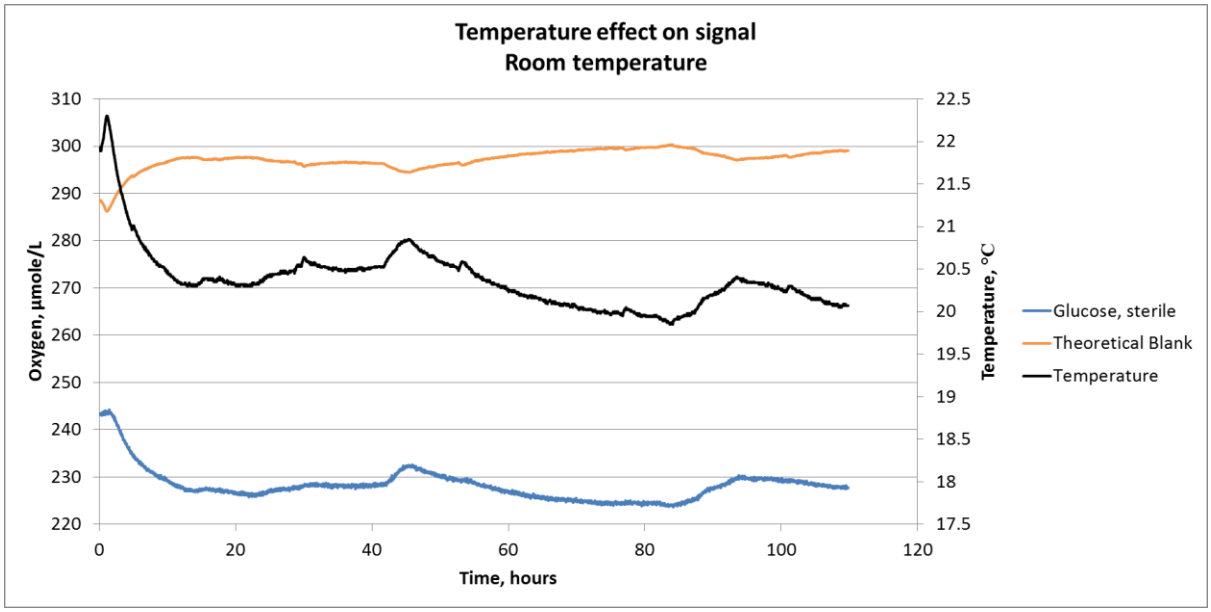

Figure 3.7: Illustrating how the temperature is causing fluctuation in the signal output. These measurements were performed without an incubator.

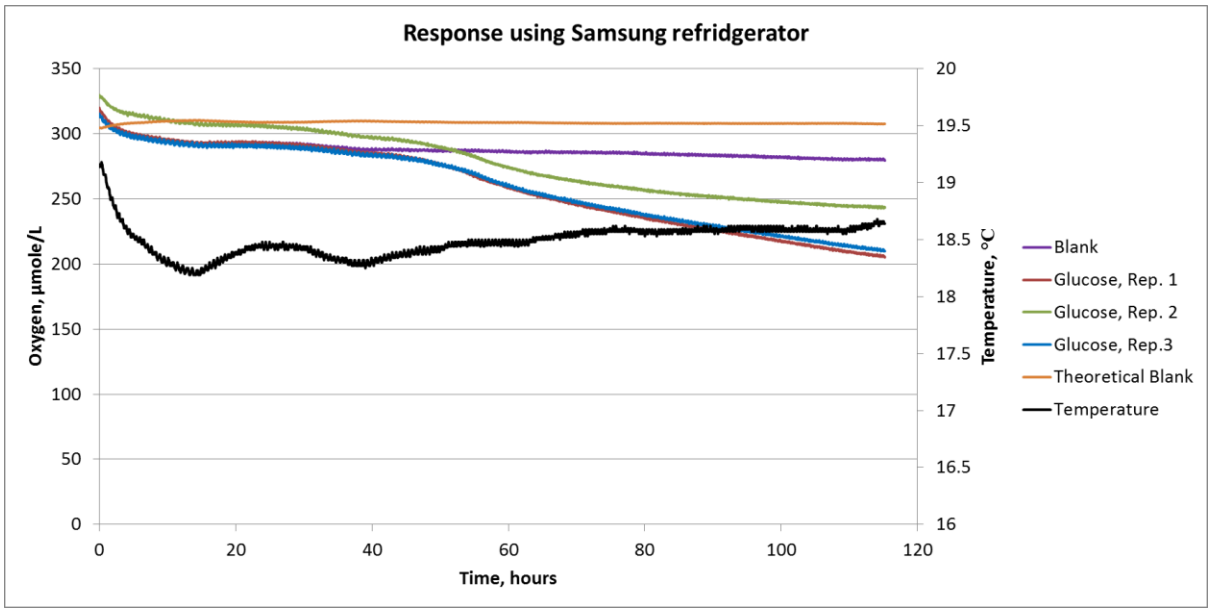

Figure 3.8: The Samsung refrigerator manages to keep the temperature approximately at the pre-set temperature of 18°C. However, significant temperature fluctuation could affect the stability of the signal output.

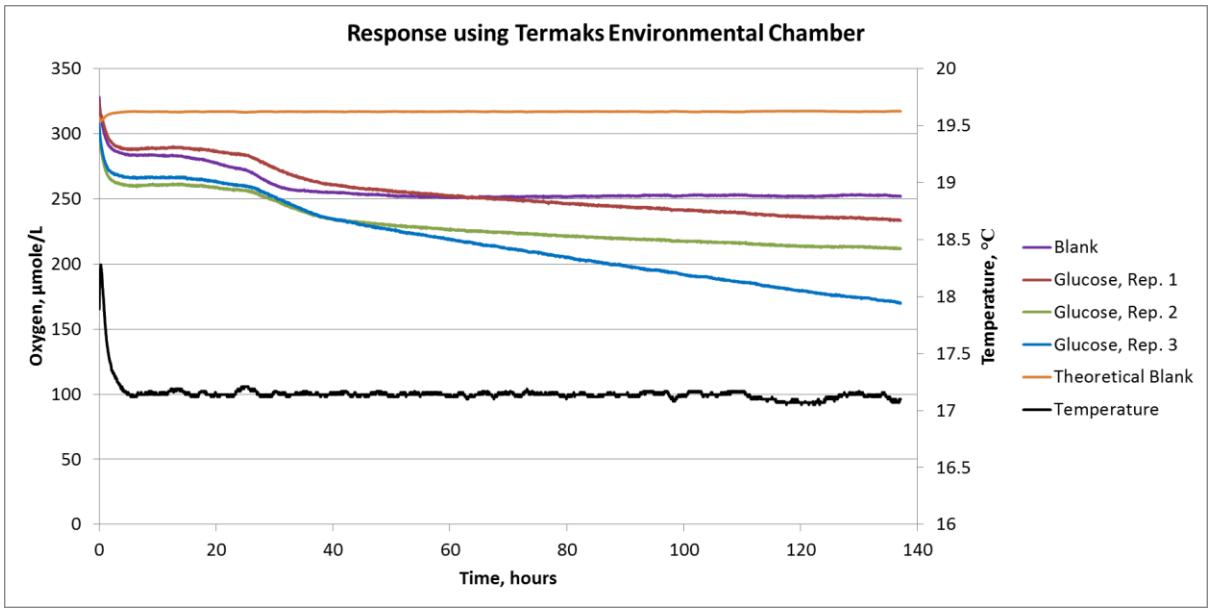

Figure 3.9: A dedicated environmental chamber provides with the most stable temperature, but technical difficulties prevented the temperature reaching 18 °C.

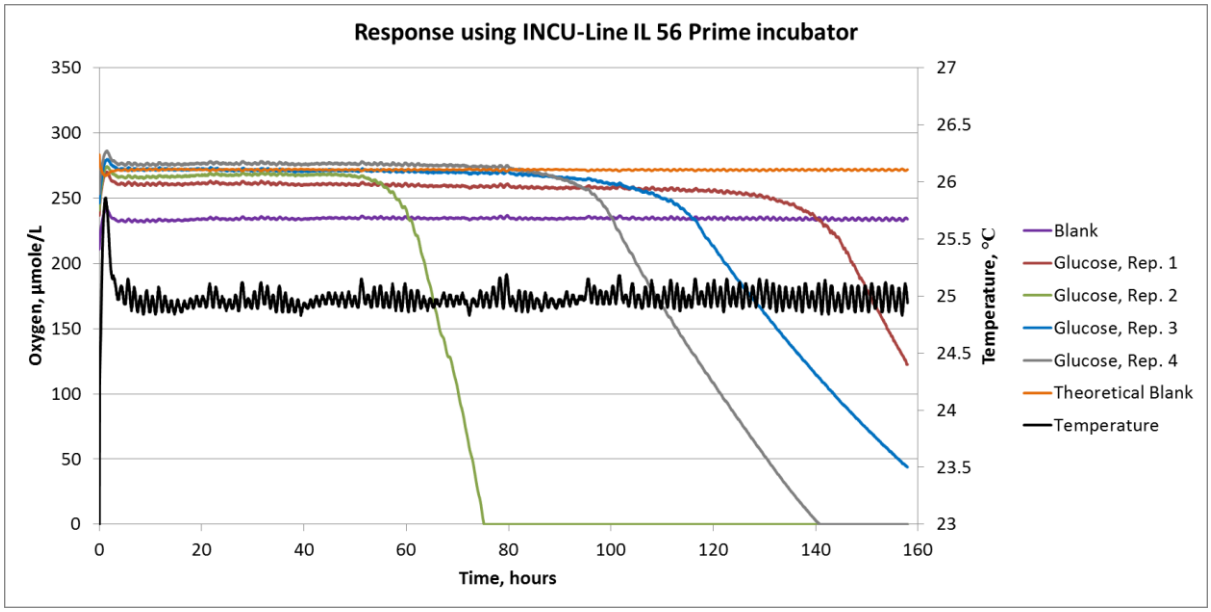

Figure 3.10: The combination with increased temperature, better sealing and adding more nutrients gave a much improved response in the signal output. The glucose solution in this experiment was doubled from 10 to 20 mg/L to match the average TOC-values of the samples.

When comparing the results presented in Figure 3.8 and 3.9 with Figure 3.10 it appears that the new approach has improved the signal output. When correlating the oxygen consumption in Figure 3.10 with the bacterial growth curves in Figure 2.15 and 2.16, Figure 3.10 illustrates in the beginning of the measurements a clear lag phase where the signal creates a flat line. This is where there is little to no oxygen consumption. Then follows a clear transition to exponential growth that rapidly consumes the oxygen in the vials. In Figure 3.8 and 3.9 the

response is more ambiguous. After the temperature has stabilised there is an apparent lag phase, but it is not represented as a straight line. Instead there is a gradual decent that slowly increases in steepness with a weak transition to what is supposed to be exponential growth, but the steepness is to shallow. The lack of an exponential curve in Figure 3.8 and 3.9 is most likely due to oxygen diffusing into the vials from the surrounding air as the concentration of oxygen inside the vials is reduced (see Table 3.2 and 3.3 and Figure 3.6). As oxygen diffuses into the vials it replaces the oxygen consumed by the bacteria thus reducing the signal output. The effect is a curve with a shallow steepness that does not represent the actual oxygen consumption rate. The end result is a perception of very low bioactivity and that the samples are poorly biodegradable.

An interesting observation is the large variation in lag time between the identical replicates of the reference samples (Figure 3.10) detected using the optimum experimental design. This emphasise the importance of assessing the data from each replicate individually and detecting at which time during the degradation the number of bacterial cells reach a sufficiently high number to induce exponential growth. As mentioned in Chapter 2.9 this number is on average 10^6 cells pr. mL (Maier et al. 2009). The cause for this variation is probably that the inoculum is added as a volume and not as a known number of cells. It is therefore impossible to ensure that each vial receives the same number of bacteria. By ensuring proper sealing to avoid diffusion of gas it becomes easier to detect when exponential growth begins and separating it from the lag time. This makes it easier to apply Equation 3.1 and calculate RR during exponential growth.

The improvement in results by using the optimum approach compared to initial experimental design is further appreciated when assessing at the differences between real blanks and theoretical blanks used to test: 1) the stability of the temperature; 2) the effect of adding bacteria to the blanks and; 3) if the vials were properly sealed. The results are presented in Table 3.4. The effect of incubating the sample at 25°C compared to using no incubator at all is clear with a much less fluctuation in the signal. When comparing the response in Samsung and Termaks the addition of inoculum to the blanks makes it impossible to determine if there is any leakage as the oxygen is consumed. The large differences in response between the two measurements are also a testament to the inconsistencies generated by the addition of an unknown number of bacteria. Given that the difference between the real blank and the theoretical blank in the INCU-Line is so small it could be argued that the use of a real blank is

un-necessary, however more experiments are needed to be performed before this is confirmed.

Table 3.4: Results from testing the effect of using different temperatures and incubators in the biodegradation experiment. RR denotes respiration rate.

Incubator	Blank, RR	Flux (min-max)	Theoretical Blank, RR	Flux (min-max)	ΔBlank, RR
No incubator (20-21°C)	0.02	2	-0.02	3.2	0.04
Samsung (18°C)	0.14	3.9	0.02	0.7	0.12
Termaks (~17°C)	0.25	10.5	-0.003	0.2	0.253
INCU-Line (25°C)	-0.0006	0.8	-0.007	0.4	0.0064

3.6.9 Summary

A summary of the experimental set-up and conditions used for the initial and optimized approaches to biodegradation assays are presented in Table 3.5.

Table 3.5: Summary of experimental set-up for initial and optimized biodegradation measurements.

Parameters	Initial approach	Optimized approach
Software	SDR_v38	SDR_v4.0.0
Measurement temperature	18°C	25°C
Incubator	Samsung Compression Refrigerator, Type 1 + Termaks KBP-6395F Environmental Chamber	INCU-Line IL 56 Prime
Sealing	Carl Roth PTFE coated, silicone rubber septum Screw caps + Parafilm	Carl Roth TY89.1 PTFE grey Screw caps + Parafilm
Blank control	Type 1 water + Inoculum + 0.1mM Phosphate	Type 1 water
Reference	D(+)- Glucose $10\ \frac{mg\ C}{L}$	D(+)- Glucose $20\ \frac{mg\ C}{L}$
Nutrients	0.1 mM phosphate	0.1 mM Phosphate + 0.1 mM Nitrate
Inoculum	2 mL	250 µL
Measurement	Sequentially from sample 1 to sample 26	In batches of 4 samples at the time. Each batch contains samples with similar TOC-values.

3.7 Calculation and statistics pertaining to the episode study

3.7.1 Analysis of correlation

In order to investigate any correlation between the different parameters measured in the different samples, the Pearson correlation coefficient, R^2 and test of significance, P were calculated. The choice of correlation coefficient was made based on determining any linear relationship between the parameters as they changed during the episode and to see if it could be correlated with changes in the respiration rate during biodegradation.

3.7.2 Determine statistical significance.

To determine if there is any significant changes in the parameters measured during the episode a two sample t-test comparing S1-S12 with S13-S25 is performed. The division between samples was selected based on Figure 4.9 in Chapter 4.4 that illustrates an increase in TOC after S12. An F-test is conducted before the t-test to check if the variance in each sample pool is equal or unequal. This ensures that the right form of t-test is performed.

4. Results and discussion

In the following discussion, the results will be presented sequentially starting with a general description of the captured storm flow episode and how the changes in hydrological flowpaths through the watershed influence the chemical characteristics of the water in the stream. Following this, the fluctuations in chemical and structural characteristics of DNOM over the discharge episode will be presented and discussed in correlation with existing theories regarding natural processes governing the quality and quantity of SOM and DNOM. There next, the results from biodegradation will be examined quantitatively and qualitatively before finally correlating these results with its solution- and intrinsic properties with the aim of this assessment is to identify natural processes that may significantly influence the biodegradability of DNOM.

4.1 Storm flow episode. Weather conditions and flow characteristics

The storm flow episode occurred in the midst of summer between 24.08.15 and 26.08.15. The average air temperature during that month was about 13°C, fluctuating between a maximum temperature of 20.6°C during daytime and a minimum temperature of 3.7°C at night. Prior to the episode the area had received little or no rain for 20 days. The area was thus relatively dry with little or no moisture in the top soil. In the stream in which samples were collected the flow had stagnated completely with the water level being only a few centimetres deep (Figure 4.1). The water had a strong dark yellow to brown colour. The first sample was collected at mid-day on the 24th at13:00, about 4 hours before the rain started and the water level began to rise in the stream.

The rain started rather abruptly around hr. 17:00, causing the water levels to rise within the hour (Figure 4.2), followed by a steady increase until peaking 28 hours later on the 25th at 21:00 (Figure 4.2 and 4.3). The short time lag (flashiness) between rainfall and water increase in the stream reflects the short travel distance for the soil water before it reaches the 1st order stream, but could also indicate that the soil has high permeability, allowing for rapid transport of water through the soil matrix. Figure 4.4 illustrates how the changing flow in the stream affects the concentration of silica. In between two storm flow events there is often a dry period of some duration where there is little or no water transported through the soil matrix (Figure 2.10). Under these conditions the concentration of silica increases due to weathering. During flash floods the silica is flushed out from the soil and into rivers and streams causing significant fluctuations in concentration that can be monitored, thus making silica suitable as a tracer for determining the contribution of ground water to the stream water flow (Hornberger

et al. 2001). As the flow starts to intensify, the Si concentration begins a slow increase as soluble silica build up in the mineral soil through weathering since the last episode and is flushed out from sequentially shallower mineral soil horizons and transported to the stream. About 20 hours into the episode, the concentration makes a sudden jump to its peak concentration likely due to "piston effect" or i.e. "plug flow". This jump is characteristic of a plug flow effect caused when the flow velocity is high enough to prevent dilution by molecular diffusion (Hiscock 2011), thus conserving the higher concentration in a body of water moving forward. This creates a sharp front where water containing higher concentration replaces water with lower concentration (Appelo and Postma 2010). When the front reaches the sampling point, it is registered as a sudden peak in concentration.

After peaking, the concentration decreases rapidly indicating the water that replenishes the soil water is from peats and organic forest floors. This soil water has not been in contact with mineral soil and is thus poor in Si (Hornberger et al. 2001). Figure 4.5 illustrates the drop in Si concentration by showing a typical clockwise (CW) loop as the concentration is generally higher before the flow peak than after.

Figure 4.1 and 4.2: Photographs showing the water level before the episode (left) and at flow peak (right). Note the instrumental set-up with autosampler.

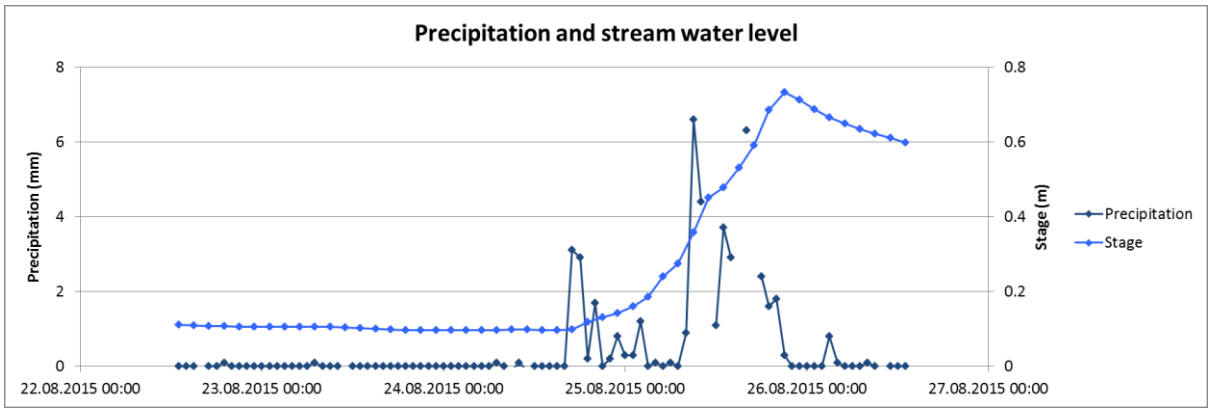

Figure 4.3: Graph illustrating precipitation and water level in the stream during the episode. Stage = water level in the stream.

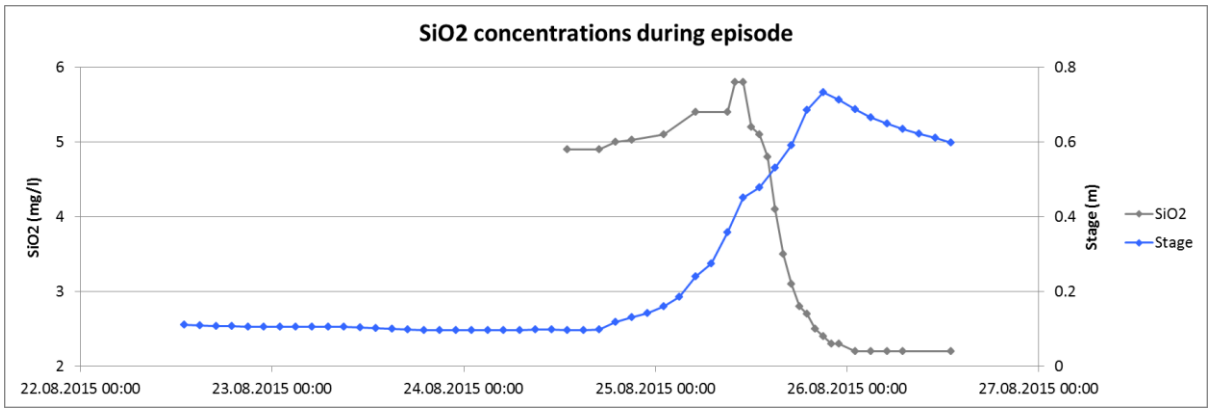

Figure 4.4: Changes in silica concentration during the episode. Note the concentration peak followed by a rapid decrease in concentration.

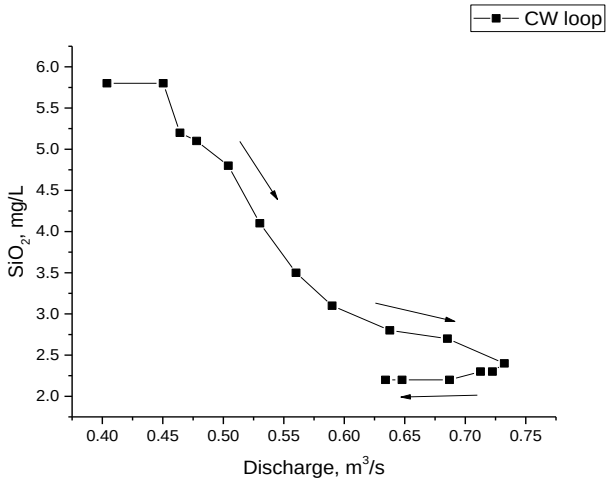

Figure 4.5: Changes in silica concentration related to changes in stream discharge. The graph illustrates a typical clockwise (CW) hysteresis loop.

4.2 Electrical Conductivity (EC) and Total organic carbon (TOC)

Conductivity was measured in all of the samples at the time of collection. Because conductivity measurements were used to select which samples to bring back to the lab and which to be discarded, more samples were measured in the field than in the lab. In Figure 4.6 the samples selected for further analysis are marked and labelled with abbreviates S1-S26 for Sample 1- Sample 26. As the water level started to raise so did the conductivity (Figure 4.6). At this stage there were no overland flow indicating that anions and cations are dissolved in the soil water and transported through the soil matrix to the sampling site. TOC seems to follow the same trend as the conductivity (Figure 4.7) indicating they both originate from the same source, i.e. the top organic rich layer of the soil and peats (Chapter 4.1). This explains the observation that neither the conductivity nor TOC follow the same concentration pattern as silica, but having a concentration peak arriving several hours later and more in conjunction with the peak in water level. EC and TOC also display a strong statistical correlation (R^2 = 0.98, $P < 0.05$) indicating that using EC-measurements as a proxy for DNOM is a reliable method.

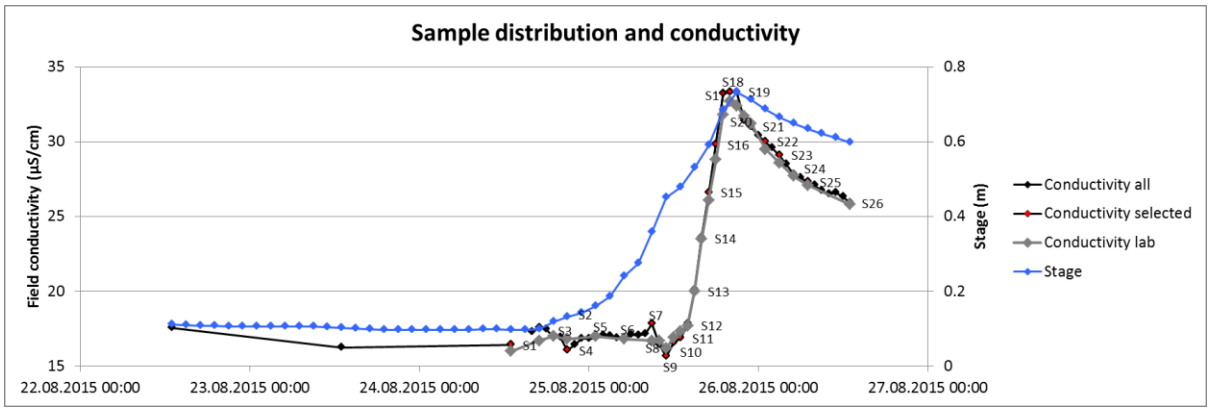

Figure 4.6: Graph illustrating changes in conductivity during the episode. Both field measurements (black line) and lab measurement (grey line) are shown. Note when the samples were collected.

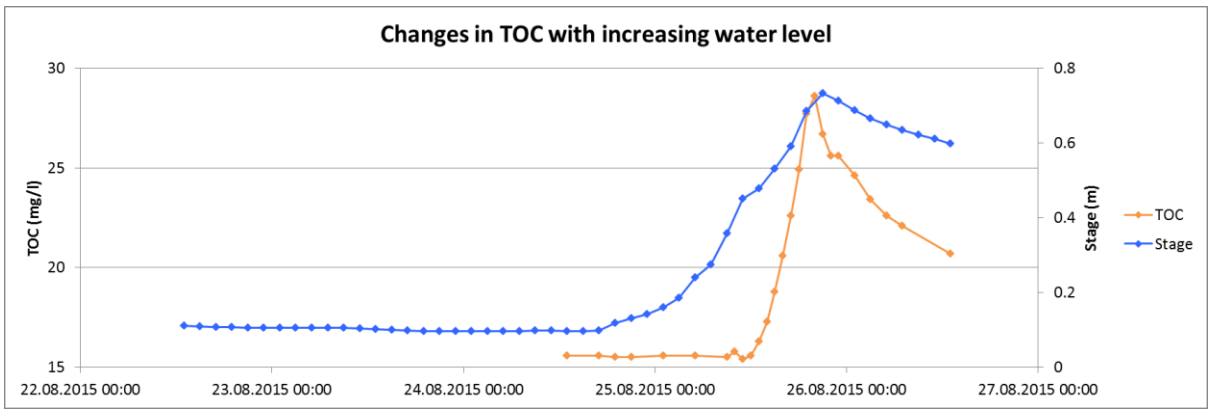

Figure 4.7: Graph illustrating how TOC changes during the episode. Note the similarities in peak concentration between TOC and conductivity (Figure 4.6).

4.3 pH

Results from pH measurement are presented in Figure 4.8 and illustrate three distinct shifts in value. In the beginning of the episode the pH remains relatively stable around 4.8 until influenced by piston (or plug) flow as described in Chapter 4.1. Rainwater in equilibrium with atmospheric gases have a pH around 5.6 (Appelo and Postma 2010). As the plug flow is caused by increase in precipitation, water flushes through the soil and in the process washes out soil water containing weathering products that has accumulated since the last rain storm. This pool of weathering products consists of soluble oxides and carbonates that consume the acidity upon dissolving and elevating the pH in the soil water (Chapter 2.4.1). This is evident from the sudden decrease in acidity correlating with peak concentration in silica (Figure 4.4) ($R^2 = 0.97$, $P < 0.05$). After the plug flow effect acidity increases rapidly. The increase is in conjunction with increasing TOC (Figure 4.7). By recalculating pH to the concentration of $H^+_{(aq)}$ and correlate with measured TOC-values it becomes evident that pH is governed by DNOM ($R^2 = 0.92$, $P < 0.05$). This is consistent with previous reports (Garmo et al. 2016) stating that the pH at Langtjern are kept at a natural low level due to a high content of humic matter.

The following discussions primarily focus on results obtained from samples filtrated through 0.2µm filters. This procedure was necessary in order to remove innate bacteria, sterilizing the sample for the biodegradation study. Chemical analyses of the filtrates revealed elevated concentrations of Cl^- and Ca^{2+} combined with lower concentrations of TOC in samples 7, 18, 23 and 26. This is consistent with contamination from tap water used to create vacuum during filtration. An analysis of the tap water using ICP-OES and IC revealed high concentrations of precisely Cl^- and Ca^{2+}. These samples were therefore omitted from the results and instead presented only in Appendix.

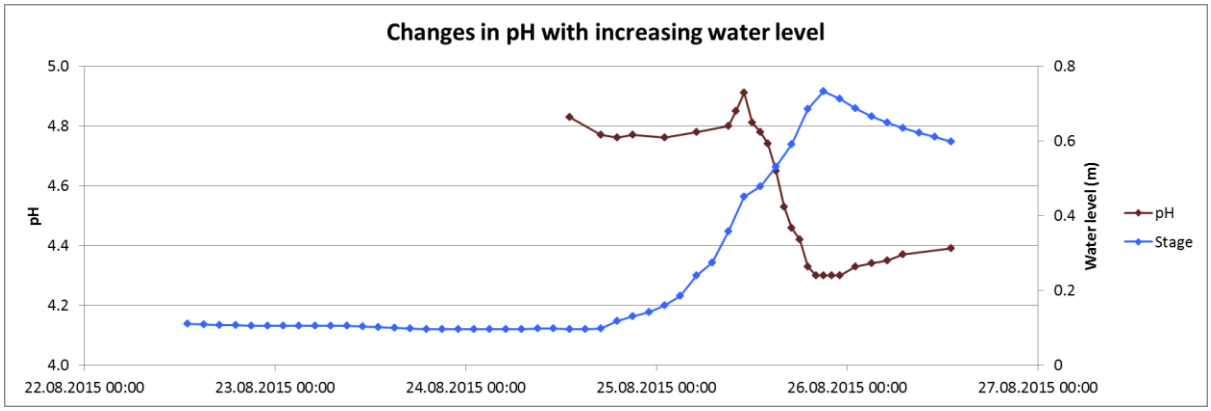

Figure 4.8: Graph illustrating changes in pH as water level increases. A peak is observed correlating with plug flow.

4.4 Total Organic Carbon

The concentration of organic carbon in each sample after filtration on 0.2µm is presented in Figure 4.9. The standard deviation between replicates is shown as error bars.

The figure illustrates an over 50% increase in TOC-loading into the stream as the rainstorm persists. A two sample t-test assuming equal variance determines there is a significant change in the amount of organic carbon during the episode ($t_{calculated} = 9.5 > t_{table} = 1.7$, $P < 0.001$). This increased loading of organic matter is strongly correlated with increasing water discharge ($R^2 = 0.73$, $P < 0.05$). However, since an increase in water content would only dilute the content of DNOM the increased concentration of TOC is a sign of a shift in flow paths that incorporates the upper organic rich soil horizons. Hysteresis analysis of TOC is presented in Figure 4.10 and illustrates a regular clockwise loop indicating the concentration is lower after the flow peak compared to before due to a slow replenishing of organic matter in the soil (Hornberger et al. 2001). Figure 4.11 illustrates hysteresis of the amount of CDOM and presents a more ambiguous picture indicating that the source of colour is not just the amount of organic carbon but may be due to changes in structural characteristics of organic molecules, chemical composition of organic matter (auxochromes) or perhaps influence from inorganic compounds such as iron (Fe) or aluminium (Al).

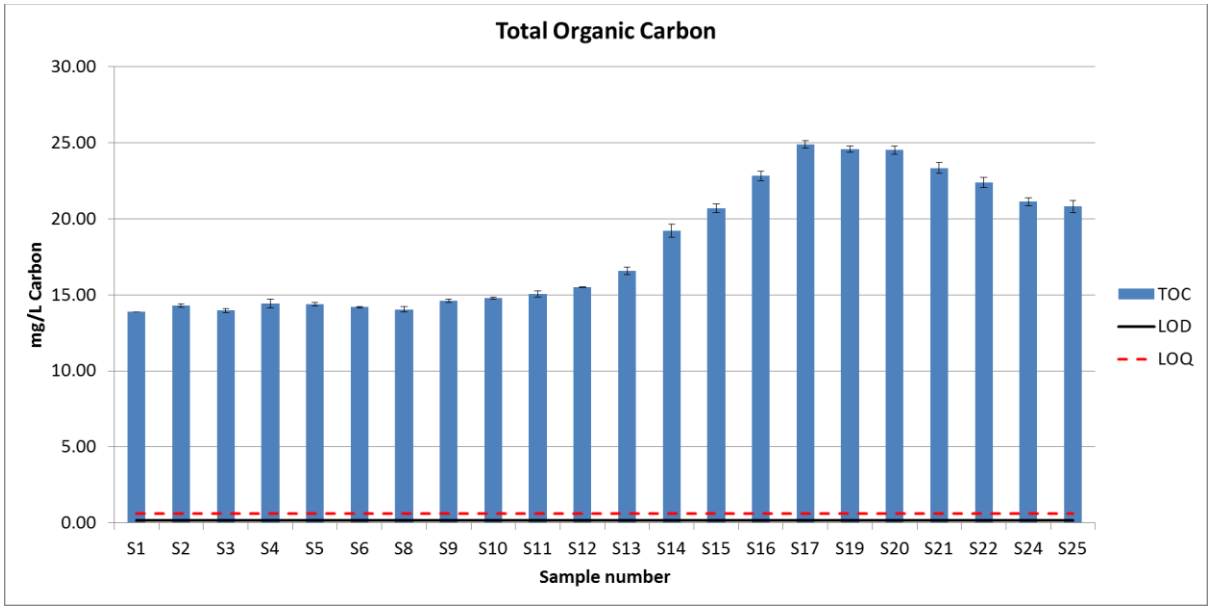

Figure 4.9: Graph illustrating how TOC increase during the episode.

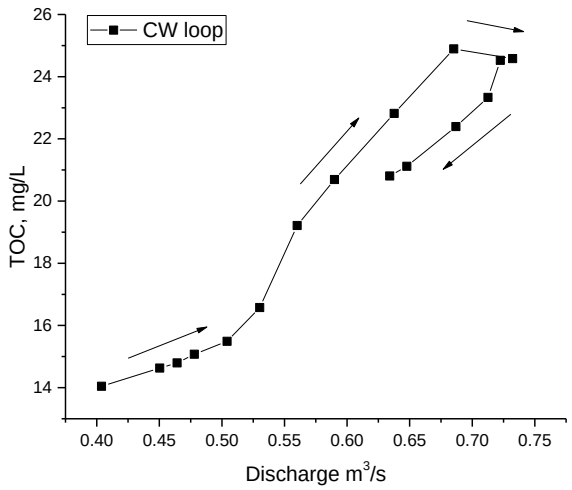

Figure 4.10: Hysteresis of TOC illustrating a typical clockwise (CW) loop.

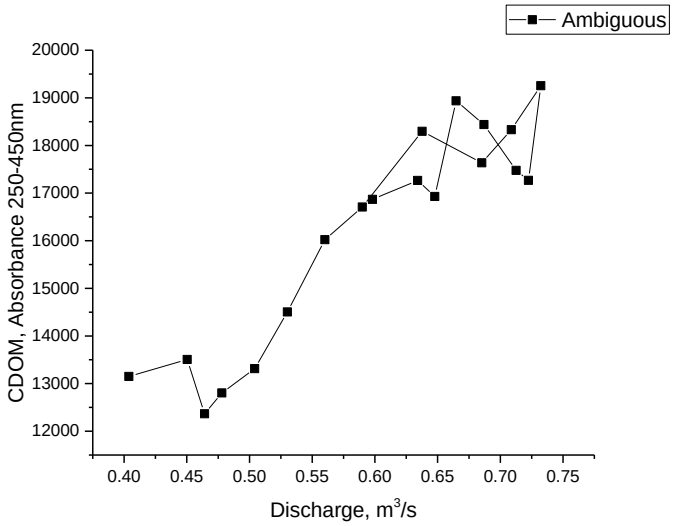

Figure 4.11: Hysteresis of CDNOM presents a more ambiguous graph indicating it's not only the amount of organic carbon that is affecting the colour in the stream.

4.5 Charge distribution of anions and cations

Overall, the ionic strength of the stream water is quite low and similar to concentrations found in rainwater (Appelo and Postma 2010). Several ions were either below limit of detection (LOD) or below limit of quantification (LOQ). Ions below LOQ are presented in Appendix. Figure 4.12 illustrates the charge balance of the cations above LOQ and is coupled with the charge contribution from DOC-[A^-] and H^+. DOC-[A^-] was the only anion detected above LOQ and therefore is the only anion in the samples that can be reliably quantified. The charge contribution from organic acids dominates in the samples and increases steadily as the water level rises. At the same time there is an increase in the concentration of H^+ making the water more acidic. The pH in the samples was after filtration on 0.2µm compared with samples filtrated through 0.45µm. This comparison revealed that the pH in the samples had increased somewhat after being filtrated on 0.2µm. However, the correlation between TOC and pH remains strong (R^2 = 0.90, $P < 0.05$) after filtration and the reason for elevated pH after filtration is most likely the removal of organic matter. It is therefore more likely that the model used to calculate DOC-[A^-] is somewhat sensitive to fluctuations in pH thus giving low DOC-[A^-] at low pH and high DOC-[A^-] at high pH. This will affect the overall charge balance between DOC-[A^-] and cations after filtration as organic matter is retained in the filter. Figure 4.14 illustrates heavy staining of the 0.2µm filters as organic matter is retained. This also affected conductivity resulting on average a 10% reduction in the electrical conductivity compared to samples filtrated at 0.45µm. This is most likely due to loss of DNOM and sub sequentially loss of H^+.

Figure 4.13 illustrates how the relative charge contribution of each ion in the samples changes during the episode. The concentration of Ca^{2+} and Mg^{2+} remains stable as these ions are strongly ion exchanged and easily bound to organic matter and thus more associated with SOM and DNOM. Meanwhile there is a steady decline in Na^+ indicating the ion is flushed from the soil. This is probably due to its high diffusion coefficient preventing the ion to precipitate. Na^+ is only weakly ion exchanged which allows it to move more or less freely through the soil and as a consequence is rapidly removed. Ca^{2+} remains the dominate cation in most of the samples but is matched by H^+ in samples 16-25 collected during peak flow. This can have a significant effect on the diffusion coefficient of humic acids (Wang et al. 2001). This allows for the positively charged Ca^{2+} to interact with humic matter causing compaction of the humic molecules thus making DNOM less soluble and thereby less mobile. As the concentration of Ca remains stable throughout the episode the diffusivity and therefore

transport of humic matter through the soil is controlled by the prevailing flow path of rainwater flushing through the soil.

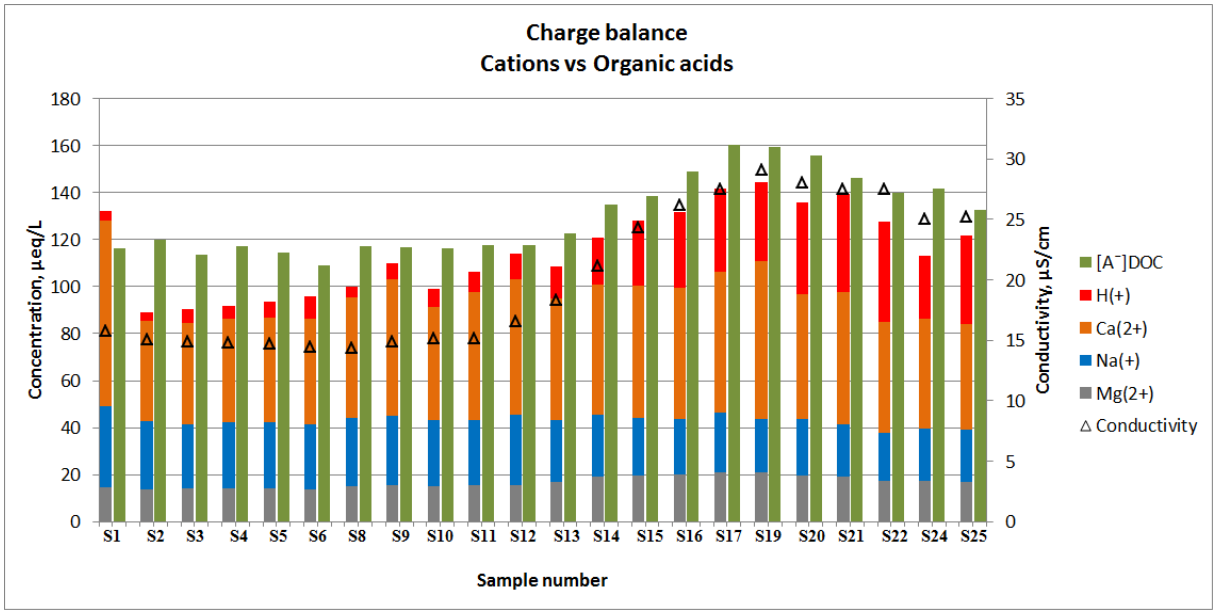

Figure 4.12: Illustrating change in conductivity and the charge balance of the major cations and organic acids.

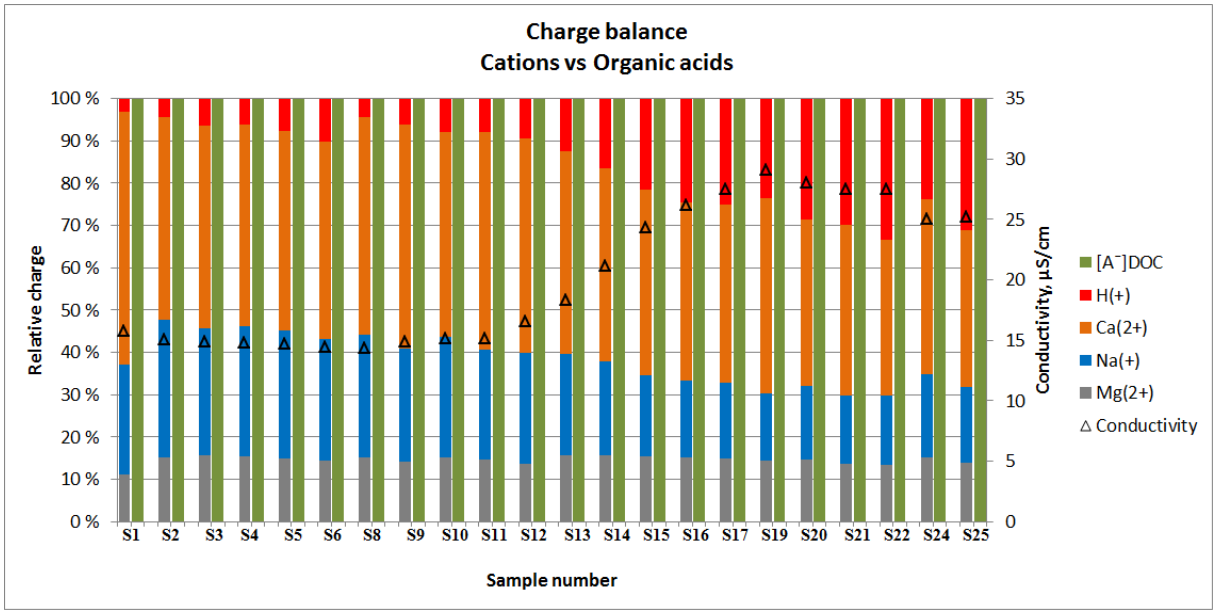

Figure 4.13: Illustrating the relative change in conductivity and the major anions and cations.

Figure 4.14: Picture of 0.2µm filters before (right) and after (left) filtration.

4.6 Aluminium and iron

The concentrations of Al and Fe in the stream water during the discharge episode are presented in Figure 4.16. Al and Fe are of particular interest in DNOM studies because of their ability to form chemical bonds with humic matter and thereby changing the chemical and optical properties of DNOM (Alberts 1982; Perdue and Lytle 1983; Hessen and Tranvik 1998; Ohno et al. 2007; Rahman et al. 2010; Xiao et al. 2015). In oxygen rich surface waters such as the conditions at Langtjern where the pH fluctuate between 4 and 5 both Fe and Al exist primarily as trivalent hydroxides such as $Fe(OH)_3$ and $Al(OH)_3$ (Waychunas et al. 2005; Appelo and Postma 2010; VanLoon and Duffy 2011). In this form they have the ability to form multidentate complexes with organic molecules called chelates (He et al. 2005; Ohno et al. 2007; Appelo and Postma 2010). Chelates tend to form a ring structure which encapsulate the metal ion and act as a carrier. This could have a significant effect on the biological uptake of organic matter (Nierop et al. 2002; He et al. 2005; Appelo and Postma 2010). If the encapsulated metal ion is of a toxic nature to microorganisms such as mercury (Hg), lead (Pb) or cadmium (Cd) to name a few, the DNOM also becomes toxic thus inhibiting biodegradation. However, if the metal ion has a nutritious value such as Fe, Mn or Mg to name a few, chelation could enhance the bioavailability of DNOM.

In waters containing both elements there will be a competition on which element to form metal-organic complexes. To which degree Al or Fe bind to DNOM depends on the structure and chemical properties of the organic molecules in the DNOM pool, but a study have shown that pH and the metal- to- DOC concentration ratio (M/C-ratio) will to a large extent dictate which of the two elements that are most likely to form chemical bonds with humic matter (Nierop et al. 2002). In samples collected from Langtjern the M/C-ratio are on average 0.02. According to Nierop et al. (2002) this will favour Al to form complexes with DNOM. A regression analysis of the data supports this with stronger correlation between TOC and Al

(R^2 = 0.82, P < 0.05) than between TOC and Fe (R^2 = 0.47, P < 0.05). This is illustrated in Figure 4.16 where Al and TOC follow roughly the same trend by showing an increase in concentration as the water level rises while Fe is more or less just flushed from the soil. In fact, Fe is exhibiting the strongest correlation with SiO_2 (R^2 = 0.76, P < 0.05) both measured on samples filtrated at 0.45µm. As mentioned earlier in Chapter 4.1, weathered SiO_2 is flushed from the soil thus exhibiting a clockwise hysteresis loop. This implies that iron exists primarily as colloidal iron hydroxides exhibiting little chemical interaction with neither DNOM nor other ligands except hydroxide in the samples (Waychunas et al. 2005) but is instead subjected to transport during high flow (Wigginton et al. 2007). Figure 4.17 illustrates hysteresis loops of both elements. Both iron and aluminium display a clockwise loop, although the loop for aluminium appears somewhat irregular. This indicates the concentration is lower after the flow peak than before. However, as iron is steadily decreasing throughout the episode aluminium increases, thus making a loop that is not very unlike the hysteresis loop of TOC illustrated in Figure 4.10. While the hysteresis of Al can be explained by its complexation with DNOM, the concentration of Fe is largely independent of organic matter. During low flow the stagnant conditions in bog water and the deep soil consumes O_2 thus creating reducing conditions. In such conditions iron exists as Fe^{2+} which is easily mobilized in the soil water. However, during high flow oxygen rich water from the top soil percolates down and flushes out the stagnant water containing Fe^{2+} while oxidizing the remaining iron to Fe^{3+} which is less mobile thus retained in the soil. This is why the highest concentration of iron can be seen in the beginning of the episode during the piston effect.

A two sample t-test assuming unequal variance determines there is a significant change in the amount of iron ($t_{calculated}$ = 4.1 > t_{table} = 2.1, P < 0.001) and aluminium ($t_{calculated}$ = 6.1 > t_{table} = 2.1, P < 0.001) during the episode.

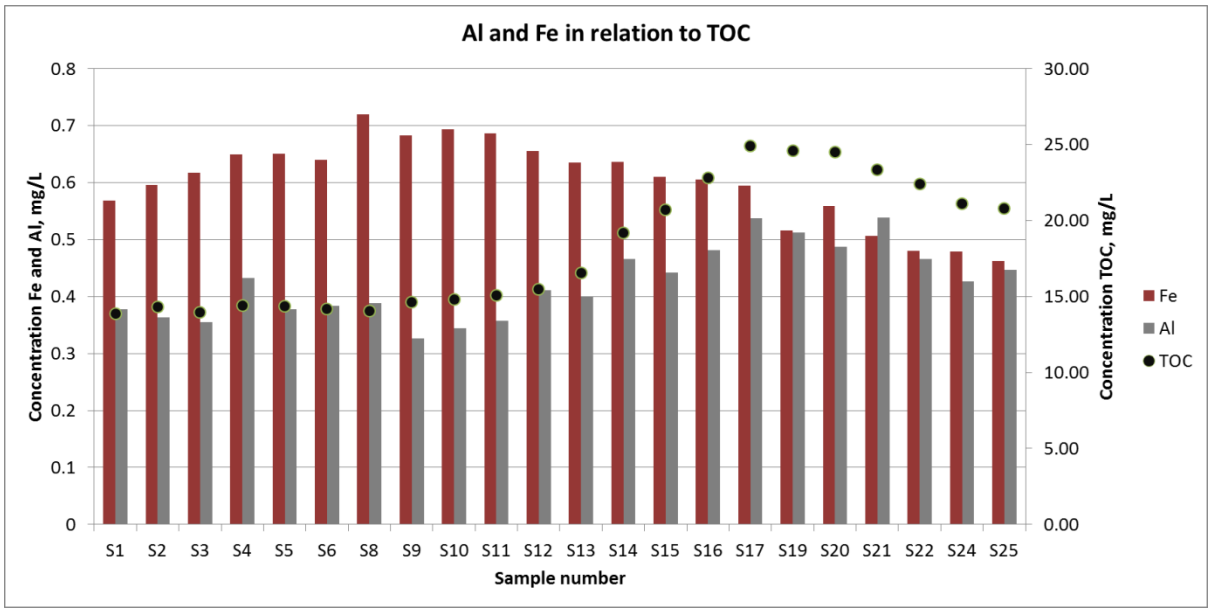

Figure 4.16: Column diagram illustrating the flux of iron and aluminium in relation to total organic carbon.

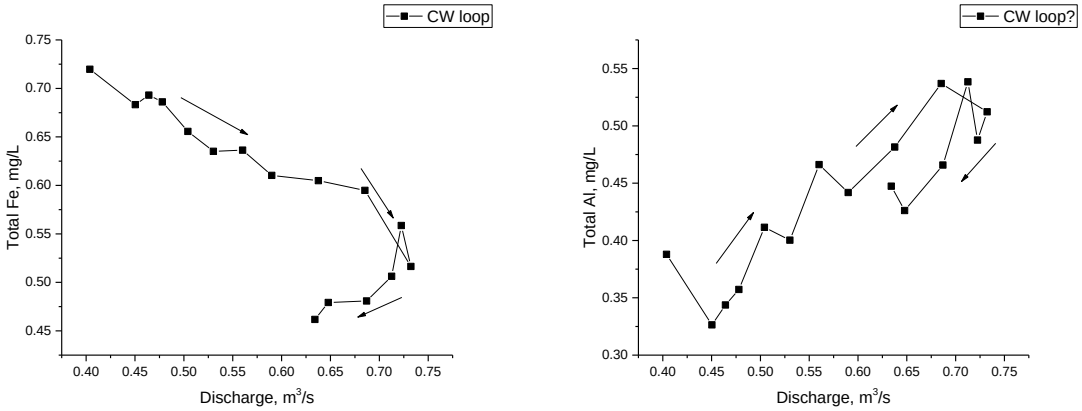

Figure 4.17 a,b: Hysteresis of iron (left) and aluminium (right) both display a clockwise loop, however as iron is steadily decreasing through the episode aluminium is increasing.

4.7 Structural characterization of DNOM

The ability of DNOM to influence the water physical and chemical characteristics, and thereby the aquatic ecosystem, is depended not only on the concentration but also the physical and chemical characteristics of the organic molecules found in the DNOM. In the following section results from UV-Vis absorbency and EEM are presented in relation to the total organic carbon (TOC) content in the samples presented in Figure 4.9. From these results it is possible to determine some of the structural characteristics by applying mathematical methods described in literature. Finally these characteristics will be statistically correlated with observed effects the increasing DNOM loading have on water quality.

4.7.1 UV-/Vis absorbency

The values of E_2/E_3-absorbance ratio of the samples from the episode study are presented in Figure 4.18. A two sample t-test assuming equal variance show that there is a significant change in E_2/E_3-values during the episode ($t_{calculated} = 13 > t_{table} = 2.1$, $P < 0.001$).

E_2/E_3 is negative correlated with molecular weight and aromaticity, thus an increase in values indicate a reduction in the numbered-average molecular weight of the organic compounds in the sample and also a lower percentage of aromatic rings (Peuravuori and Pihlaja 1997). As illustrated by Figure 4.18, the values of E_2/E_3 remains at a stable level until sample 10 when the values begin to increase. As illustrated in Figures 4.4 and 4.18-4.20 the plug- flow effect described in Chapter 4.1 occurred right before sample 10 were collected. Therefore all samples collected from this point represent "new" soil water derived from precipitation replacing the "older" water that has been residing in the soil for duration of time. This effect is perhaps better illustrated by incorporating the E_2/E_3-values in models (Equation 3.1 and 3.2) by Peuravuori and Pihlaja (1997) to calculate the numbered- average molecular weight and the percent of aromaticity presented in Figure 4.19 and 4.20 respectively.

The significant changes in E2/E3-ratio are further supported by fluctuations in sUVa, sVISa and SAR presented in Figures 4.21, 4.22 and 4.23 respectively. A two sample t-test concludes that there is a significant change in both sUVa ($t_{calculated} = 7.7 > t_{table} = 2.1$, $P < 0.001$) (unequal variance), sVISa ($t_{calculated} = 9.4 > t_{table} = 2.1$, $P < 0.001$) (equal variance) and SAR ($t_{calculated} = 13 > t_{table} = 2.1$, $P < 0.001$) (unequal variance) during the episode. For sUVa and sVISa the limit of detection and limit of quantification in the determination of TOC are illustrated as horizontal lines while the standard deviation are presented as error bars.

As sUVa reflects the degree of aromaticity the values illustrates a gradual reduction in the average number of aromatic compound over the discharge peak. At the same time sVISa is also reduced in the same samples indicating a shift towards lower molecular weight compounds over the peak of discharge. This is also reflected by an increase in SAR over the discharge peak. As higher values of SAR are indicative of LMW compounds it is also consistent with an increase in oxygen content which is expected with smaller organic molecules (Chapter 2.10.1). In Chapter 2.1 SOM were described as the decomposition of organic compounds into increasingly smaller molecules by both biotic and abiotic degradation processes. As time passed the more degraded SOM would be buried in the deeper soil horizons while fresh SOM accumulated at the top of the soil profile. Based on this model the opposite response of what is illustrated in Figures 4.18-4.23 would occur because the DNOM characteristics down through a soil profile decrease in aromaticity and MW. However, the area surrounding the stream in which the samples were collected there are several patches of peat containing DNOM with high aromaticity and MW compared to the mineral soil (Aitkenhead et al. 1999; Kononova 2013). The response of increasingly smaller molecules with less aromaticity can thus only be explained by a shift in the main contribution of runoff to the stream. At low flow the peat provides the largest contribution of DNOM while at high flow DNOM from the mineral soil starts to dominate which contains smaller compounds containing less aromaticity. Similar results have been obtained in another episode study (Austnes et al. 2010) showing an increase in E_2/E_3-ratio and a reduction in sUVa during an rainstorm in peatland.

As LMW compounds tends to be less hydrophobic than HMW compounds an increase in solubility is expected thus elevating the DOC-concentration over the discharge peak in the water. There is also a reduction in pH while at the same time there is a steady increase in DOC concentration. This indicates that it is the organic acids themselves that are making the water more acidic. This interaction is further explained in Chapter 4.3.

The slope ratios, SR were practically constant throughout the episode with an average value of 0.71 ± 0.005. Such low values is associated with CDNOM subjected to dark aerobic microbial alteration consistent with DNOM-rich wetlands and forest areas (Helms et al. 2008a). The only deviation is Sample 2 with a $S_R = 1$. This is most likely explained by direct dilution with rainwater as this sample was collected during heavy rain but before any significant supply of soil water into the stream.

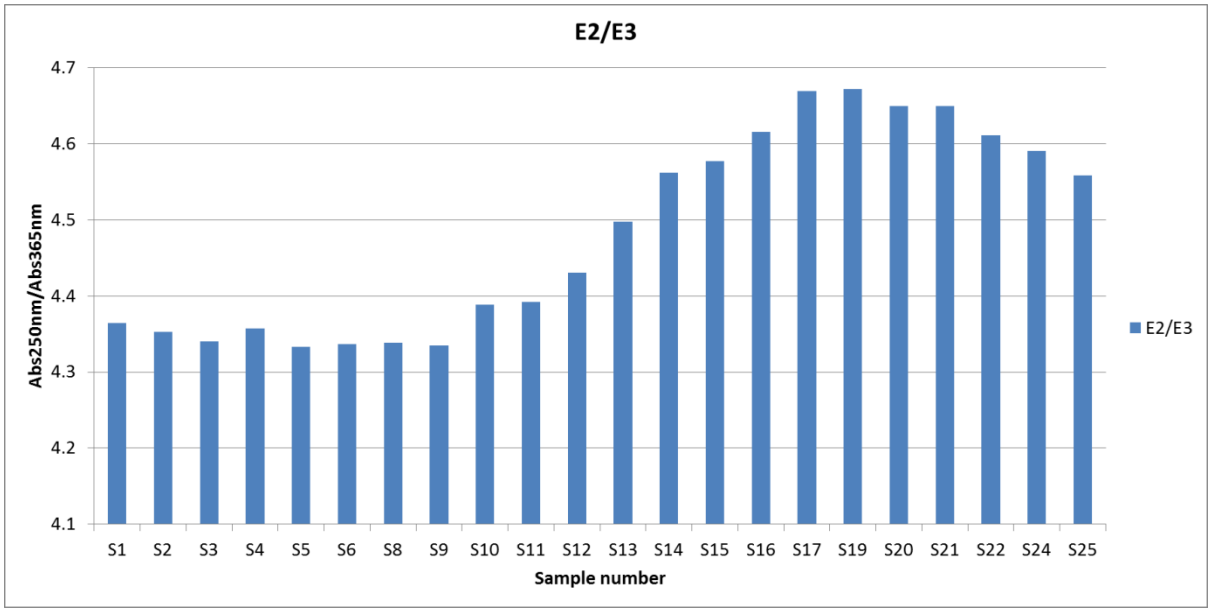

Figure 4.18: The changes in the absorbance ratio E2/E3 is indicating a reduction in both molecular weight and the degree of aromaticity as the storm-flow episode persists.

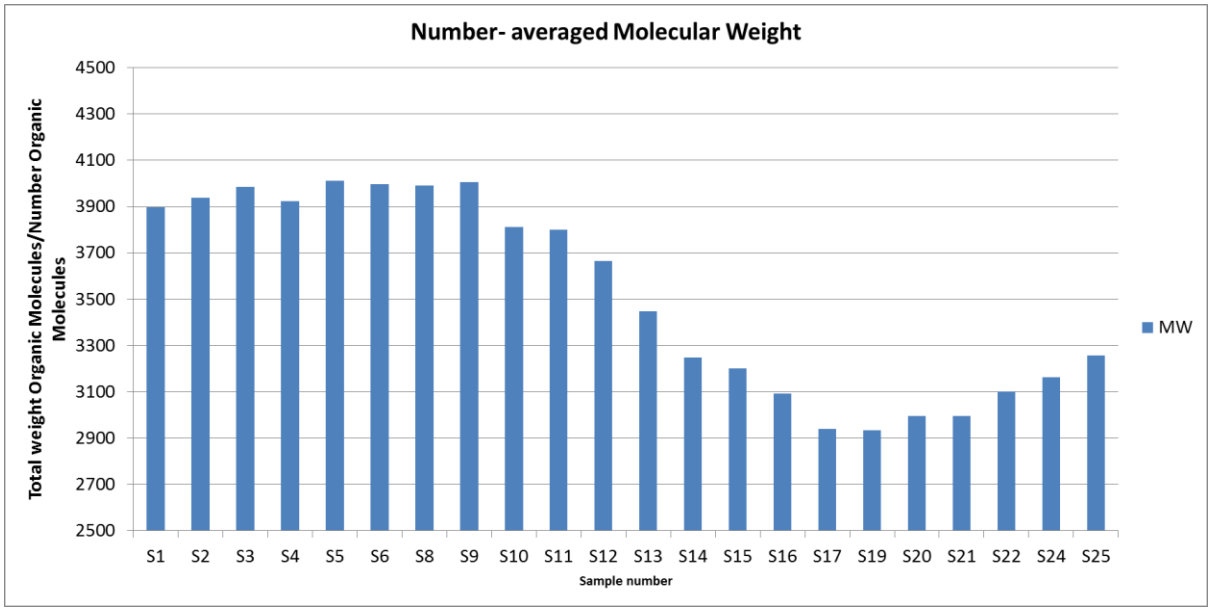

Figure 4.19: The drop in number-averaged molecular weight indicate a shift towards a higher proportion of LMW compounds in the stream.

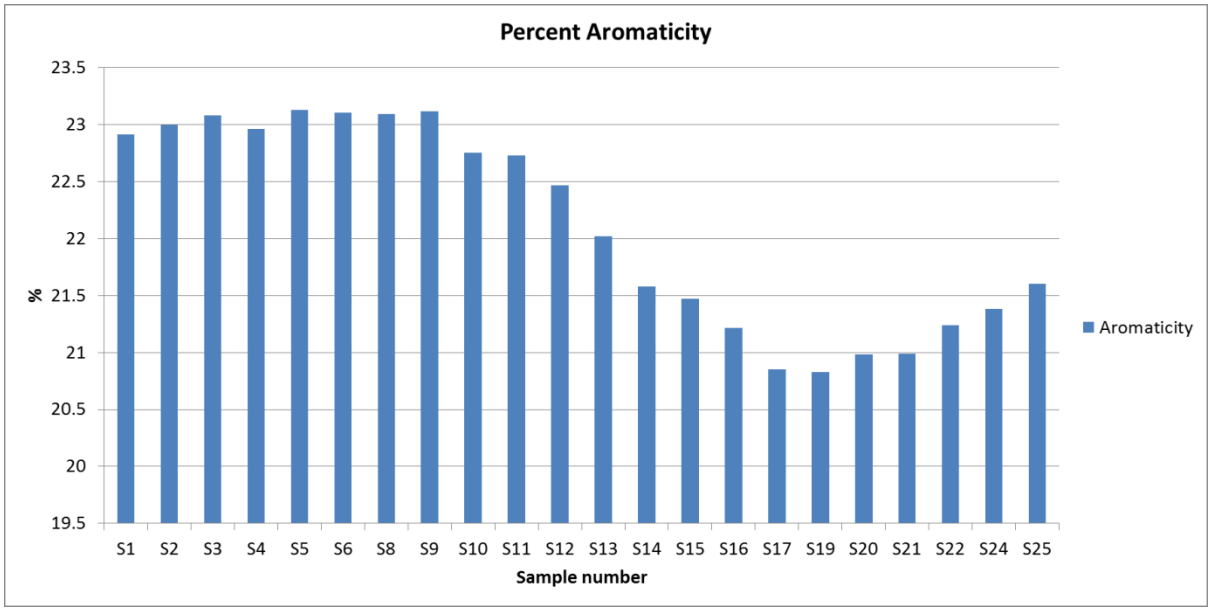

Figure 4.20: Accompanying the higher proportion of LMW DNOM illustrated in Figure 4.19 there is also a reduction in the percent of aromaticity.

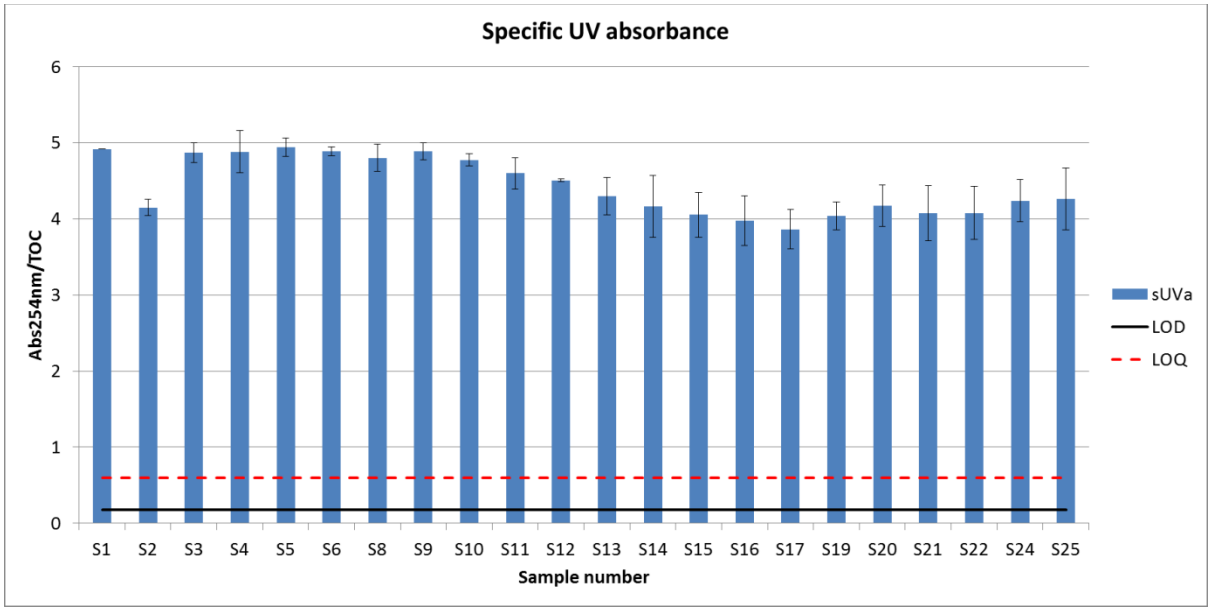

Figure 4.21: sUVa is reflecting the degree aromaticity of DNOM. The gradual shift towards lower values is consistent with findings from other analytical methods.

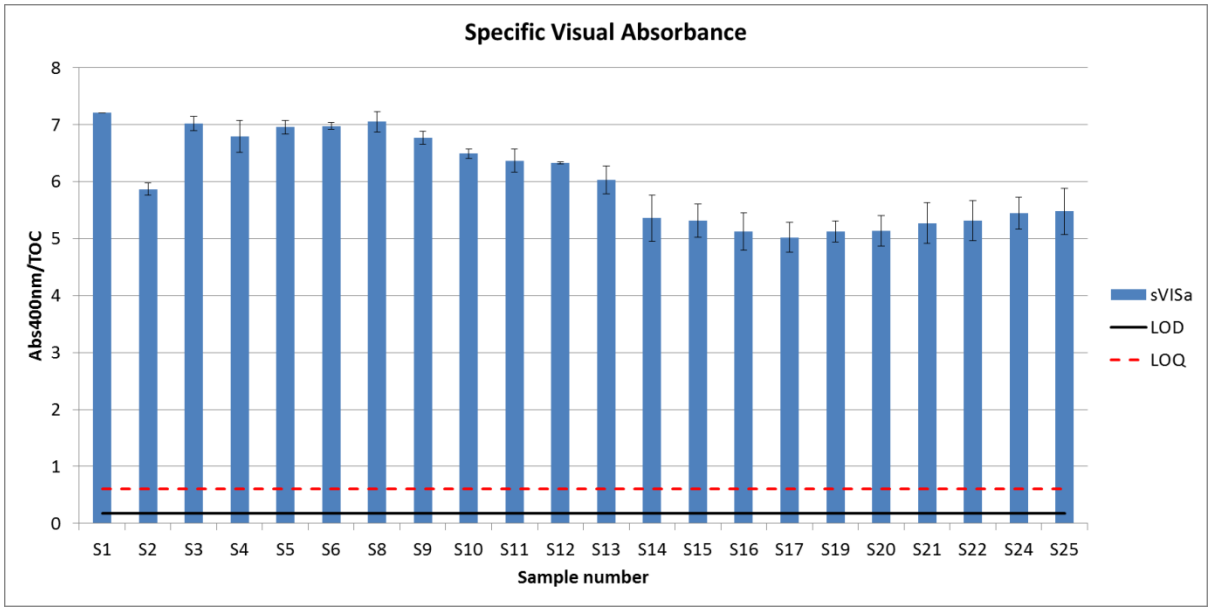

Figure 4.22: Absorption in the visual spectre reveals a shift towards LMW compounds.

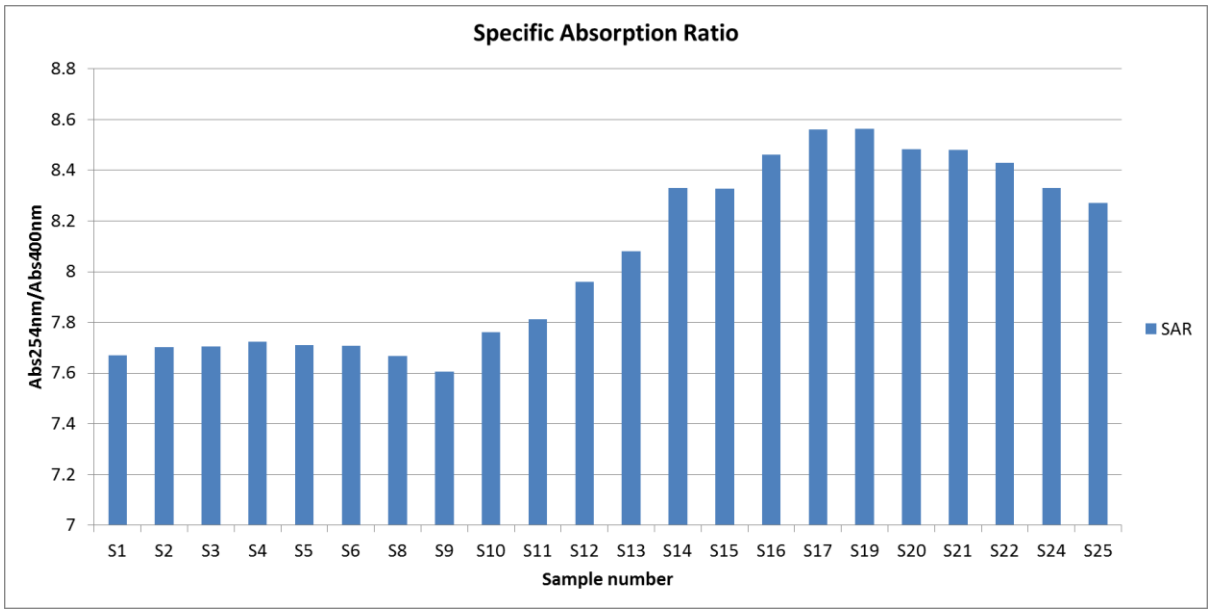

Figure 4.23: Inversely correlated with MW and condensed aromatic rings, higher values are indication more LMW compounds and an increase in oxygen content.

4.7.2 UV-/Vis- Fluorescence Excitation-Emission Matrix (EEM) spectra

The fluorescence EEM spectrum for each sample is presented in Appendix (Chapter 8.3.2). The peaks used for further calculations were extracted using software and corrected for inner filtering (Ohno 2002). The fluorescence index, FI and the freshness index, β:α were calculated by method described in literature (Fellman et al. 2010) and are presented in Figure 31 and 32 respectively. Each EEM spectra is mainly dominated by two distinct peaks designated Fulvic (λ_{ex}= 240-245nm, λ_{em}= 444-458nm) and Humic (λ_{ex}= 335-345nm, λ_{em}= 444-458nm). The peak designated bioavailable proteins (λ_{ex} = 270-280nm, λ_{em}=304-368nm) (Fellman et al. 2010) exhibit very low intensity and due to the poor signal-to-noise-ratio is exempted from further analysis. The excitation and emission wavelengths and the intensity of the humic and fulvic peaks are presented in Table 4.1. The intensity is also presented in Figure 4.24 to illustrate how the amount of each size fractions is fluctuating during the episode. The fulvic fraction dominates in all samples and increasing as the episode intensifies. This is consistent with sVISa and SAR presented in Figure 4.22 and 4.23 respectively, showing an increase in the relative amount of LMW compounds over the discharge episode. The humic fraction remains at a more constant level throughout the episode although both fractions fluctuate in intensity. The most likely explanation for these fluctuations is as described in Chapter 4.7. The contribution to runoff is shifted from peat during low flow that contains DNOM characteristic of high MW and aromaticity to mineral soil during high flow containing DNOM of lower MW and is less aromatic. This fluctuation is even more pronounced when examining the fluorescence index (FI) and freshness index (α:β) in Figure 4.25 and 4.26 respectively. A two sample t-test reveals there is a significant change in both fluorescence index ($t_{calculated}$ = 4.9 > t_{table} = 2.1, P < 0.001) (equal variance) and freshness index index ($t_{calculated}$ = 6.5 > t_{table} = 2.1, P < 0.001) (equal variance) during the episode. As described in Chapter 2.10.2, the FI is primarily used to differentiate between two sources of DNOM, microbial derived and terrestrial derived with higher values of FI (~ 1.8-1.9) indicating microbial and lower values (~1.2) indicating terrestrial (McKnight et al. 2001; Fellman et al. 2010). The FI values in Figure 4.26 are fluctuating between 1.37 and 1.80, and do so in a rather erratic pattern with no consistent trends of increase or decrease. This indicates that the contribution of microbial and terrestrial derived DNOM remains the same independent weather the DNOM is from peat or mineral soil. The average FI-value of the samples is rather high at 1.57 with several peaks approaching 1.80 while none is in the range of 1.2. This indicates that there is a high microbial activity in the soil producing a constant supply of microbial derived DNOM. This could have a significant effect on the further bioavailability of

DNOM as microbial processing increase the degree of humification (Wickland et al. 2007) which incorporates loss of labile compounds and an increase in oxygen content (VanLoon and Duffy 2011). As the labile fraction of DNOM is consumed, the recalcitrant fraction left behind exhibits a more uniform chemical characteristic affecting the chemical diversity of the DNOM pool (Wickland et al. 2007) and could explain the rather uniform FI-values and the values of sUVa, sVISa and SAR in the beginning of the episode (S1-S9).

The freshness index illustrated in Figure 4.25 is exhibiting the same erratic fluctuation pattern as the fluorescence index, but with a marked increase in average values beginning in sample 12 and peaking in sample 16- 19. This peak in freshness is consistent with increasing water level reaching the upper layers of the soil where the more recently derived organic matter resides. Due to the younger age it is expected that organic matter leaching from the upper soil horizons has not been subjected to the same extensive degradation as organic matter from the lower soil horizons and by extension should contain more labile compounds, exhibit less aromaticity and contain a higher $\frac{H}{C}$ – ratio. This hypothesis is partly supported by the dataset. sUVa and the E_2/E_3-ratio show a reduction in aromaticity and an increase in SAR which is consistent with a lower content of condensed aromatic rings. The increase in DOC (Figure 4.7 and 4.9) could signify an increase in hydrophilic functional groups causing increased dissolution but the high content of fulvic acids is the most likely explanation given the high solubility of this particular fraction. This will also have an effect on SAR as fulvic acids is smaller in size and have in general a higher oxygen content. The high FI accompanying the freshness index indicate that even this comparatively young pool of organic matter has been subjected to extensive microbial alteration before it is transported to the stream.

Table 4.1: Relative peak intensity normalized for the concentration of organic matter and the location of the peaks in the fluorescence spectra based on the excitation and emission wavelengths.

Sample Number	Fulvic peak			Humic peak			Peak Ratio Ful/Hum
	λ_{ex}	λ_{em}	$\frac{Intensity}{TOC}$	λ_{ex}	λ_{em}	$\frac{Intensity}{TOC}$	
S1	245	456	4.6±0.11	340	456	2.6±0.11	1.8
S2	240	458	3.2±0.13	335	458	2.2±0.13	1.4
S3	245	454	3.5±0.28	340	452	2.3±0.28	1.5
S4	245	456	3.5±0.12	335	454	2.3±0.12	1.5
S5	240	454	3.8±0.06	340	456	2.3±0.06	1.6
S6	240	452	3.7±0.18	340	458	2.3±0.18	1.6
S8	245	450	3.5±0.11	345	458	2.2±0.11	1.6
S9	240	456	3.7±0.08	345	444	2.2±0.08	1.6
S10	245	456	3.4±0.21	345	458	2.2±0.21	1.5
S11	240	458	3.7±0.02	340	456	2.1±0.02	1.7

S12	240	444	3.5±0.24	345	454	2.1±0.24	1.7
S13	240	458	3.3±0.40	340	458	2.0±0.40	1.6
S14	245	456	3.4±0.29	340	450	2.1±0.29	1.6
S15	240	456	3.9±0.33	345	458	2.2±0.33	1.8
S16	240	454	4.3±0.26	350	458	2.0±0.26	2.1
S17	250	454	3.2±0.18	345	456	2.2±0.18	1.5
S19	240	452	5.3±0.27	345	458	2.3±0.27	2.3
S20	240	458	5.6±0.36	345	458	2.3±0.36	2.4
S21	240	444	5.5±0.35	340	458	2.5±0.35	2.2
S22	245	456	4.0±0.28	335	458	2.2±0.28	1.8
S24	240	452	4.5±0.41	335	458	2.4±0.41	1.9
S25	240	458	4.4±0.27	350	454	2.3±0.27	1.9

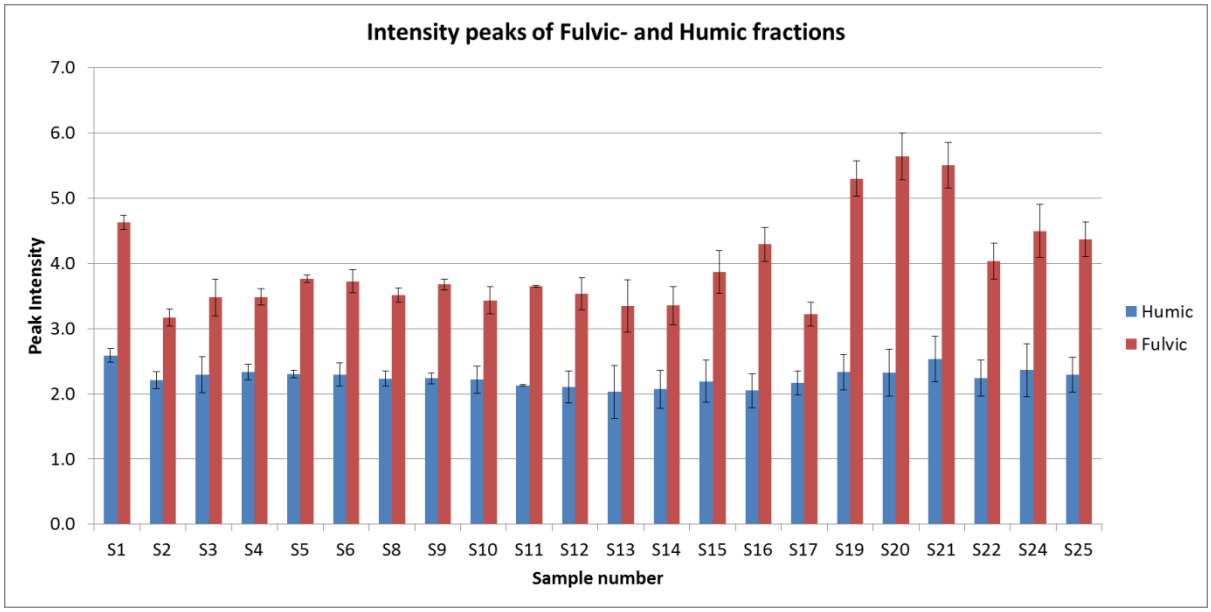

Figure 4.24: Illustrating the difference in the relative intensity between the fulvic and humic peaks. The error bars represents the uncertainty in the TOC measurements.

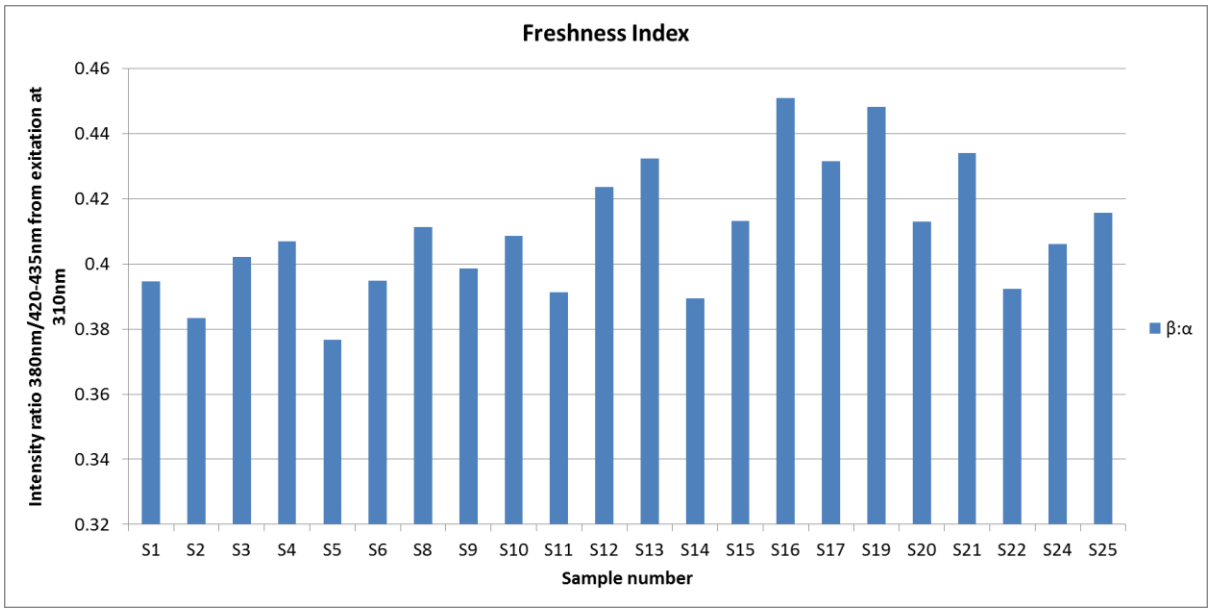

Figure 4.25: The freshness index is fluctuating but a steady increase can be seen from Sample 12. This indicates that DNOM of a younger age is flushed into the stream.

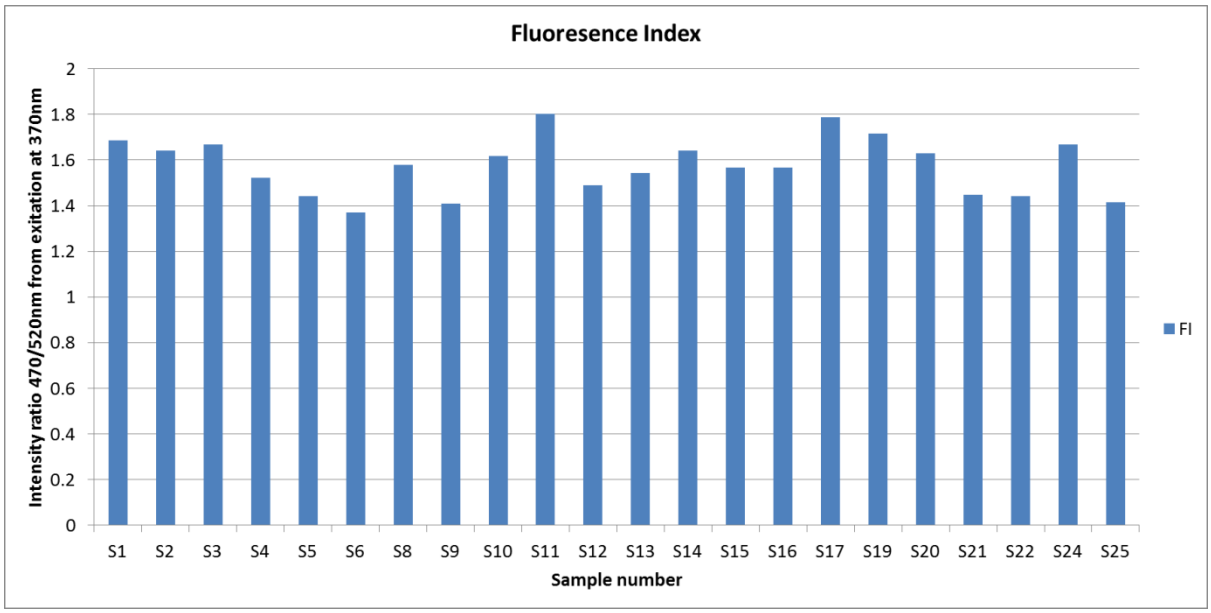

Figure 4.26: FI show some fluctuation but remains at a relative high level.

4.9 Biodegradation

The results from the initial and improved approaches to conduct measurements of the biodegradability of DNOM are presented and compared in Table 4.2 and Figure 4.27. Due to the improved signal-to-noise ratio from the improved approach the values are higher than those from the initial approach. A two sample t-test reveals there is a significant difference between the two methods ($t_{calculated} = 5.5 > t_{table} = 1.7$, $P < 0.001$) (unequal variance). Another interesting observation is the large variation in lag time in the different reference samples (Figure 3.10) detected using the improved approach. This emphasise the importance of treating each replicate individually and detecting at which time during the degradation the number of bacterial cells reach a sufficiently high number to induce exponential growth. As mentioned earlier this number is on average 10^6 cells pr mL (Maier et al. 2009). The reason for this variation is probably that the inoculum is added as a volume and not as a known number of cells to induce bioactivity. When each sample is prepared and distributed between the individual vials, it is impossible to ensure that each vial receives the same number of bacteria thus the response is a variation in lag time. By ensuring proper sealing to avoid leakage it becomes easier to detect when exponential growth begins and separating it from the lag time. The response in Figure 3.8 and 3.9 demonstrate neither a proper lag time nor any phase that resembles exponential growth, thus making it hard to observe any changes in bioactivity. This forces the user to calculate the biodegradation from the start of the experiment which will incorporate the lag time. The end result is a perception of very low bioactivity and that the samples are poorly biodegradable.

The method failed however to determine any significant change in the bioavailability through the episode. A two sample t-test indicates there is no difference between samples collected before and during the discharge peak, however the P-value is too high for the result to be significant ($t_{calculated} = 1.1 < t_{table} = 2.1$, $P = 0.29$) (unequal variance). The high P-value could indicate that the number of samples is too low for there to be any statistic determination. However, the lack of difference in bioavailability coincides with FI in Figure 4.26 showing that the DNOM at Langtjern is primarily microbial derived despite the potential high input of terrestrial derived DNOM. This indicates that the DNOM has already been subjected to extensive biodegradation which will have consumed the more labile compounds and sub sequentially making the DNOM pool more recalcitrant. This could explain some of the problems in getting a proper signal-to-noise ratio during the experiments as the signal output are reduced due to the lack of bioavailability. The graphs from the biodegradation

experiments are listed in Appendix (Chapter 8.3.3). By comparing the graphs with Figure 2.15 and 2.16 it appears that there are variations in in both lag time and the overall shape of the curves. However, the variations do not seem to follow any systematic pattern that correlate with the rest of the dataset. Given Equation 2.7 and Figure 2.14 a higher degradation rate was expected for Sample 12-24 compared with Sample 2-11 due to the increasing carbon content illustrated by Figure 4.9. Another hypothesis was to expect a lower degradation rate in Sample 12-24 due to the increase in SAR as is illustrated in Figure 4.23 which also signify an increase in oxygen content (Chapter 2.9.1). According to Equation 2.8 this will have a significant negative effect on the bioavailability of DNOM. However, as determined by t-test there is neither a net increase nor decrease in the biodegradation rate when comparing samples collected before and during flow peak.

With the exception of Sample 20 (Figure 8.78) all of the graphs appear to correlate with a standard Monod growth curve (Figure 2.15). Only Sample 20 shows a typical bi-phasic growth curve with a secondary lag phase occurring at approximately after 1200 minutes (20 hours). However, most of the samples show a distinct change in curve steepness during the experiment which indicate that the bacteria is consuming the more labile moieties of DNOM first before the more recalcitrant moieties. The lack of any distinct increase or decrease in RR during the episode and the evidence of bi-phasic growth curves questions the theory of aquatic priming effect (PE) presented in Chapter 2.8.1. PE hypothesized that as DNOM of different character are mixed together during storm flow conditions the increased input of labile DNOM would have a significant effect on the bioavailability of the recalcitrant moieties as well and sub sequentially increase the overall biodegradation rate. The findings in this thesis indicate that is not the case. However, it should be emphasised that given the lack of statistical significance (indicated by a high P-value) it is not possible to reach any conclusion based on the biodegradation data presented in this thesis.

Table 4.2: Results from the two approaches to biodegradation. On average the response using the improved approach gave higher signal output and lower standard deviation. This gave a significant improvement in signal-to-noise ratio.

Sample number	RR (µmole O_2/hour) Initial Approach	SD	SD%	RR (µmole O_2/hour) Improved Approach	SD	SD%
S1	0.10	0.03	30.72	-	-	-
S2	0.12	0.02	13.16	0.1	0.008	8
S3	0.3	0.1	34.41	0.3	0.1	33
S4	0.1	0.1	81.04	0.41	0.03	7
S5	0.1	0.1	59.66	0.3	0.2	67

S6	0.15	0.03	16.48	0.21	0.03	14
S8	0.24	0.02	8.38	-	-	-
S9	0.3	0.1	46.24	0.18	0.006	3
S10	0.07	0.03	45.89	0.33	0.01	2.98
S11	0.13	0.04	31.52	0.29	0.03	10.99
S12	0.16	0.05	30.19	0.35	0.01	4.28
S13	0.2	0.1	32.27	0.34	0.03	7.88
S14	0.2	0.2	80.07	0.3	0.1	23.22
S15	0.01	0.1	987.86	0.44	0.03	6.40
S16	0.07	0.01	14.50	0.2	0.1	24.70
S17	0.0	0.1	12385.46	0.53	0.03	5.13
S19	0.0	0.1	2112.58	0.40	0.04	10.61
S20	0.0	0.1	251.46	0.16	0.009	6
S21	0.0	0.1	410.32	0.13	0.008	6
S22	-0.01	0.05	471.98	0.23	0.03	11.72
S24	0.0	0.1	758.76	0.40	0.05	11.33
S25	-0.02	0.1	472.32	-	-	-

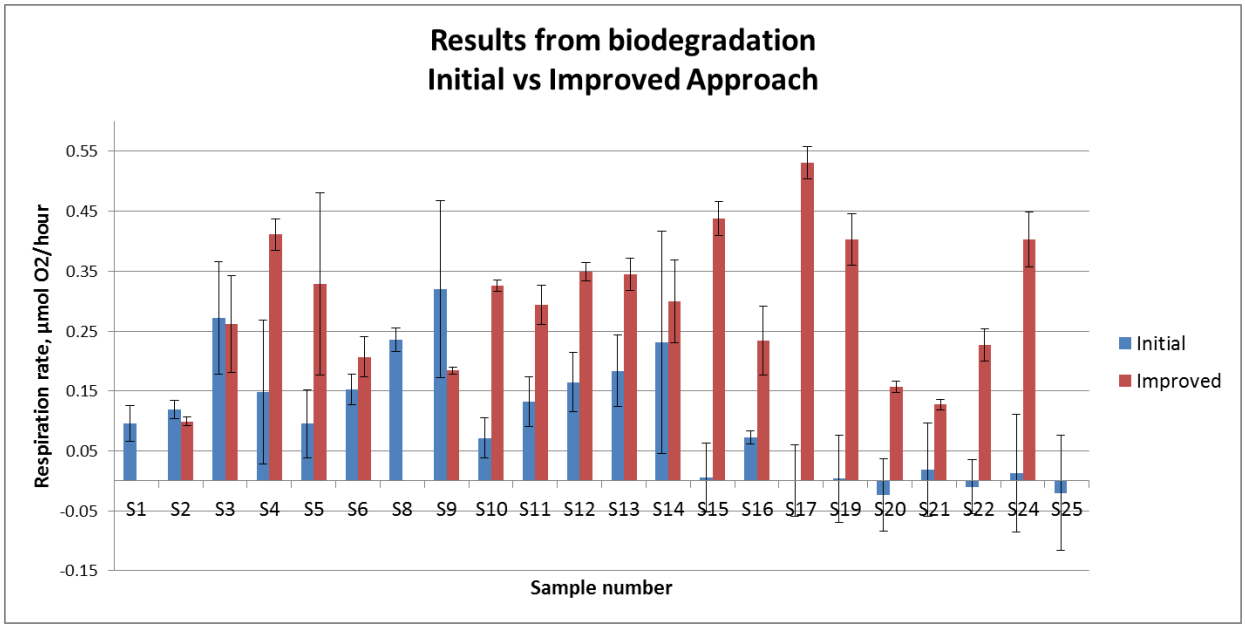

Figure 4.27: Large variation in results from the biodegradation experiments. However, the improved approach shows a much better response compared to the initial approach.

5. Conclusion

It has been hypothesized that the darkening colour and the increased concentration of DOC in surface waters, observed in the Nordic countries and North- East America during the past 30 years, is partly due to changes in precipitation patterns. The resulting change in hydrology is also postulated to have caused a change in the characteristics of DNOM towards more high molecular weight and increased degree of aromaticity. The results from analysis presented in this thesis revealed the opposite. As precipitation persists during the episode the DNOM supplied to the stream did show an increased in the concentration of DOC, however with a gradual change in character to having a lower molecular weight and being less aromatic. It is clear that changes in water levels during heavy precipitation changes the flow patterns of water supplying the stream. In the study area there is a mix of shallow mineral soil and bogs. As a consequence there is a shift in the overall contribution of DNOM coming from the different soil types that resides in the area. During low flow conditions the water supplying the stream is from ground water seepage originating primarily from the water saturated peats. The DNOM found in peats typically contain more high molecular weight DNOM with a high degree of aromaticity. With the onset of rain, the increasing water levels cause flushing of water through the mineral soils and over the peats. The DNOM from the mineral soil generally contain DNOM of low molecular weight and less degree of aromaticity. An increase flux of water from the mineral soil during runoff episodes thus change the overall character of DNOM in the steam. This is consistent with previous episode studies performed in area with mixed soil types.

An extensive part of this thesis was to develop and improving a method for measuring the biodegradability of DNOM. When comparing the signal output from the initial approach with the optimized method the results are encouraging. The optimized method produces a much improved response with a consistent higher signal output with lower signal-to-noise ratio. Moreover, the improved method produces results that are more consistent with theory.

The measured biodegradability of the DNOM using the optimized method revealed no significant changes in the bioavailability of DNOM through the episode. This is supported by the fluorescence index (FI) showing that the DNOM in all of the samples collected during the episode is primarily microbial derived regardless of the source. It is therefore hypothesized that the conditions at Langtjern is favourable for microbial activity causing an effective biodegradation of labile organic compounds thus making the remaining DNOM more recalcitrant and less bioavailable. However, it must be emphasized that the number of samples

studied in this thesis is limited. The biodegradability of the DNOM in a larger number of samples from different sources needs to be measured using the improved method in order to verify if it is able to yield reliable results.

Based on the findings in this thesis an argument could be made that as climate change persists, a change in temperature and precipitation patterns could significantly affect the supply and character of DNOM in to natural surface waters.

6. Recommended future work

The results produced in this thesis are from one single episode. It is therefore highly recommended that many more episode studies is performed in order to see if the results are from an anomaly or if they represents a trend explaining a larger spatial and temporal variation. This will produce a larger sample pool to which conduct statistics and thereby trend analysis.

A major obstacle in collecting large number of samples in remote areas is the physical labour involved. Due to limit capacity there is only a certain amount of water samples that can be carried back to the lab. This puts limits to the number of samples to which conduct analysis and thereby limits the basis for statistical analysis. It is therefore recommended to either involve more personnel when doing field work or arrange for mechanistic transport so that more samples can be brought back for analysis.

Sample pre-treatment were conducted by filtrating the sample raw water directly on 0.2µm filters. Due to the high content of particulate matter this process was at times painstakingly slow due to clogging of filters. It is therefore highly recommended to pre-filter the raw water on 0.7µm to remove most of the particulate matter before performing another filtration on 0.2 µm for sterilization.

References

Abbt-Braun G, Frimmel FH (1999) Basic characterization of Norwegian NOM samples - Similarities and differences. Environ Int 25:161–180. doi: 10.1016/S0160-4120(98)00118-4

Aiken GR, Hsu-Kim H, Ryan JN (2011) Influence of dissolved organic matter on the environmental fate of metals, nanoparticles, and colloids. Environ Sci Technol 45:3196–3201. doi: 10.1021/es103992s

Aitkenhead JA, Hope D, Billett MF (1999) The relationship between dissolved organic carbon in stream water and soil organic carbon pools at different spatial scales. Hydrol Process 13:1289–1302.

Al-Faiyz YSS (2013) CPMAS 13C NMR characterization of humic acids from composted agricultural Saudi waste. Arab J Chem 10:S839–S853. doi: 10.1016/j.arabjc.2012.12.018

Alberts JJ (1982) The effect of metal ions on the ultraviolet spectra of humic acid, tannic acid and lignosulfonic acid. Water Res 16:1273–1276. doi: 10.1016/0043-1354(82)90146-4

Allison SD, Wallenstein MD, Bradford MA (2010) Soil-carbon response to warming dependent on microbial physiology. Nat Geosci 3:336–340. doi: 10.1038/ngeo846

Amon RMW, Benner R (1996) Bacterial utilization of different size classes of dissolved matter organic. Limnol Oceanogr 41:41–51.

Appelo CAJ, Postma D (2010) Geochemistry, groundwater and pollution, 2nd edn. A.A. Balkema Publishers

Arrigo KR (2005) Marine microorganisms and global nutrient cycles. Nature 437:349–355. doi: 10.1038/nature04159

Atkins P, De Paula J (2010) Physical Chemistry, 9th edn. W.H. Freeman and Company

Austnes K, Evans CD, Eliot-Laize C, Naden PS, Old GH (2010) Effects of storm events on mobilisation and in-stream processing of dissolved organic matter (DOM) in a Welsh peatland catchment. Biogeochemistry 99:157–173. doi: 10.1007/s10533-009-9399-4

Azam F, Fenchel T, Field J, Gray J, Meyer-Reil L, Thingstad F (1983) The Ecological Role of Water-Column Microbes in the Sea. Mar Ecol Prog Ser 10:257–263. doi: 10.3354/meps010257

Badis A, Ferradji FZ, Boucherit A, Fodil D, Boutoumi H (2009) Characterization and biodegradation of soil humic acids and preliminary identification of decolorizing actinomycetes at Mitidja plain soils (Algeria). African J Microbiol Res 3:997–1007.

Baker A (2001) Fluorescence excitation - Emission matrix characterization of some sewage-impacted rivers. Environ Sci Technol 35:948–953. doi: 10.1021/es000177t

Barré P, Plante AF, Cécillon L, Lutfalla S, Baudin F, Bernard S, Christensen BT, Eglin T, Fernandez JM, Houot S, Kätterer T, Le Guillou C, Macdonald A, van Oort F, Chenu C (2016) The energetic and chemical signatures of persistent soil organic matter. Biogeochemistry 130:1–12. doi: 10.1007/s10533-016-0246-0

Bengtsson MM, Wagner K, Burns NR, Herberg ER, Wanek W, Kaplan LA, Battin TJ (2015a) No evidence of aquatic priming effects in hyporheic zone microcosms. Sci Rep 4:5187. doi: 10.1038/srep05187

Bengtsson MM, Wagner K, Burns NR, Herberg ER, Wanek W, Kaplan LA, Battin TJ (2015b) No evidence of aquatic priming effects in hyporheic zone microcosms. Sci Rep 4:5187. doi: 10.1038/srep05187

Biggs W, Nambiar HS (2016) Horizons - Wikimedia Commons. https://commons.wikimedia.org/w/index.php?curid=46207693. Accessed 4 May 2017

Blackman AG, Gahan LR (2014) Aylward and Findley`s SI chemical data/Allan Blackman; Lawrence Gahan., 7th edn. John Wiley & Sons Australia Ltd, Milton

Brooker RJ, Widmaier EP, Graham LE, Stiling PD (2011) Biology, 2nd edn. McGraw-Hill

Catalán N, Kellerman AM, Peter H, Carmona F, Tranvik LJ (2015) Absence of a priming effect on dissolved organic carbon degradation in lake water. Limnol Oceanogr 60:159–168. doi: 10.1002/lno.10016

Chen J, Gu B, LeBoeuf EJ, Pan H, Dai S (2002) Spectroscopic characterization of the structural and functional properties of natural organic matter fractions. Chemosphere 48:59–68. doi: 10.1016/S0045-6535(02)00041-3

Chen W, Westerhoff P, Leenheer JA, Booksh K (2003) Fluorescence Excitation-Emission Matrix Regional Integration to Quantify Spectra for Dissolved Organic Matter. Environ Sci Technol 37:5701–5710. doi: 10.1021/es034354c

Chen Y, Senesi N, Schnitzer M (1977) Information Provided on Humic Substances by E4/E6 Ratios1. Soil Sci Soc Am J 41:352–358. doi: 10.2136/sssaj1977.03615995004100020037x

Correll DL (1999) Phosphorus: a rate limiting nutrient in surface waters. Poult Sci 78:674–82.

Cory RM, Mcknight DM (2005) Fluorescence Spectroscopy Reveals Ubiquitous Presence of Oxidized and Reduced Quinones in Dissolved Organic Matter Fluorescence Spectroscopy Reveals Ubiquitous Presence of Oxidized and Reduced Quinones in Dissolved Organic Matter. Environ Sci Technol 39:8142–8149. doi: 10.1021/es0506962

Cotner JB, Hall EK, Scott JT, Heldal M (2010) Freshwater bacteria are stoichiometrically flexible with a nutrient composition similar to seston. Front Microbiol 1:1–11. doi: 10.3389/fmicb.2010.00132

Cotrufo MF, Soong JL, Horton AJ, Campbell EE, Haddix ML, Wall DH, Parton WJ (2015) Formation of soil organic matter via biochemical and physical pathways of litter mass loss. Nat Geosci 8:776–779. doi: 10.1038/ngeo2520

Cotrufo MF, Wallenstein MD, Boot CM, Denef K, Paul E (2013) The Microbial Efficiency-Matrix Stabilization (MEMS) framework integrates plant litter decomposition with soil organic matter stabilization: Do labile plant inputs form stable soil organic matter? Glob Chang Biol 19:988–995. doi: 10.1111/gcb.12113

Danger M, Cornut J, Chauvet E, Chavez P, Elger A, Lecerf A (2013) Benthic algae stimulate leaf litter decomposition in detritus-based headwater streams: a case of aquatic priming effect? Ecology 94:1604–1613. doi: 10.1890/12-0606.1

De Haan H, De Boer T (1987) Applicability of light absorbance and fluorescence as measures of concentration and molecular size of dissolved organic carbon in humic Lake Tjeukemeer. Water Res 21:731–734. doi: 10.1016/0043-1354(87)90086-8

de Wit H (2015) Langtjern – long term ecological monitoring - NIVA - Norsk institutt for

vannforskning. http://www.niva.no/en/langtjern. Accessed 4 May 2017

Dijkstra FA, Cheng W (2007) Interactions between soil and tree roots accelerate long-term soil carbon decomposition. Ecol Lett 10:1046–1053. doi: 10.1111/j.1461-0248.2007.01095.x

Dore MHI (2005) Climate change and changes in global precipitation patterns: What do we know? Environ Int 31:1167–1181. doi: 10.1016/j.envint.2005.03.004

Elser JJ, Bracken MES, Cleland EE, Gruner DS, Harpole WS, Hillebrand H, Ngai JT, Seabloom EW, Shurin JB, Smith JE (2007) Global analysis of nitrogen and phosphorus limitation of primary producers in freshwater, marine and terrestrial ecosystems. Ecol Lett 10:1135–1142. doi: 10.1111/j.1461-0248.2007.01113.x

Fasching C, Behounek B, Singer GA, Battin TJ, Saccomandi F (2015) Microbial degradation of terrigenous dissolved organic matter and potential consequences for carbon cycling in brown-water streams. Sci Rep 4:4981. doi: 10.1038/srep04981

Fellman JB, Hood E, Spencer RGM (2010) Fluorescence spectroscopy opens new windows into dissolved organic matter dynamics in freshwater ecosystems: A review. Limnol Oceanogr 55:2452–2462. doi: 10.4319/lo.2010.55.6.2452

Fierer N, Schimel JP, Holden PA (2003) Variations in microbial community composition through two soil depth profiles. Soil Biol Biochem 35:167–176. doi: 10.1016/S0038-0717(02)00251-1

Finstad AG, Andersen T, Larsen S, Tominaga K, Blumentrath S, de Wit HA, Tømmervik H, Hessen DO (2016) From greening to browning: Catchment vegetation development and reduced S-deposition promote organic carbon load on decadal time scales in Nordic lakes. Sci Rep 6:31944. doi: 10.1038/srep31944

Fitzgerald WF, Engstrom DR, Mason RP, Nater E a. (1998) The Case for Atmospheric Mercury Contamination in Remote Areas. Environ Sci Technol 32:1–7. doi: 10.1021/es970284w

Fovet O, Ruiz L, Hrachowitz M, Faucheux M, Gascuel-Odoux C (2015) Hydrological hysteresis and its value for assessing process consistency in catchment conceptual models. Hydrol Earth Syst Sci 19:105–123. doi: 10.5194/hess-19-105-2015

Garmo Ø, Skancke LB, Høgåsen T (2016) Overvåking av langtransportert forurenset luft og nedbør. Årsrapport - Vannkjemiske effekter 2015.

Grasshoff K, Erhardt M, Kremling K, Koroleff F (1985) Determination of silicone. In: Methods of Seawater Analysis. Wiley, pp 174–185

Grinhut T, Hertkorn N, Schmitt-Kopplin P, Hadar Y, Chen Y (2011) Mechanisms of Humic Acids Degradation by White Rot Fungi Explored Using ^{1}H NMR Spectroscopy and FTICR Mass Spectrometry. Environ Sci Technol 45:2748–2754. doi: 10.1021/es1036139

Groisman PY, Karl TR, Easterling DR, Knight RW, Jamason PF, Hennessy KJ, Suppiah R, Page CM, Wibig J, Fortuniak K, Razuvaev VN, Douglas A, Førland E, Zhai PM (1999) Changes in the probability of heavy precipitation: Important indicators of climatic change. Clim. Change 42:243–283.

Guenet B, Danger M, Harrault L, Allard B, Jauset-Alcala M, Bardoux G, Benest D, Abbadie

L, Lacroix G (2014) Fast mineralization of land-born C in inland waters: first experimental evidences of aquatic priming effect. Hydrobiologia 721:35–44. doi: 10.1007/s10750-013-1635-1

Guenet B, Danger M, Abbadie L, Lacroix G (2010) Priming effect: bridging the gap between terrestrial and aquatic ecology. Ecology 91:2850–2861. doi: 10.1890/09-1968.1

Gundersen CB, Andersen T, Lindahl S, Linke D, Vogt RD (2014) Bacterial response from exposure to selected aliphatic nitramines. Energy Procedia 63:791–800. doi: 10.1016/j.egypro.2014.11.089

Haitzer M, Aiken GR, Ryan JN (2002) Binding of mercury(II) to dissolved organic matter: The role of the mercury-to-DOM concentration ratio. Environ Sci Technol 36:3564–3570. doi: 10.1021/es025699i

Hall BD, Aiken GR, Krabbenhoft DP, Marvin-DiPasquale M, Swarzenski CM (2008) Wetlands as principal zones of methylmercury production in southern Louisiana and the Gulf of Mexico region. Environ Pollut 154:124–134. doi: 10.1016/j.envpol.2007.12.017

Hanssen-Bauer I, Drange H, Førland EJ, Roald LA, Børsheim KY, Hisdal H, Lawrence D, Nesje A, Sandven S, Sorteberg A, Others (2015) Klima i Norge 2100.

Hanssen B, Forland E (1998) Long-term trends in precipitation and temperature in the Norwegian Artctic: can they be explained by changes in the atmospheric circulation patterns? Int J Climatol 20:143–153. doi: 10.3354/cr010143

Hardie AG, Dynes JJ, Kozak LM, Huang P. (2009) The role of glucose in abiotic humification pathways as catalyzed by birnessite. J Mol Catal 114–126.

Hautala K, Peuravuori J, Pihlaja K (2000) Measurement of aquatic humus content by spectroscopic analyses. Water Res 34:246–258. doi: 10.1016/S0043-1354(99)00137-2

He ZL, Yang XE, Stoffella PJ (2005) Trace elements in agroecosystems and impacts on the environment. J Trace Elem Med Biol 19:125–140. doi: 10.1016/j.jtemb.2005.02.010

Helms JR, Stubbins A, Ritchie JD, Minor EC, Kieber DJ, Mopper K (2008a) Absorption spectral slopes and slope ratios as indicators of molecular weight, source, and photobleaching of chromophoric dissolved organic matter. Limnol Oceanogr 53:955–969. doi: 10.4319/lo.2008.53.3.0955

Helms JR, Stubbins A, Ritchie JD, Minor EC, Kieber DJ, Mopper K (2008b) Absorption spectral slopes and slope ratios as indicators of molecular weight, source, and photobleaching of chromophoric dissolved organic matter. Limonology Oceanogr 53:955–969. doi: 10.4319/lo.2008.53.3.0955

Henriksen A, Grande M (2002) Lake Langtjern - fish studies in the Langtjern area 1966-2000.

Hessen DO, Tranvik LJ (1998) Aquatic Humic Substances : Ecology and Biogeochemistry. Springer Berlin Heidelberg

Hiscock KM (2011) Hydrogeology: principles and practice. Blackwell Publishing

Hornberger GM, Scanlon TM, Raffensperger JP (2001) Modelling transport of dissolved silica in a forested headwater catchment: The effect of hydrological and chemical time scales on hysteresis in the concentration-discharge relationship. Hydrol Process 15:2029–2038. doi: 10.1002/hyp.254

Hov Ø, Cubasch U, Fischer E, Höppe P, Iversen T, Kvamstø NG, Kundzewicz ZW, Rezacova D, Rios D, Santos FD, Schädler B, Veisz O, Zerefos C, Benestad R, Murlis J, Donat M, Leckebusch GC, Ulbrich U (2013) Extreme Weather Events in Europe: preparing for climate change adaptation. Det Norske Videnskaps Akademi

International Standard (1998) ISO11259 - Soil Quality - Simplified Soil Description. 1998:1–48.

IPCC IP on CC (2013) Climate Change 1995. The Science of Climate Cliange. J Chem Inf Model 53:1689–1699. doi: 10.1017/CBO9781107415324.004

Jensen IS, Eriksen TG, Skålin R (2017) Climate statistics for Austlandet. http://www.yr.no/place/Norway/Austlandet/climate.html?spr=eng. Accessed 4 May 2017

Jordan RN, Yonge DR, Hathhorn WE (1997) Enhanced mobility of Pb in the presence of dissolved natural organic matter. J Contam Hydrol 29:59–80. doi: 10.1016/S0169-7722(96)00087-3

Kellerman AM, Dittmar T, Kothawala DN, Tranvik LJ (2014) Chemodiversity of dissolved organic matter in lakes driven by climate and hydrology. Nat Commun 5:1–8. doi: 10.1038/ncomms4804

Khan E, Subramania-Pillai S (2006) EFFECT OF LEACHING FROM FILTERS ON LABORATORY ANALYSES OF COLLECTIVE ORGANIC CONSTITUENTS.

Kiikkilä O, Kitunen V, Smolander A (2011) Properties of dissolved organic matter derived from silver birch and Norway spruce stands: Degradability combined with chemical characteristics. Soil Biol Biochem 43:421–430. doi: 10.1016/j.soilbio.2010.11.011

Kononova MM (2013) Soil Organic Matter : Its Nature, Its Role in Soil Formation and in Soil Fertility. Elsevier Science

Korshin G V, Li C, Benjamin MM (1997) Organic Matter Through Uv Spectroscopy : Water Res 31:1787–1795. doi: 10.1016/S0043-1354(97)00006-7

Kothawala DN, von Wachenfeldt E, Koehler B, Tranvik LJ (2012) Selective loss and preservation of lake water dissolved organic matter fluorescence during long-term dark incubations. Sci Total Environ 433:238–246. doi: 10.1016/j.scitotenv.2012.06.029

Lampmann GM, Pavia DL, Kriz GS, Vyvyan JR (2010) Spectroscopy, 4th edn. Mary Finch

Leeben A, Heinsalu A, Alliksaar T, Vassiljev J (2010) High-resolution spectroscopic study of pore-water dissolved organic matter in Holocene sediments of Lake Peipsi (Estonia/Russia). Hydrobiologia 646:21–31. doi: 10.1007/s10750-010-0174-2

Lehmann J, Kleber M (2015) The contentious nature of soil organic matter. Nature. doi: 10.1038/nature16069

Madigan MT, Martinko JM (2006) Brock Biology of Microorganisms, 11th edn. Pearson Education, Inc.

Maier RM (2010) Bacterial Growth. Environ Microbiol 37–54. doi: 10.1007/978-94-017-8908-0

Maier RM, Pepper IL, Gerba CP (2009) Environmental microbiology. Academic Press

Marschner B, Kalbitz K (2003) Controls of bioavailability and biodegradability of dissolved

organic matter in soils. Geoderma 113:211–235. doi: 10.1016/S0016-7061(02)00362-2

McKnight DM, Boyer EW, Westerhoff PK, Doran PT, Kulbe T, Andersen DT (2001) Spectrofluorometric characterization of dissolved organic matter for indication of precursor organic material and aromaticity. Limnol Oceanogr 46:38–48. doi: 10.4319/lo.2001.46.1.0038

Moore DS, McCabe GP, Craig BA (2012) Introduction to the Practice of Statistics, 7th edn. W.H. Freeman and Company, New York

Moravcová J, Pavlíček T, Koupilová M, Ondr P, Váchal J (2010) Landscape Studies Behavior of selected c-q hysteresis parameters by extreme rainfall-runoff events in artificially drained localities. J Landsc Stud 2:77–88.

Neidhardt FC, Ingraham JL, Schaechter M (1990) PHYSIOLOGY OF THE BACTERIAL CELL: A MOLECULAR APPROACH, 1st edn. Sinauer Associates, Inc.

Nieder R, Harden T, Martens R, Benbi DK (2008) Microbial biomass in arable soils of Germany during the growth period of annual crops. J Plant Nutr Soil Sci 171:878–885. doi: 10.1002/jpln.200700024

Nierop KGJ., Jansen B, Verstraten JM (2002) Dissolved organic matter, aluminium and iron interactions: precipitation induced by metal/carbon ratio, pH and competition. Sci Total Environ 300:201–211. doi: 10.1016/S0048-9697(02)00254-1

NIST (2016) NIST. Oxygen. Henry`s Law data. http://webbook.nist.gov/cgi/cbook.cgi?ID=C7782447&Units=SI&Mask=10#Solubility. Accessed 11 Apr 2017

NVE (2017) Nedbørfelt (REGINE). https://gis3.nve.no/link/?link=nedborfelt. Accessed 3 May 2017

Ohno T (2002) Fluorescence inner-filtering correction for determining the humification index of dissolved organic matter. Environ Sci Technol 36:742–746. doi: 10.1021/es0155276

Ohno T, Chorover J, Omoike A, Hunt J (2007) Molecular weight and humification index as predictors of adsorption for plant- and manure-derived dissolved organic matter to goethite. Eur J Soil Sci 58:125–132. doi: 10.1111/j.1365-2389.2006.00817.x

Oliver BG, Thurman EM, Malcolm RL (1983) The contribution of humic substances to the acidity of colored natural waters. Geochim Cosmochim Acta 47:2031–2035. doi: 10.1016/0016-7037(83)90218-1

Perdue EM, Lytle CR (1983) Distribution Model for Binding of Protons and Metal Ions by Humic Substances. Environ Sci Technol 17:654–660. doi: 10.1021/es00117a006

Perdue EM, Ritchie JD (2003) Dissolved organic matter in freshwaters. Treatise Geochemistry Vol 5 Surf Gr Water, Weather Soils 273–318.

Peuravuori J, Pihlaja K (1997) Molecular size distribution and spectroscopic properties of aquatic humic substances. Anal Chim Acta 337:133–149. doi: 10.1016/S0003-2670(96)00412-6

PreSens (2017) Stern-Volmer-equation Optical Sensor Basics. https://www.presens.de/knowledge/basics/detail/the-stern-volmer-relationship-900.html. Accessed 3 May 2017

PreSens (2016) SensorDishes & SensorVials - Instruction Manual. Regensburg, Germany

Rahman MA, Hasan AM, Rahim A, Alam AMS (2010) Characterization of Humic Acid from the River Bottom Sediments of Burigonga : Complexation Studies of Metals with Humic Acid. Pakistan J Anal Environ Chem 11:42–52.

Redfield AC (1934) ON THE PROPORTIONS OF ORGANIC DERIVATIVES IN SEA WATER AND THEIR RELATION TO THE COMPOSITION OF PLANKTON. In: James Johnstone Memorial Volume, 1st edn. University Press of Liverpool, Liverpool, pp 176–192

Schmidt MWI, Torn MS, Abiven S, Dittmar T, Guggenberger G, Janssens I a., Kleber M, Kögel-Knabner I, Lehmann J, Manning D a. C, Nannipieri P, Rasse DP, Weiner S, Trumbore SE (2011) Persistence of soil organic matter as an ecosystem property. Nature 478:49–56. doi: 10.1038/nature10386

Seip HM (2016) Nedbør og tørke - fortsatt en klimagåte. Klima

Senesi N, Xing B, Huang PM (2009) Biophysico-Chemical Processes Involving Natural Nonliving Organic Matter in Environmental Systems, 1st edn. John Wiley & Sons, Inc., Hoboken, New Jersey

Skjelkvåle BL (2003) The 15-year report: Assessment and monitoring of surface waters in Europe and North America; acidification and recovery, dynamic modelling and heavy metals.

Stedmon C a., Markager S, Kaas H (2000) Optical Properties and Signatures of Chromophoric Dissolved Organic Matter (CDOM) in Danish Coastal Waters. Estuar Coast Shelf Sci 51:267–278. doi: 10.1006/ecss.2000.0645

Stevenson FJ (1994) Humus chemistry : genesis, composition, reactions, 2nd edn. Wiley

Sun L, Perdue EM, Meyer JL, Weis J (1997) Use of elemental composition to predict bioavailability of dissolved organic matter in a Georgia river. Limnol Oceanogr 42:714–721. doi: 10.4319/lo.1997.42.4.0714

Tananaev NI (2015) Hysteresis effects of suspended sediment transport in relation to geomorphic conditions and dominant sediment sources in medium and large rivers of the Russian Arctic. Hydrol Res 46:232. doi: 10.2166/nh.2013.199

Tipping E, Somerville CJ, Luster J (2016) The C:N:P:S stoichiometry of soil organic matter. Biogeochemistry 130:117–131. doi: 10.1007/s10533-016-0247-z

Twardowski MS, Boss E, Sullivan JM, Donaghay PL (2004) Modeling the spectral shape of absorption by chromophoric dissolved organic matter. Mar Chem 89:69–88. doi: 10.1016/j.marchem.2004.02.008

Vallino JJ, Hopkinson CS, Hobbie JE (1996) Modeling bacterial utilization of dissolved organic matter: Optimization replaces Monod growth kinetics. Limnol Oceanogr 41:1591–1609. doi: 10.4319/lo.1996.41.8.1591

VanLoon GW, Duffy SJ (2011) Environmental chemistry : a global perspective, 3rd edn. Oxford University Press

Vogt RD (2005) Soil Profile descriptions. Oslo: Department of Chemistry, University of Oslo. Unpublished material.

Vogt RD, Akkanen J, Andersen DO, Brüggemann R, Chatterjee B, Gjessing E, Kukkonen JVK, Larsen HE, Luster J, Paul A, Pflugmacher S, Starr M, Steinberg CEW, Schmitt-Kopplin P, Zsolnay Á (2004) Key site variables governing the functional characteristics of Dissolved Natural Organic Matter (DNOM) in Nordic forested catchments. Aquat Sci 66:195–210. doi: 10.1007/s00027-004-0710-0

Wang Y, Combe C, Clark MM (2001) The effects of pH and calcium on the diffusion coefficient of humic acid. J Memb Sci 183:49–60. doi: 10.1016/S0376-7388(00)00555-X

Waychunas GA, Kim CS, Banfield JF (2005) Nanoparticulate Iron Oxide Minerals in Soils and Sediments: Unique Properties and Contaminant Scavenging Mechanisms. J Nanoparticle Res 7:409–433. doi: 10.1007/s11051-005-6931-x

Weishaar JL, Aiken GR, Bergamaschi BA, Fram MS, Fujii R, Mopper K (2003) Evaluation of specific ultraviolet absorbance as an indicator of the chemical composition and reactivity of dissolved organic carbon. Environ Sci Technol 37:4702–4708. doi: 10.1021/es030360x

Wickland KP, Neff JC, Aiken GR (2007) Dissolved organic carbon in Alaskan boreal forest: Sources, chemical characteristics, and biodegradability. Ecosystems 10:1323–1340. doi: 10.1007/s10021-007-9101-4

Wigginton NS, Haus KL, Hochella Jr MF (2007) Aquatic environmental nanoparticles. J Environ Monit 9:1306. doi: 10.1039/b712709j

Williams GP (1989) Sediment concentration versus water discharge during single hydrologic events in rivers. J Hydrol 111:89–106. doi: 10.1016/0022-1694(89)90254-0

Xiao YH, Räike A, Hartikainen H, Vähätalo A V. (2015) Iron as a source of color in river waters. Sci Total Environ 536:914–923. doi: 10.1016/j.scitotenv.2015.06.092

Zheng W, Liang L, Gu B (2012) Mercury reduction and oxidation by reduced natural organic matter in anoxic environments. Environ Sci Technol 46:292–299. doi: 10.1021/es203402p

8. Appendix

8.1 Balancing chemical equation

$a(C_6H_{12}O_6) + b(NH_3) + c(O_2) \rightarrow d(C_5H_7NO_2) + e(CO_2) + f(H_2O)$ (2.9)

Table 8.1: The molecular weight of the different compounds in Equation 2.9. Only the MW of the cell mass and glucose are needed for balancing the equation.

Compound	Molecular weight (g/mole)
Cell mass, $C_5H_7NO_2$	113
Glucose, $C_6H_{12}O_6$	180
Ammonia, NH_3	17
Oxygen, O_2	32
Carbon dioxide, CO_2	44
Water, H_2O	18

Assuming a = 1 mole of glucose and a cell yield of Y = 0.4

Balancing the cell mass with glucose using the cell yield:

d*113 = a*180*Y

$\underline{d} = \frac{a*180*Y}{113} = \frac{1*180*0.4}{113} \approx \underline{0.64}$

Balancing glucose with ammonia using nitrogen:

$\underline{b}*1 = d*1 \approx \underline{0.64}$

Balancing carbon dioxide with glucose and cell mass using carbon:

e*1 + d*5 = a*6

$\underline{e} = a*6 - d*5 = 1*6 - 0.64*5 = \underline{2.8}$

Balancing water with glucose, ammonia and cell mass:

f*2 + d*7 = a*12 + b*3

$\underline{f} = \frac{a*12+b*3-d*7}{2} = \frac{1*12+0.64*3-0.64*7}{2} = \underline{4.72}$

Balancing oxygen with glucose, cell mass, carbon dioxide and water using oxygen:

c*2 + a*6 = d*2 + e*2 + f*1

$\underline{c} = \frac{d*2+e*2+f*1-a*6}{2} = \frac{0.64*2+2.8*2+4.72-1*6}{2} = \underline{2.8}$

Result

$(C_6H_{12}O_6) + 0.64(NH_3) + 2.8(O_2) \rightarrow 0.64(C_5H_7NO_2) + 2.8(CO_2) + 4.72(H_2O)$ (2.9a)

Table 8.2: Showing that Equation 2.9a were properly balanced by having an equal number of elements on both sides of the equation.

Balance check			
	Right side		Left side
Carbon	**6**	=	0.64*5 + 2.8 = **6**
Hydrogen	12 +0.64*3 = **13.92**	=	0.64*7 + 4.72*2 =**13.92**
Oxygen	6 + 2.8*2 = **11.6**	=	0.64*2 + 2.8*2 + 4.72 = **11.6**
Nitrogen	**0.64**	=	**0.64**

The amount of carbon consumed pr. oxygen = $\frac{6}{11.6} \approx$ **0.52.**

Assuming a = 1 mole of glucose and a cell yield of Y = 0.2

(Applying the same calculations as above)

Result

$(C_6H_{12}O_6) + 0.32(NH_3) + 4.41(O_2) \rightarrow 0.32(C_5H_7NO_2) + 4.41(CO_2) + 5.36(H_2O)$ (2.9b)

Table 8.3: Showing that Equation 2.9b were properly balanced by having an equal number of elements on both sides of the equation.

Balance check			
	Right side		Left side
Carbon	**6**	=	0.64*5 + 2.8 = **6**
Hydrogen	12 +0.32*3 = **13**	=	0.32*7 + 5.36*2 =**13**
Oxygen	6 + 4.41*2 = **14.8**	=	0.32*2 + 4.41*2 + 5.36 = **14.8**
Nitrogen	**0.32**	=	**0.32**

The amount of carbon consumed pr. oxygen = $\frac{6}{14.8} \approx$ **0.41**

8.2 Element analysis

8.2.1 Ion Chromatography

Table 8.4: Instrumental conditions for IC when determining the concentration of anions in the samples.

Instrument and operating conditions Anions	
Instrument	Dionex AS40
Anion guard Column	Dionex AG 18
Anion separator column	Dionex AS 18
Anion self-regenerating suppressor	Dionex AERS 300 4mm
Detector	Dionex Conductivity Detector DS6 cell
Eulent	28 mM KOH
AERS current	70 mA
Column temperature	30°C
Sample loop	25 µL
Flow rate	1.0 mL/min

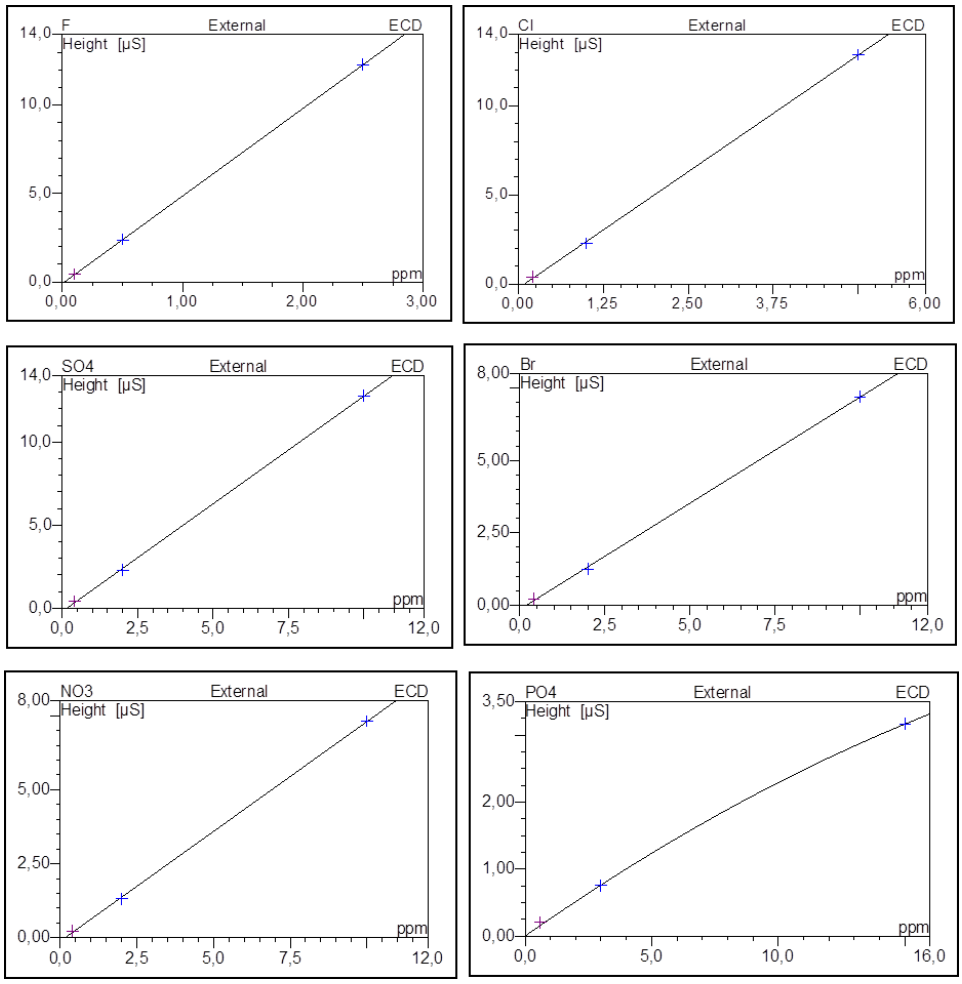

Figure 8.1: Presentation of the calibration curves used to determine the concentration of anions at the Dep. of Geoscience.

Table 8.5: The results from the calibration. The calibration equations were not available and the concentrations were calculated by the instrument.

Compound	Cal. type	SD	R^2	LOD	LOQ
Fluoride	Linear	0.017	1	0.052	0.175
Chloride	Linear	0.145	0.9998	0.436	1.455
Sulphate	Linear	0.135	0.9998	0.406	1.355
Bromium	Linear	0.101	0.9996	0.303	1.008
Nitrate	Linear	0.074	0.9998	0.221	0.735
Phosphate	Quadratic	0.045	0.9996	0.136	0.454

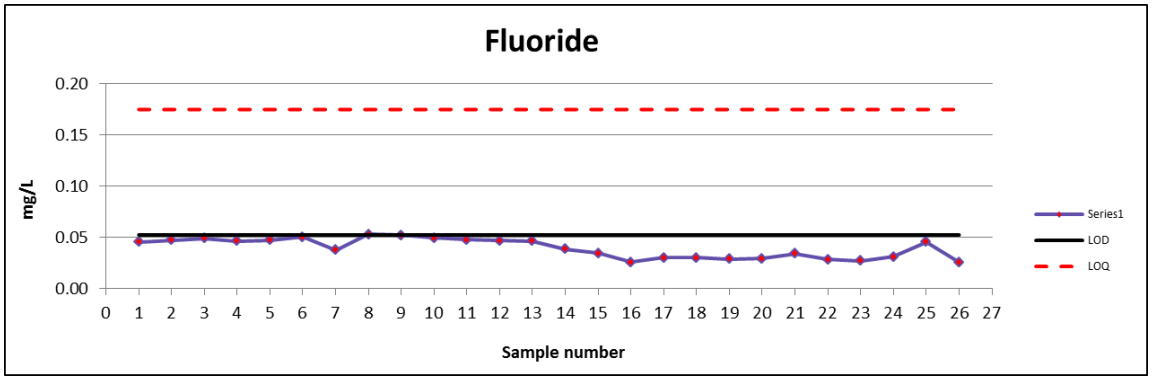

Figure 8.2: The concentration of fluoride was below LOD for all the samples.

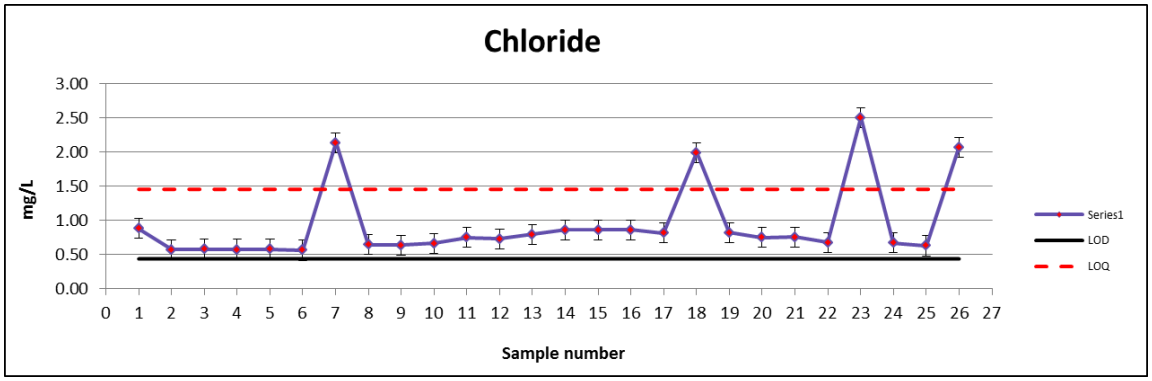

Figure 8.3: The concentration of chloride was below LOQ for all samples except those contaminated by spring water.

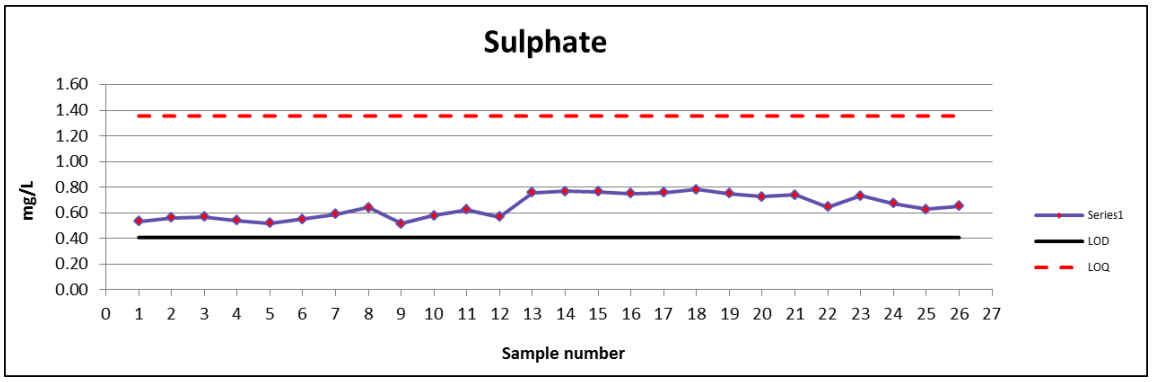

Figure 8.4: The concentration of sulphate was below LOQ for all samples.

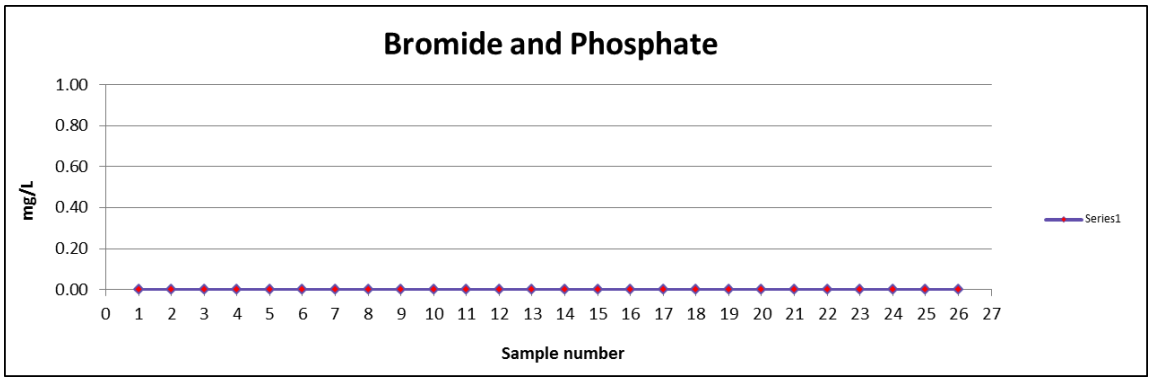

Figure 8.5: The instrument was unable to detect any concentration levels of neither bromide nor phosphate.

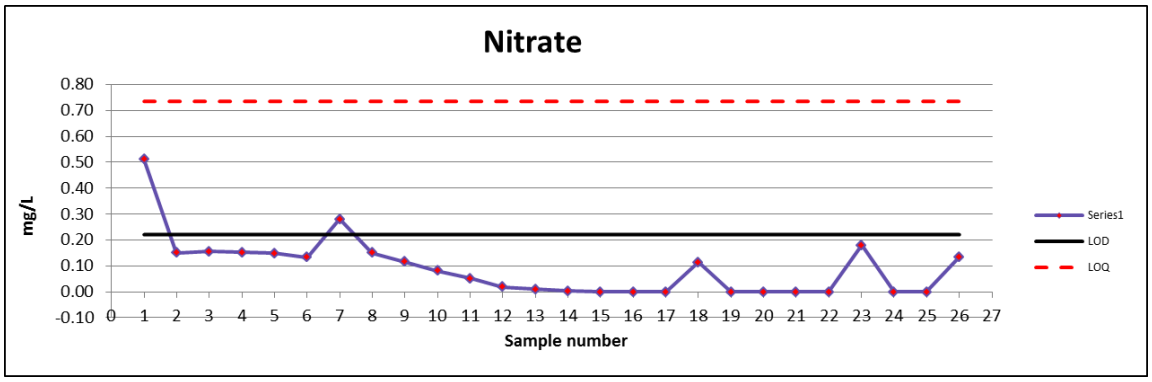

Figure 8.6: The concentration of nitrate was below LOQ in all samples and below LOD for most in the samples.

Table 8.6: Instrumental conditions for IC when determining the concentration of cations in the samples.

Instrument and operating conditions Cations	
Instrument	Dionex AS40
Cation guard Column	Dionex CG16
Cation separator column	Dionex IonPac CS16 Analytical 3x250mm
Cation self-regenerating suppressor	Dionex CSRS300 4mm
Detector	Dionex Conductivity Detector DS6 cell
Eulent	30 mM MSA
AERS current	32 mA
Column temperature	30°C
Sample loop	25 µL
Flow rate	0.36 mL/min

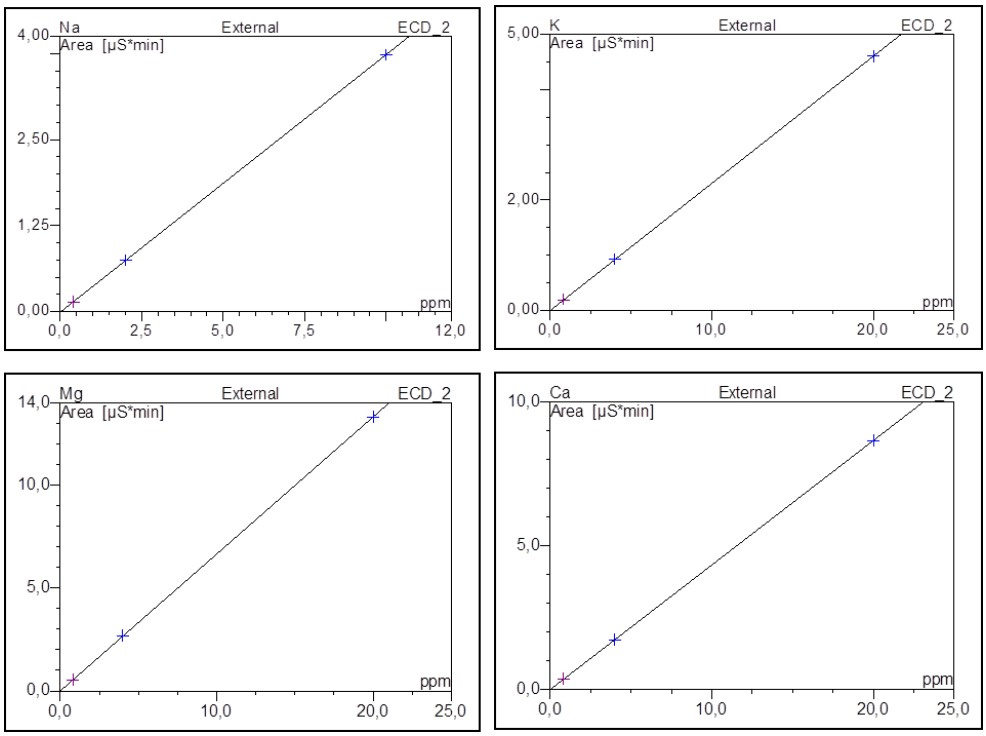

Figure 8.7: Presentation of the calibration curves used to determine the concentration of cations at the Dep. of Geoscience.

Table 8.7: The results from the calibration. The calibration equations were not available and the concentrations were calculated by the instrument.

Element	Cal. type	SD	R^2	LOD	LOQ
Sodium	Linear	0.003	1	0.008	0.027
Potassium	Linear	0.007	0.99999	0.02	0.066
Manganese	Linear	0.013	1	0.039	0.13
Calcium	Linear	0.005	1	0.015	0.05

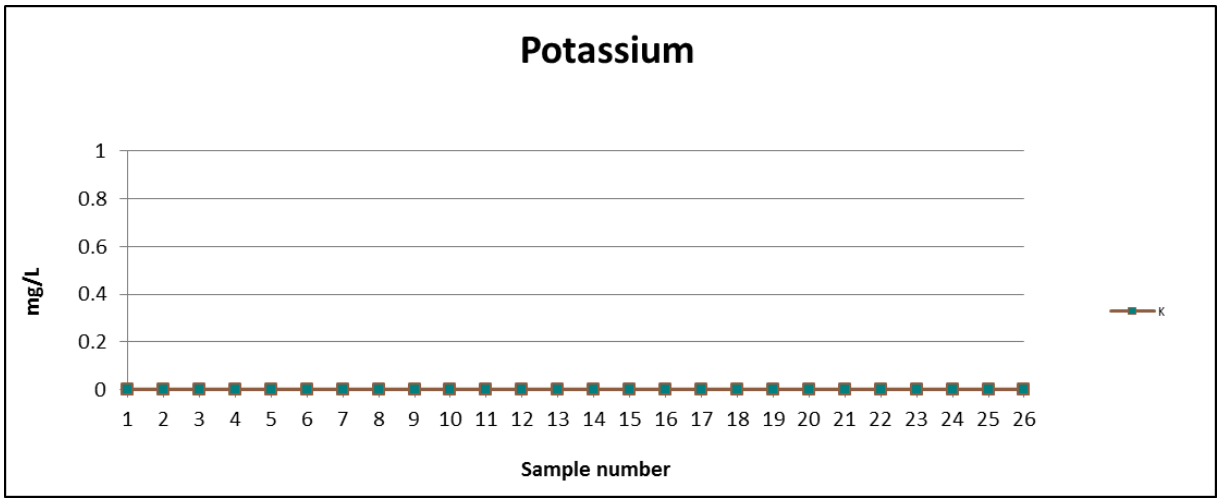

Figure 8.8: The concentration of potassium could not be determined by the instrument in any of the samples.

8.2.2 Test of spring water to verify source of anion contamination

Table 8.8: Instrumental conditions for IC when determining the concentrations of anions in spring water.

Instrument and operating conditions Anions	
Instrument	Dionex Integrion HPLC
Anion guard Column	Dionex IonPac AG 18, 4µm
Anion separator column	Dionex IonPac AS 18, 4µm
Anion self-regenerating suppressor	Dionex AERS 500, 2mm
Detector	Dionex Conductivity Detector DS6 cell
Eulent	2.25 mM $NaHCO_3$ / 2.25mM Na_2CO_3
AERS current	29 mA
Column temperature	30°C
Sample loop	5 µL
Flow rate	2.0 mL/min

Table 8.9: Calibration equations used to calculate the concentrations in spring water

Calibration		
Compound	**Equation**	**R^2**
Chloride	y = 1.5352x – 0.029	0.9998
Fluoride	y = 2.4111x + 0.0325	0.9999
Bromide	y = 1.6817x – 0.084	0.9997
Nitrate	y = 0.8553x – 0.087	0.9998
Nitrite	y = 0.9891x + 0.3095	1.0000

Table 8.10: Results from the analysis of spring water. Elevated levels of chloride correlate with the levels detected in sample 7, 18, 23 and 26.

Results			
Compound	**Concentration**	**LOD**	**LOQ**
Chloride	7.8 ± 0.1 mg/L	0.4 mg/L	1.2 mg/L
Fluoride	0.02 ± 0.09 mg/L	0.3 mg/L	0.9 mg/L
Bromide	1.3 ± 0.3 mg/L	0.8 mg/L	2.8 mg/L
Nitrate	0.7 ± 0.2 mg/L	0.6 mg/L	1.9 mg/L
Nitrite	1.39 ± 0.02 mg/L	0.05 mg/L	0.16 mg/L

8.2.3 ICP-OES

The analysis where performed using Varian Vista AX CCD simultaneous axial view ICP-OES equipped with cone spray nebulizer and Sturman Masters spray chamber. Conditions used for the analysis is presented in table 12 below.

Table 8.11: Instrumental conditions set for ICP-OES.

Instrumental conditions	
RF Power	1.05 kW
Plasma argon flow	15.0 L/min
Auxiliary argon flow	1.50 L/min
Nebulizer argon flow	0.90 L/min
Read time	1.00 s
Rinse time	20 s
Sample update delay	30 s
Pump rate	20 rpm

Table 8.12: Calibration equations form ICP-OES used to calculate the concentrations of cations in the samples. Due to the high number of samples the instrument was re-calibrated after every 15th sample to compensate for instrumental drift.

Calibration					
Element	**Equation**	**R^2**	**LOD**	**LOQ**	**Wavelength**
Aluminium	y = 487.26x + 48.385 (S1-11) y = 501.35x + 48.443 (S12-26)	0.9996 0.9996	0.03	0.09	237.312nm
Calcium	y = 36848x + 37128 (S1-11) y = 38047x + 42364 (S12-26)	0.9985 0.9967	0.14	0.45	422.673nm
Iron	y = 4709.8x + 124.53 (S1-11) y = 4835.5x + 137.91 (S12-26)	0.9999 0.9998	0.01	0.05	259.940nm
Potassium	y = 14793x + 10971 (S1-11) y = 15329x + 12148 (S12-26)	0.9992 0.9981	0.12	0.39	766.491nm
Magnesium	y = 12211x + 11701 (S1-11) y = 12546x + 12463 (S12-26)	0.9972 0.9962	0.13	0.45	285.213nm
Manganese	y = 41220x + 513.46 (S1-11) y = 42257x + 585.04 (S12-26)	0.9998 0.9998	0.008	0.03	257.610nm
Sodium	y = 65948x – 10315 (S1-11) y = 65560x + 19460 (S12-26)	0.9995 0.9971	0.08	0.27	588.995nm

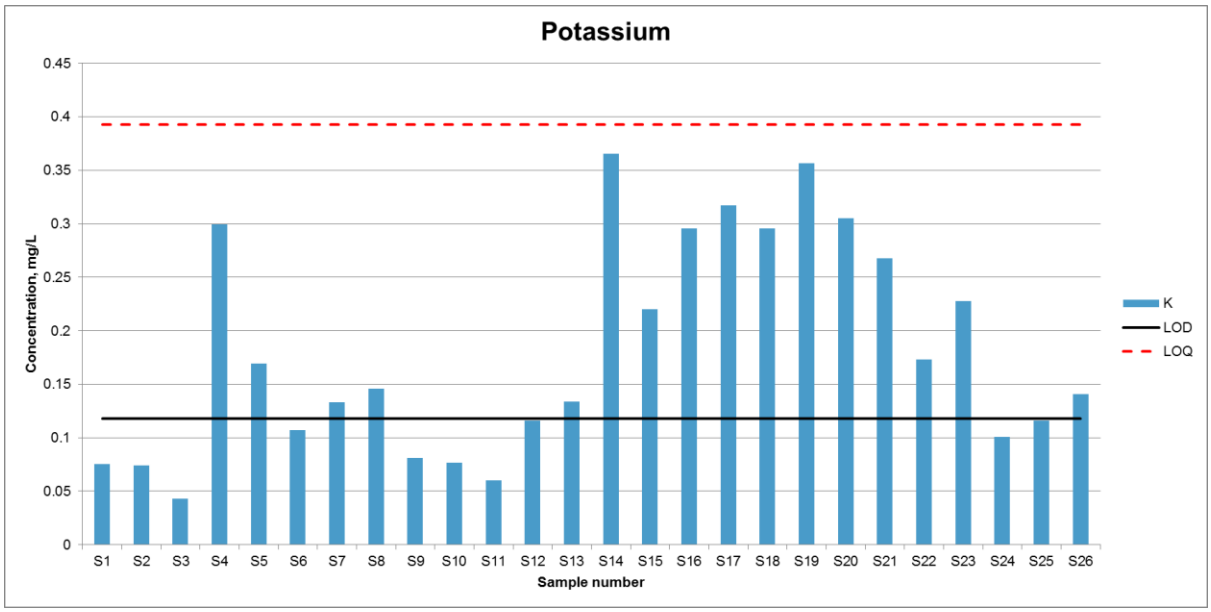

Figure 8.9: The concentration of potassium was below LOQ in all of the samples.

8.2.4 Test of spring water to verify source of cation contamination.

Table 8.13: An overview of the equations used to calculate the concentration of the respective elements in the samples.

Calibration			
Element	**Equation**	**R^2**	**Wavelength**
Aluminium	$y = 8.1x^2 + 1077.3x + 438.6$	0.9999	308.215nm
Calcium	$y = -11.4x^2 + 28594.2x + 10820.2$	0.9999	422.673nm
Iron	$y = 40.8x^2 + 3251.1x + 115.9$	0.9999	259.940nm
Potassium	$y = 1.3x^2 + 11683.6x + 2517.9$	0.9999	766.491nm
Magnesium	$y = -8.7x^2 + 9857.0x + 245.5$	0.9999	285.213nm
Manganese	$y = 520.6x^2 + 29059.2x + 260.0$	0.9999	257.610nm
Sodium	$y = 125.9x^2 + 42799.0 + 8759.6$	0.9999	589.592nm

Table 8.14: The concentration of Calcium (Ca) was much higher in spring water than in any of the samples. This could explain why the contaminated samples (Sample 7, 18, 23 and 26) measured higher concentration of Ca.

Results		
Element	**Concentration**	**SD**
Aluminium	-	-
Calcium	15.6 mg/L	0.2
Iron	-	-
Magnesium	0.378 mg/L	0.006
Sodium	1.34 mg/L	0.02
Potassium	-	-
Manganese	-	-

8.2.5 Total Organic Carbon

Table 8.15: An overview of the instrumental settings of the TOC-instrument during analysis.

Instrumental settings	
Maximum number of injections	4
Minimum number of injections	3
Number of washes before analysis	8
Flow rate	150 mL/min
Pressure	5 bar
Sparge time	1 min

Table 8.16: Calibration equation used to calculate the concentration of total organ carbon in the samples.

Calibration				
Compound	Equation	R^2	LOD	LOQ
Organic carbon	y = 3.3252x + 0.8053	0.99999	0.19 mg/L	0.65 mg/L

8.3 Structural characterization

8.3.1 UV-/ViS absorption spectra

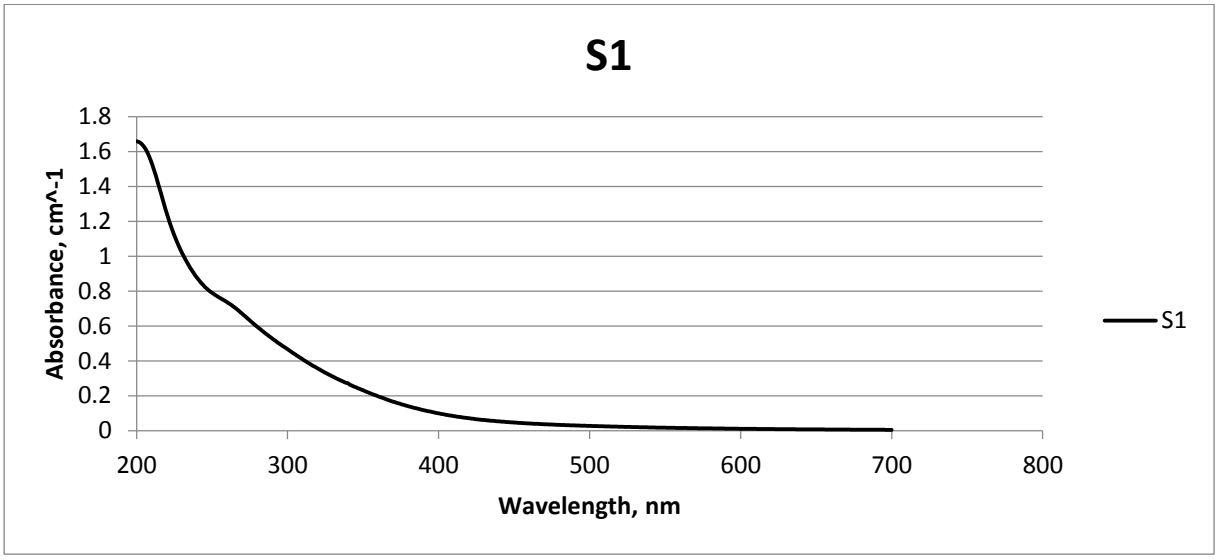

Figure 8.10: UV-/ViS absorbance spectra for Sample 1.

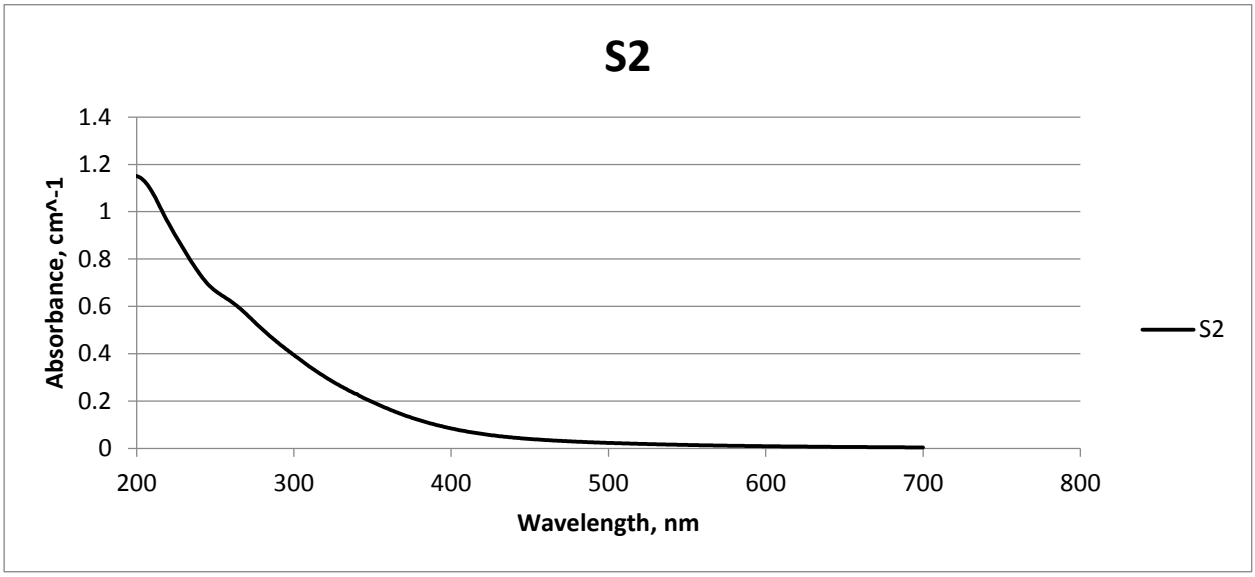

Figure 8.11: UV-/ViS absorbance spectra for Sample 2.

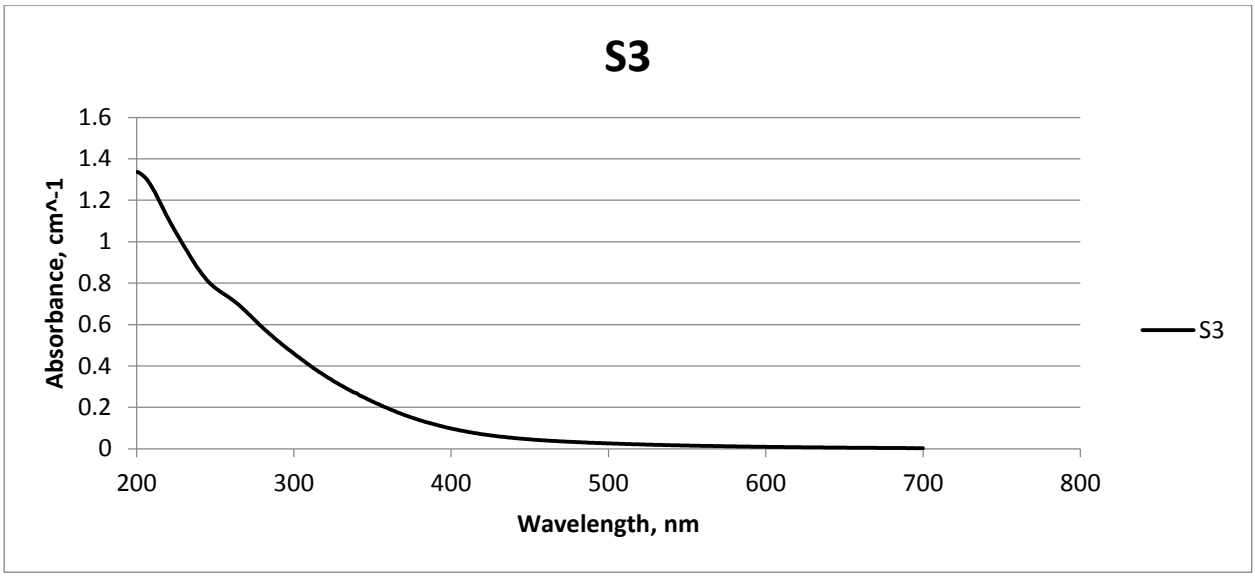

Figure 8.12: UV-/ViS absorbance spectra for Sample 3.

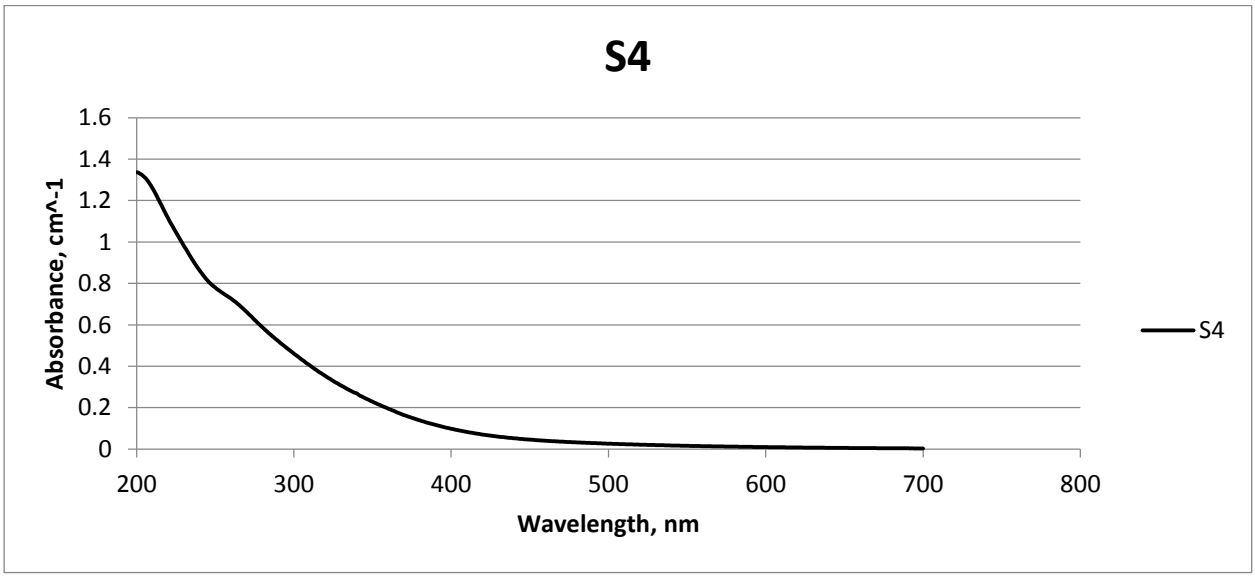

Figure 8.13: UV-/ViS absorbance spectra for Sample 4.

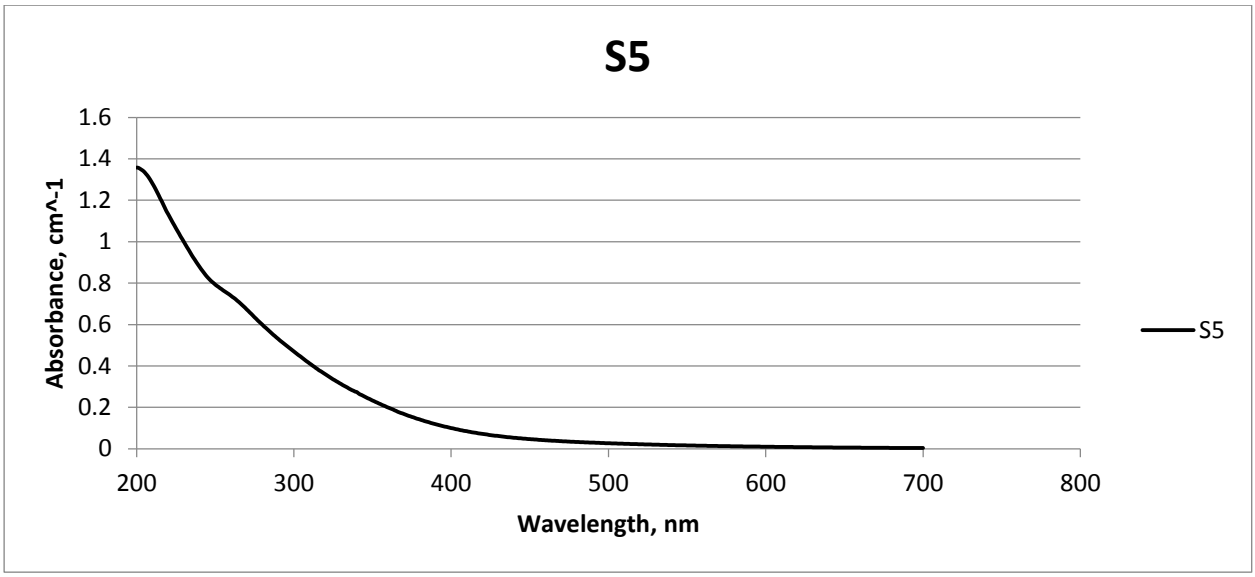

Figure 8.14: UV-/ViS absorbance spectra for Sample 5.

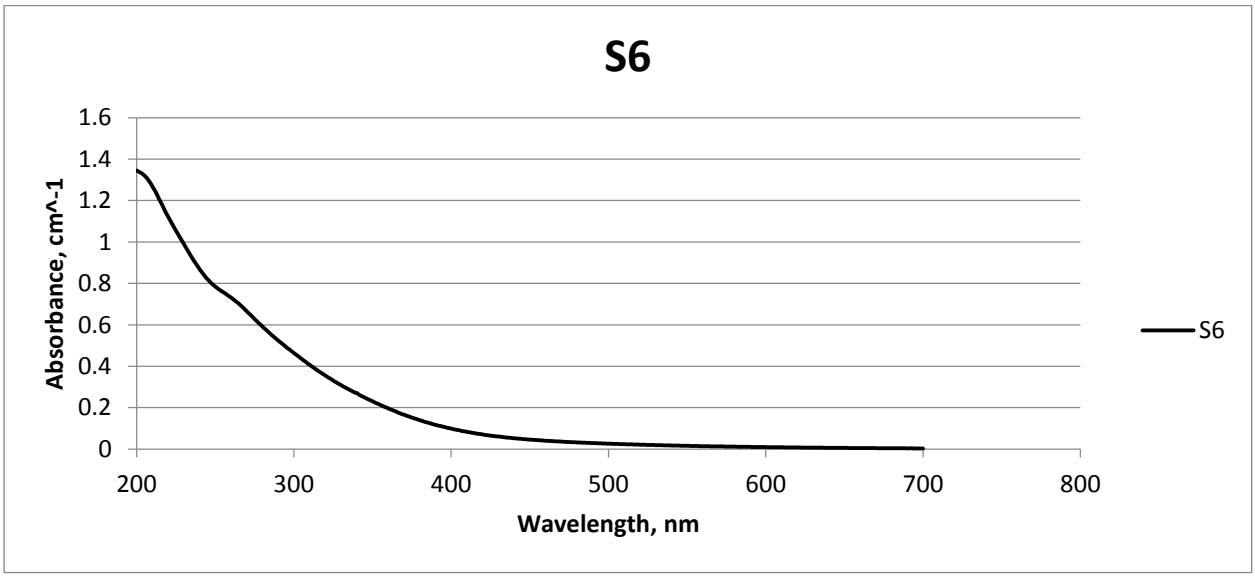

Figure 8.15: UV-/ViS absorbance spectra for Sample 6.

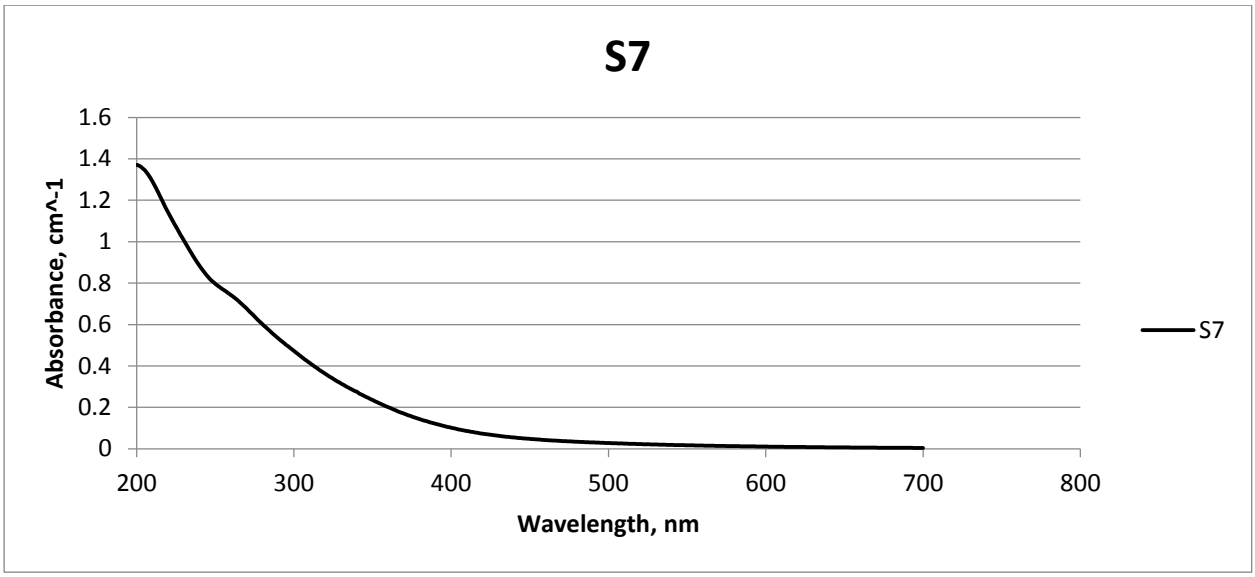

Figure 8.16: UV-/ViS absorbance spectra for Sample 7.

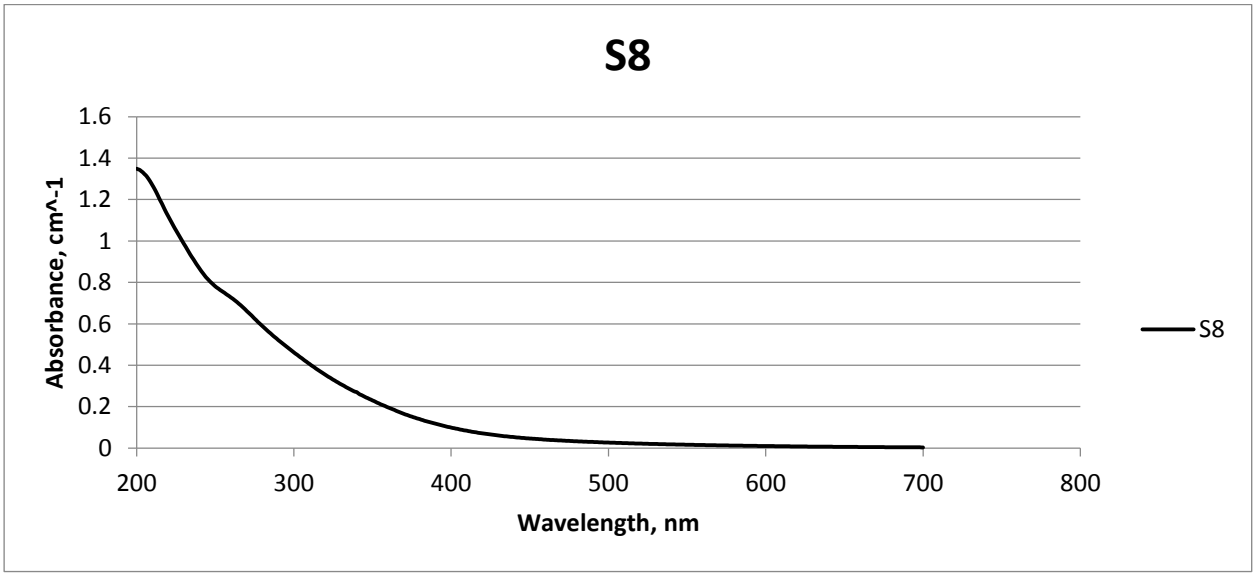

Figure 8.17: UV-/ViS absorbance spectra for Sample 8.

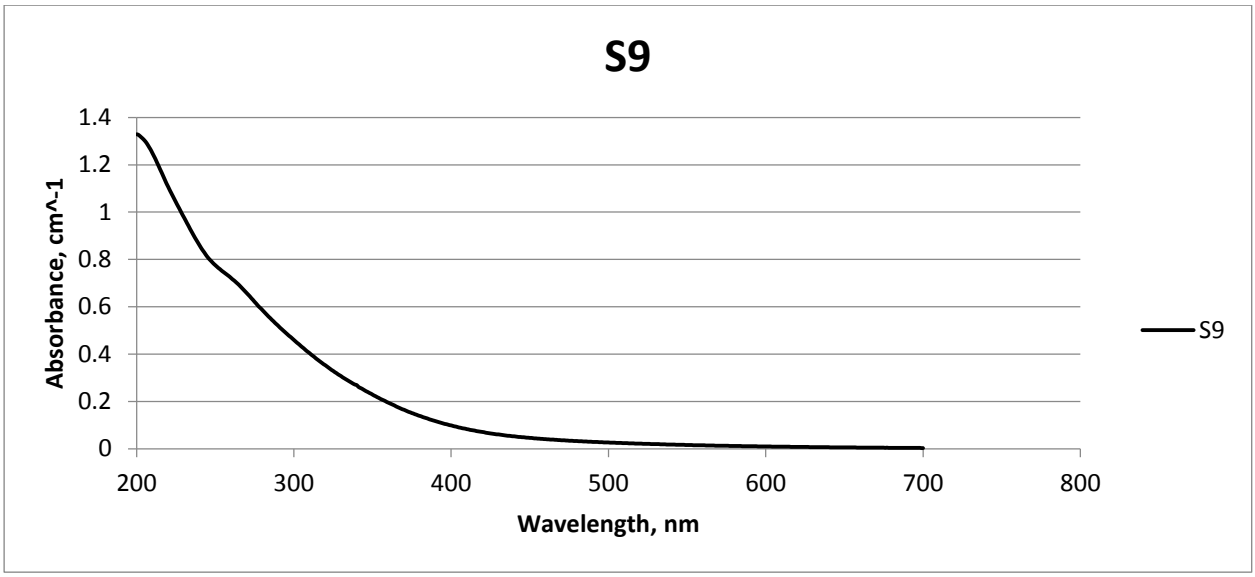

Figure 8.18: UV-/ViS absorbance spectra for Sample 9.

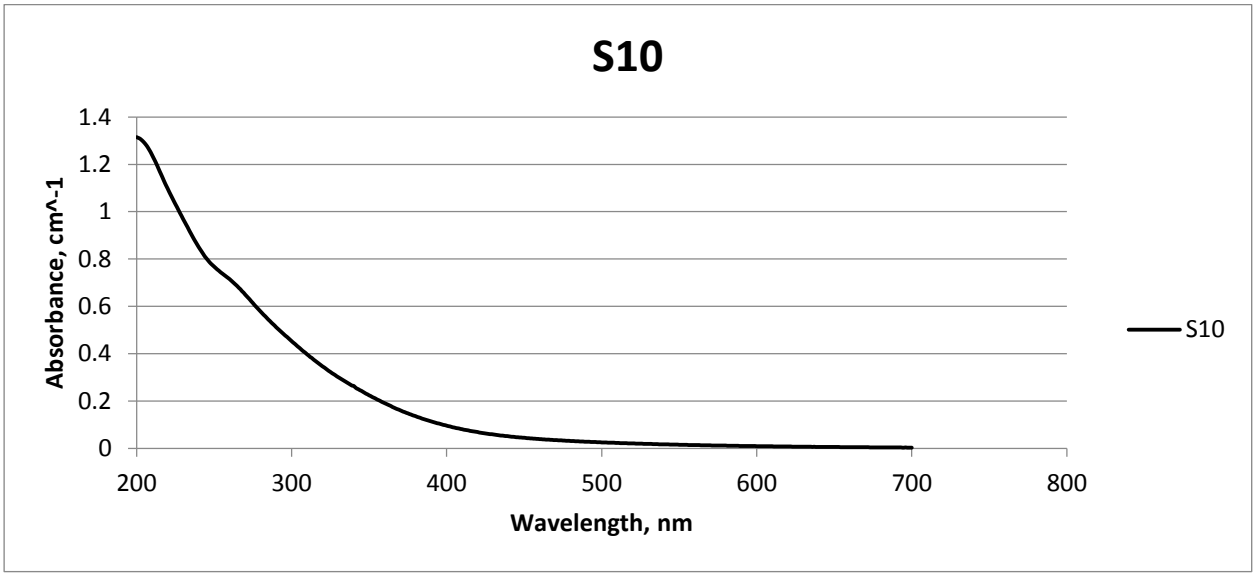

Figure 8.19: UV-/ViS absorbance spectra for Sample 10.

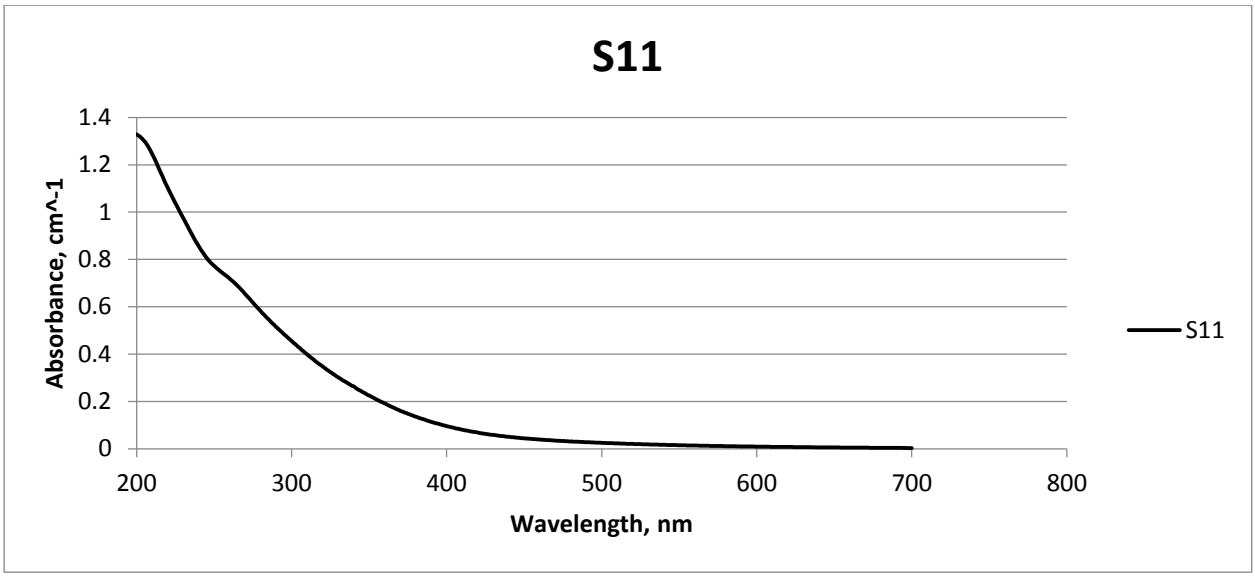

Figure 8.20: UV-/ViS absorbance spectra for Sample 11.

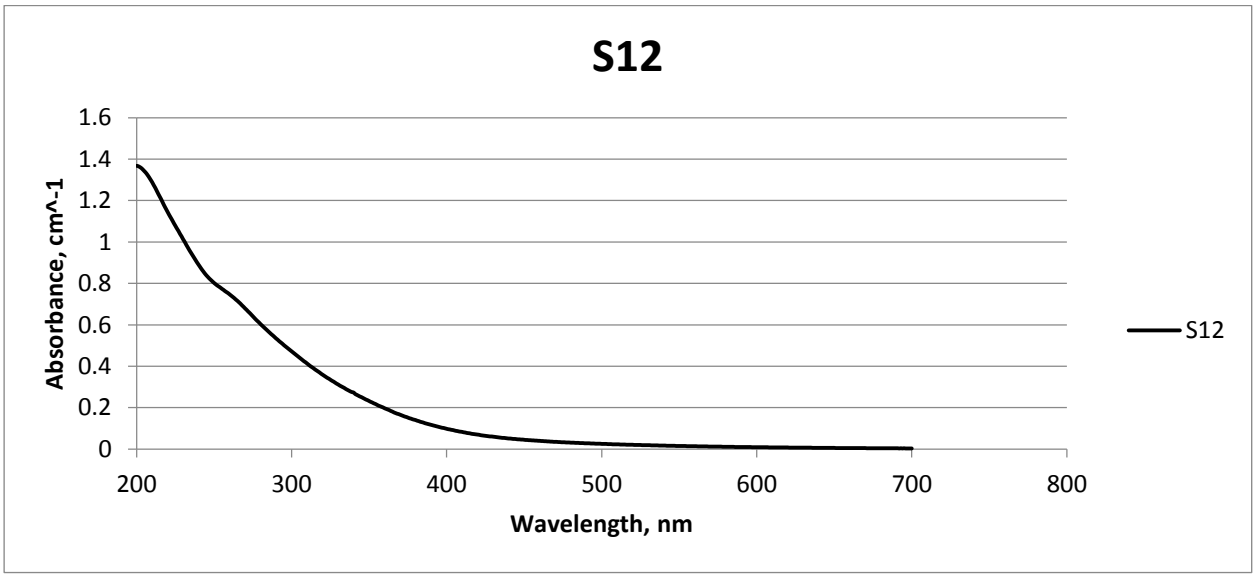

Figure 8.21: UV-/ViS absorbance spectra for Sample 12.

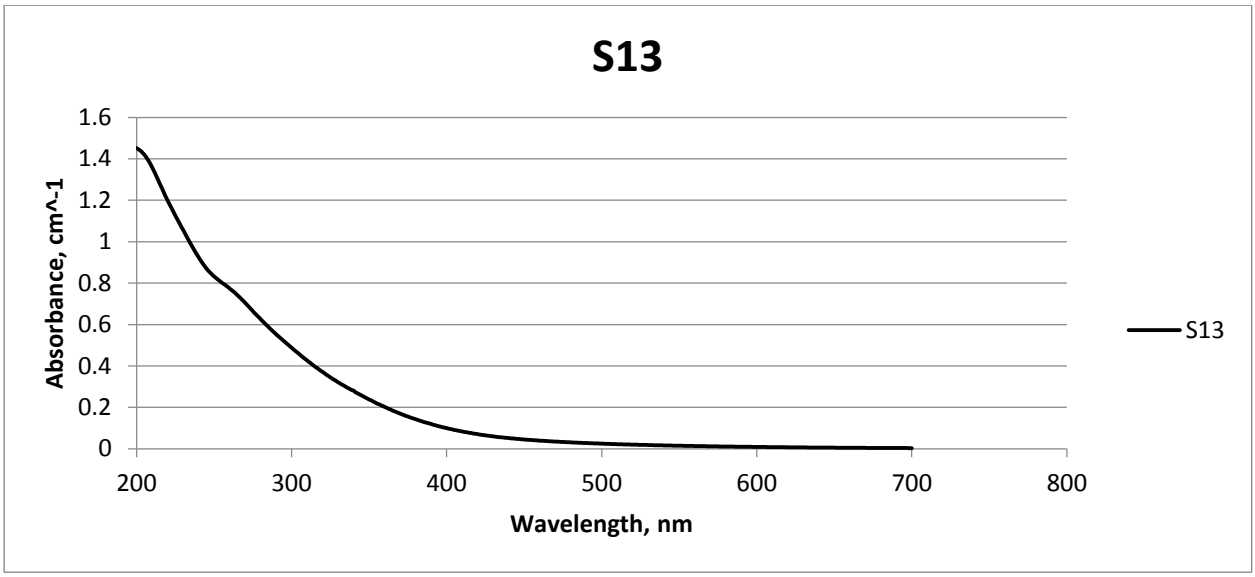

Figure 8.22: UV-/ViS absorbance spectra for Sample 13.

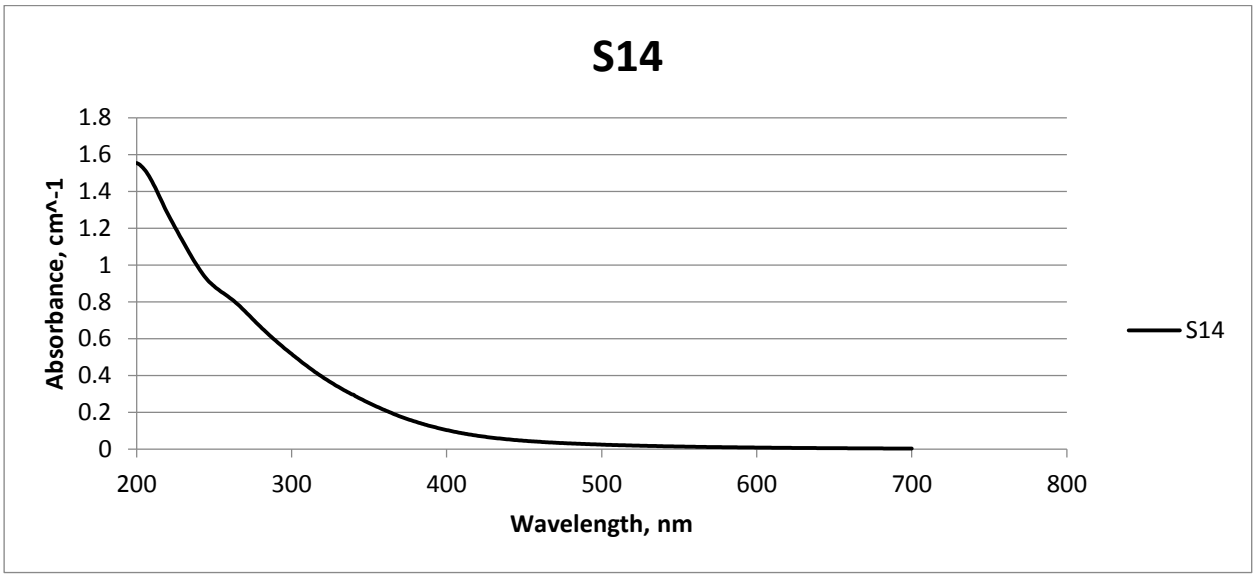

Figure 8.23: UV-/ViS absorbance spectra for Sample 14.

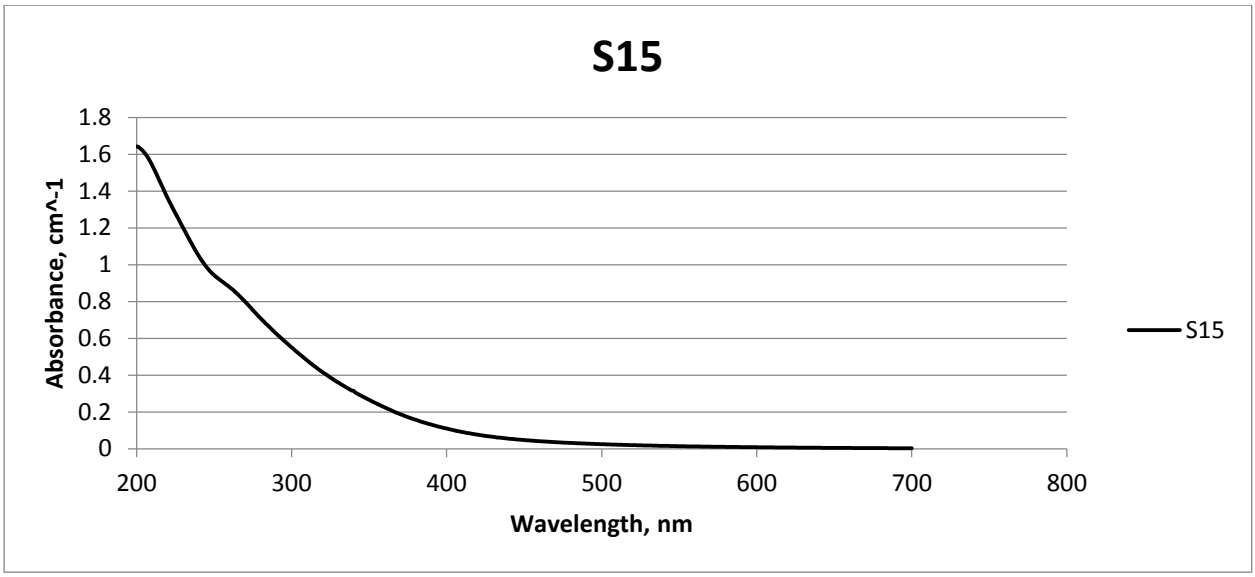

Figure 8.24: UV-/ViS absorbance spectra for Sample 15.

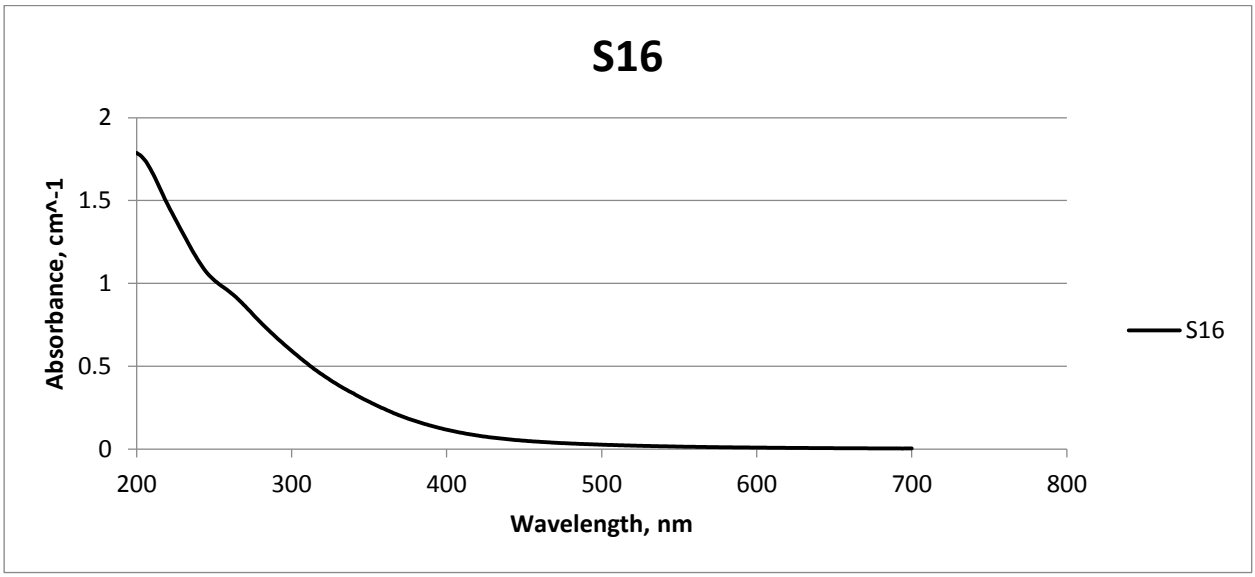

Figure 8.25: UV-/ViS absorbance spectra for Sample 16.

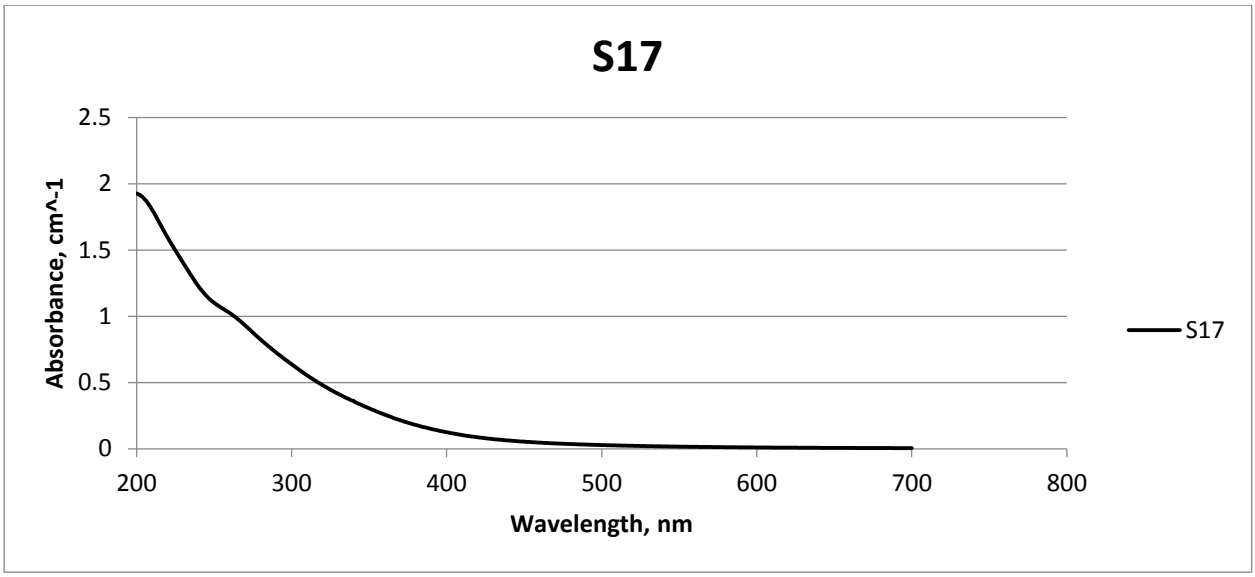

Figure 8.26: UV-/ViS absorbance spectra for Sample 17.

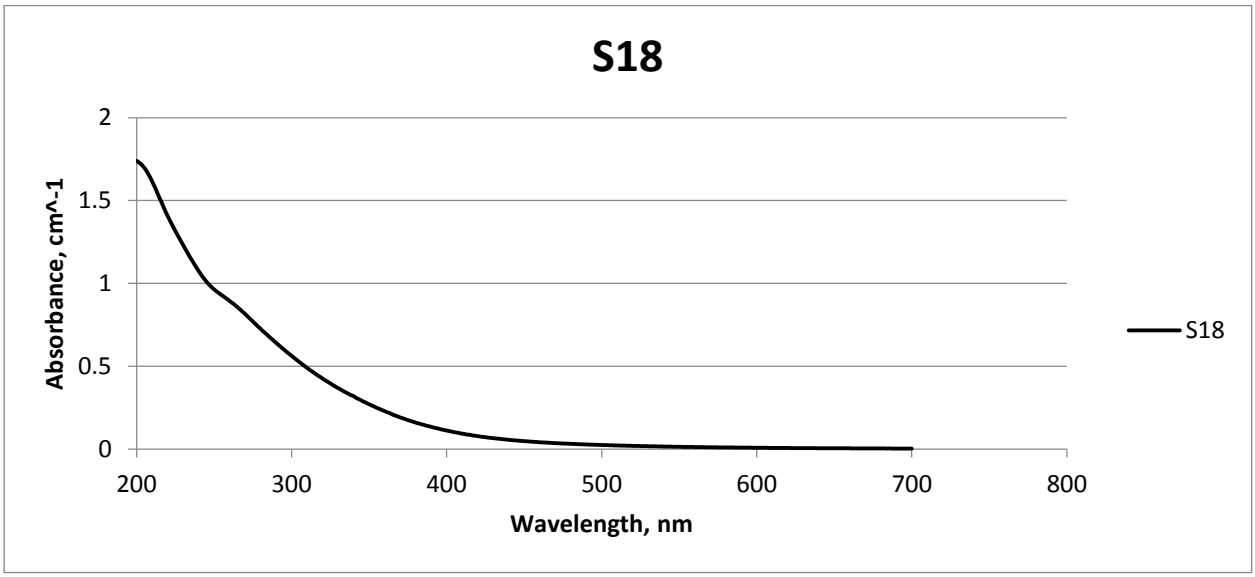

Figure 8.27: UV-/ViS absorbance spectra for Sample 18.

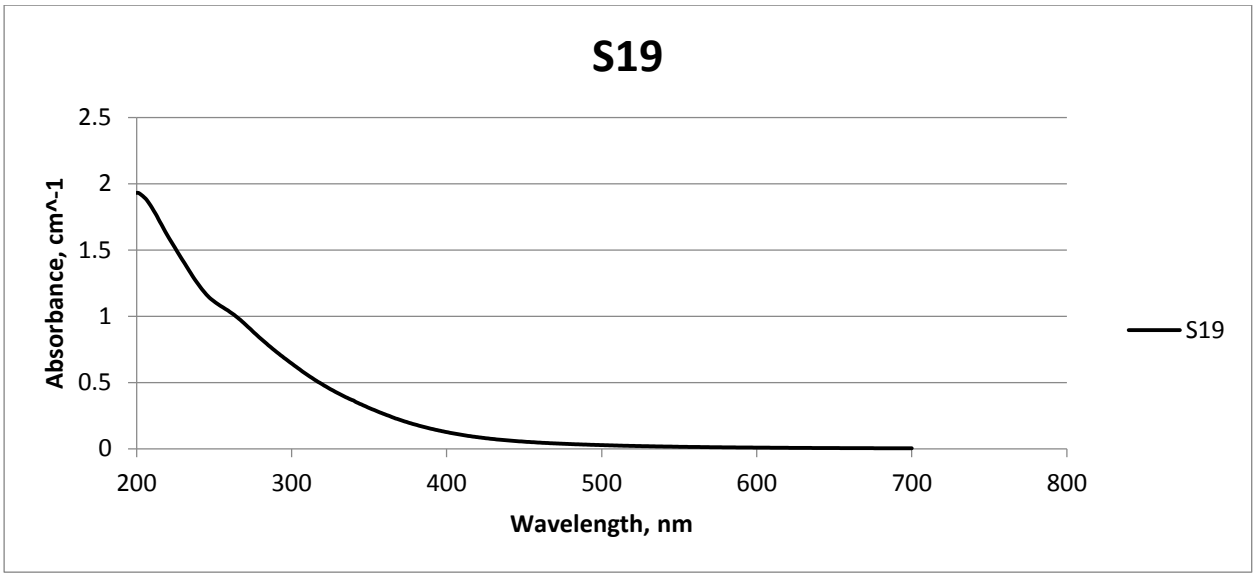

Figure 8.28: UV-/ViS absorbance spectra for Sample 19.

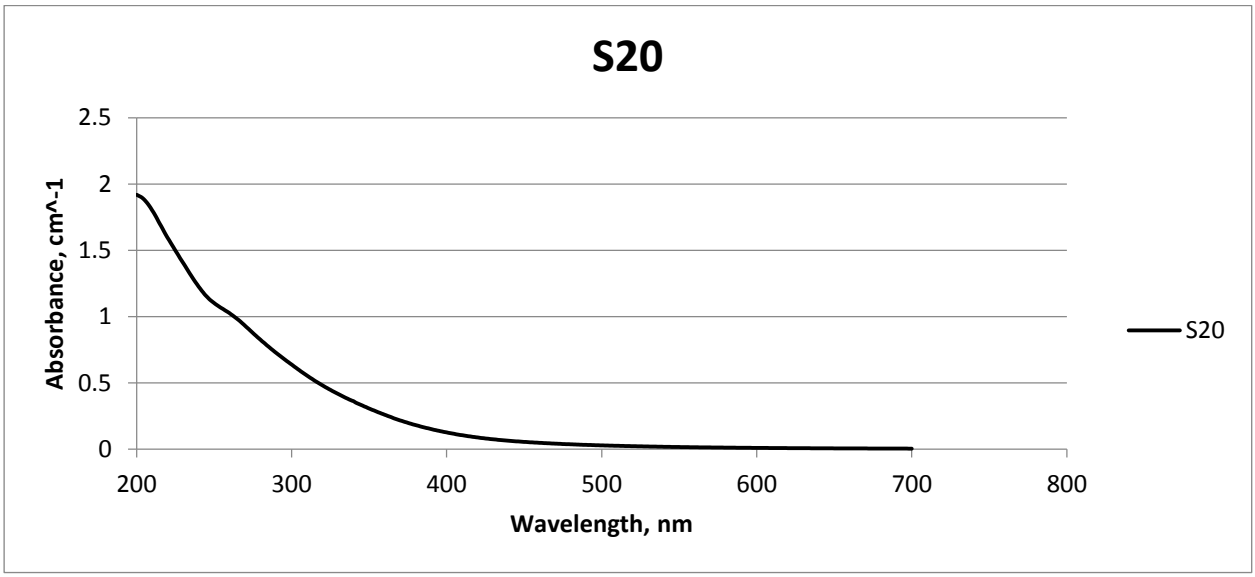

Figure 8.29: UV-/ViS absorbance spectra for Sample 20.

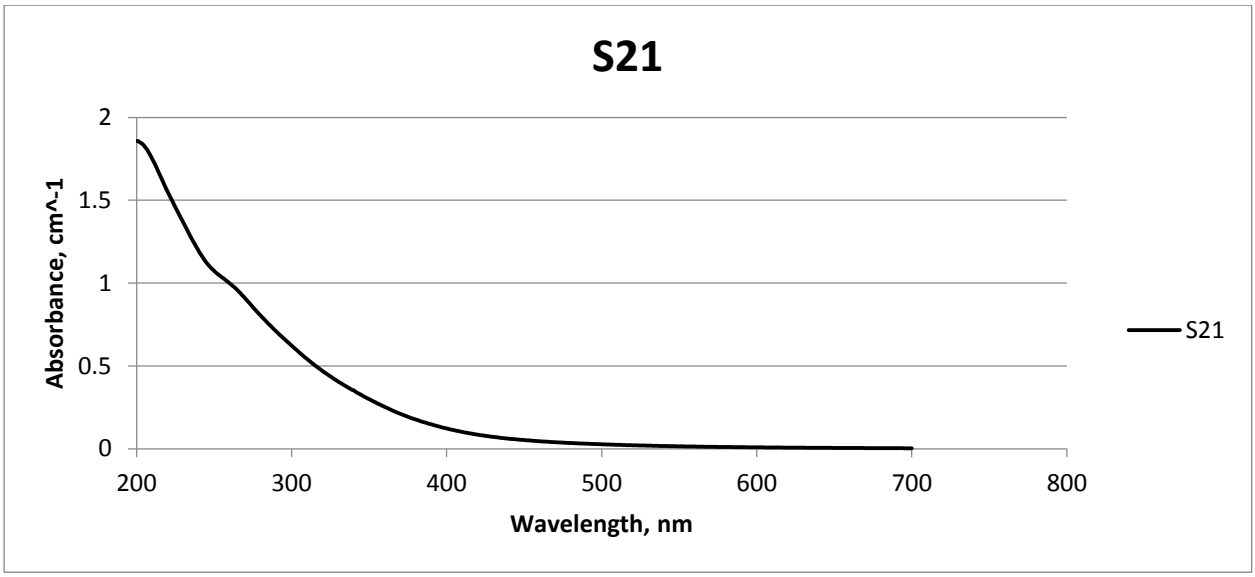

Figure 8.30: UV-/ViS absorbance spectra for Sample 21.

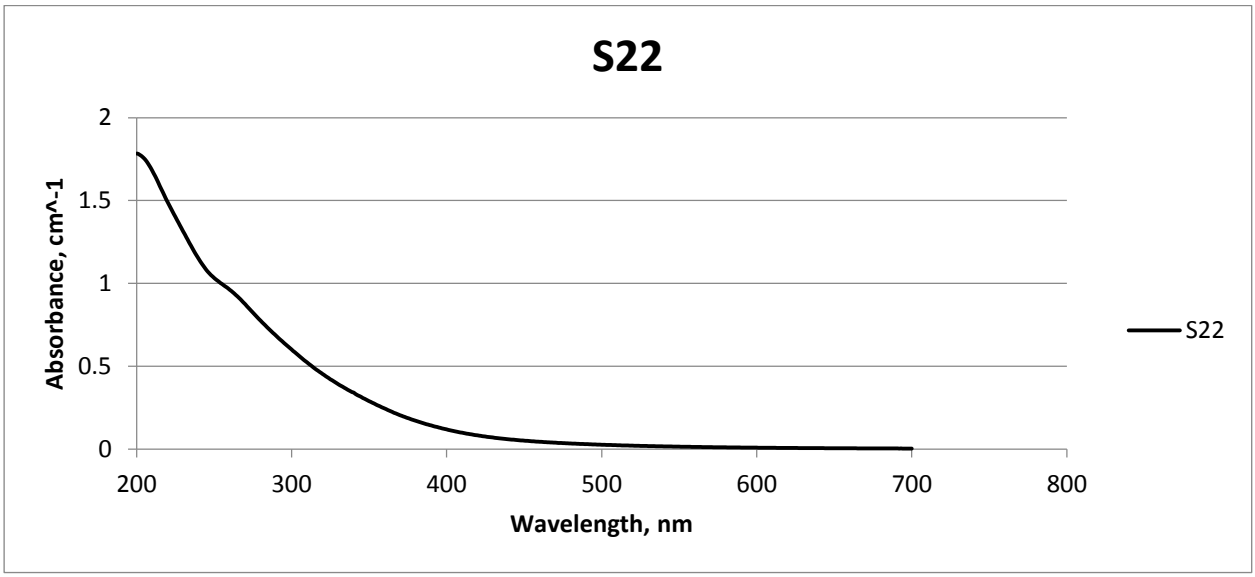

Figure 8.31: UV-/ViS absorbance spectra for Sample 22.

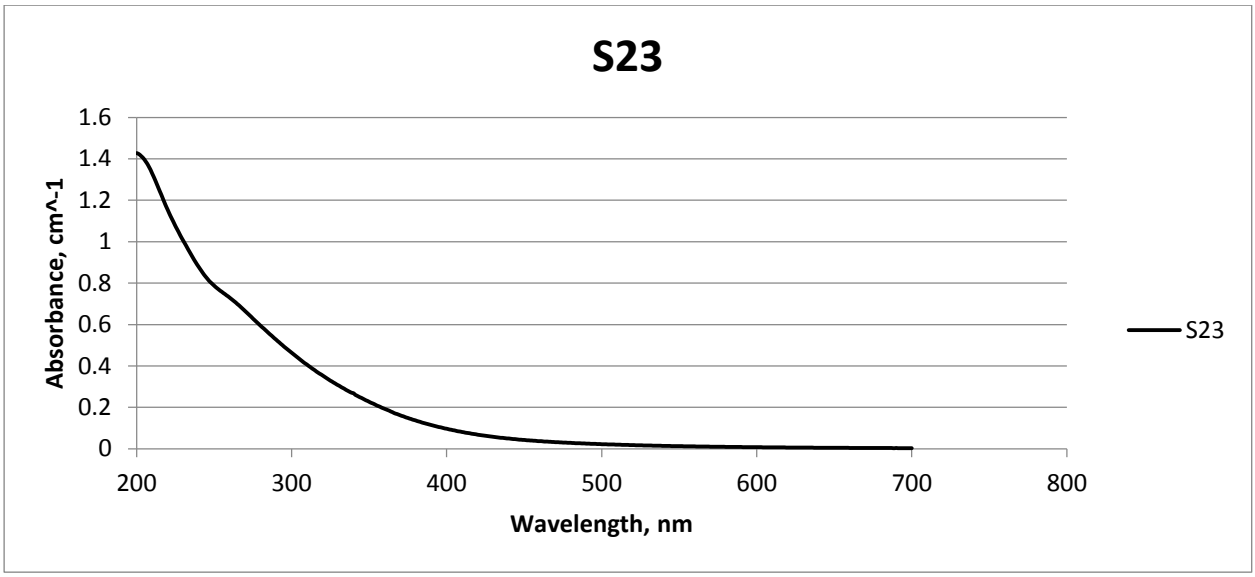

Figure 8.32: UV-/ViS absorbance spectra for Sample 23.

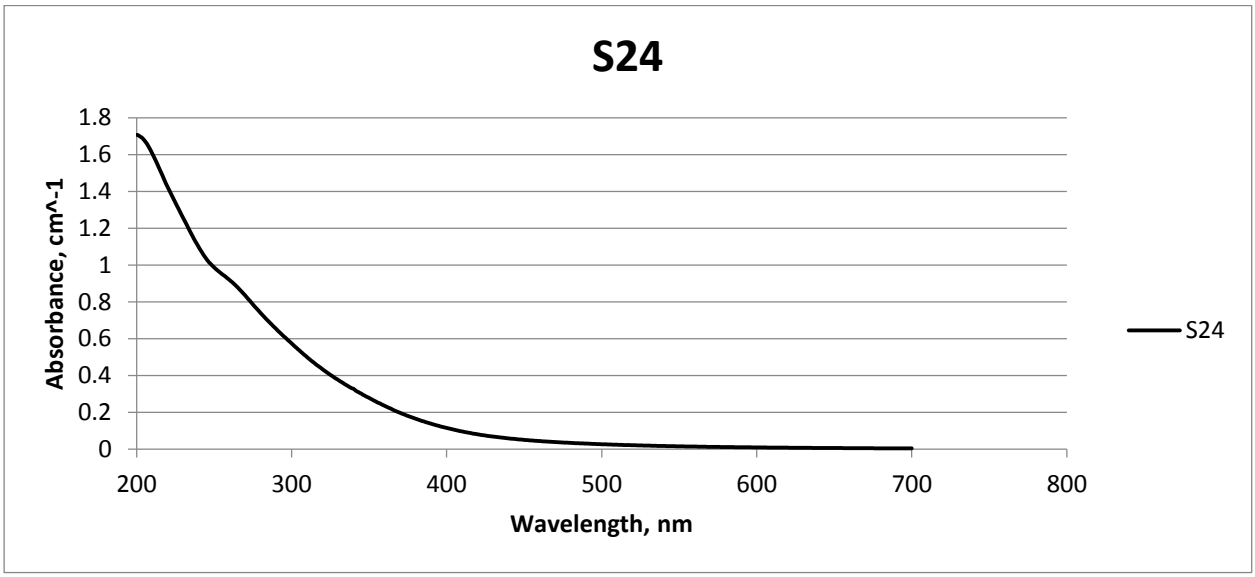

Figure 8.33: UV-/ViS absorbance spectra for Sample 24.

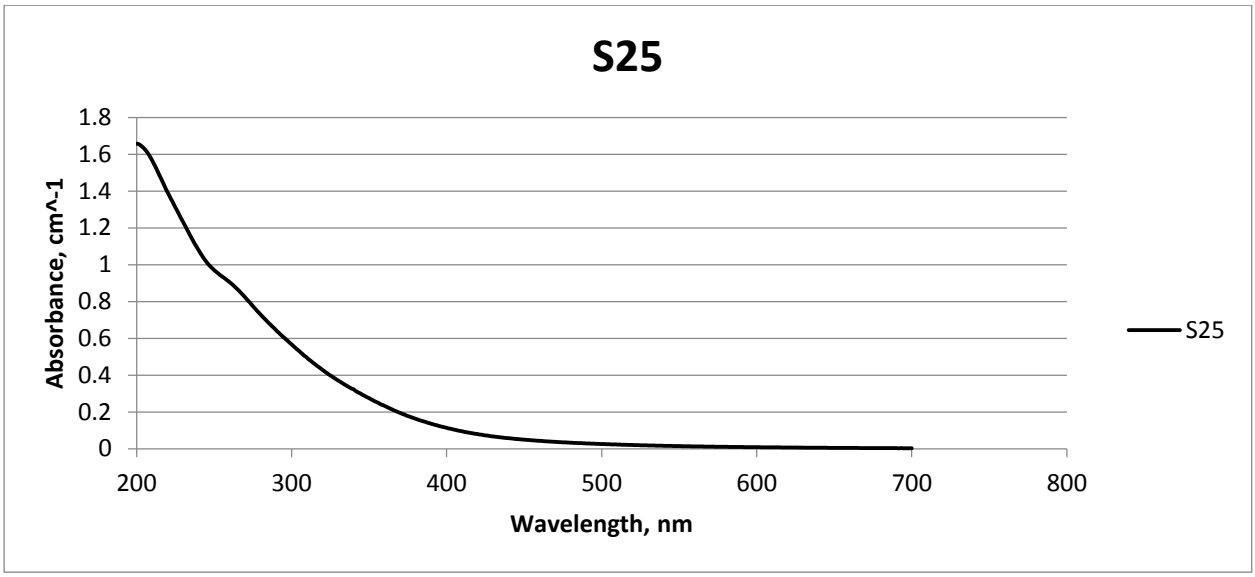

Figure 8.34: UV-/ViS absorbance spectra for Sample 25.

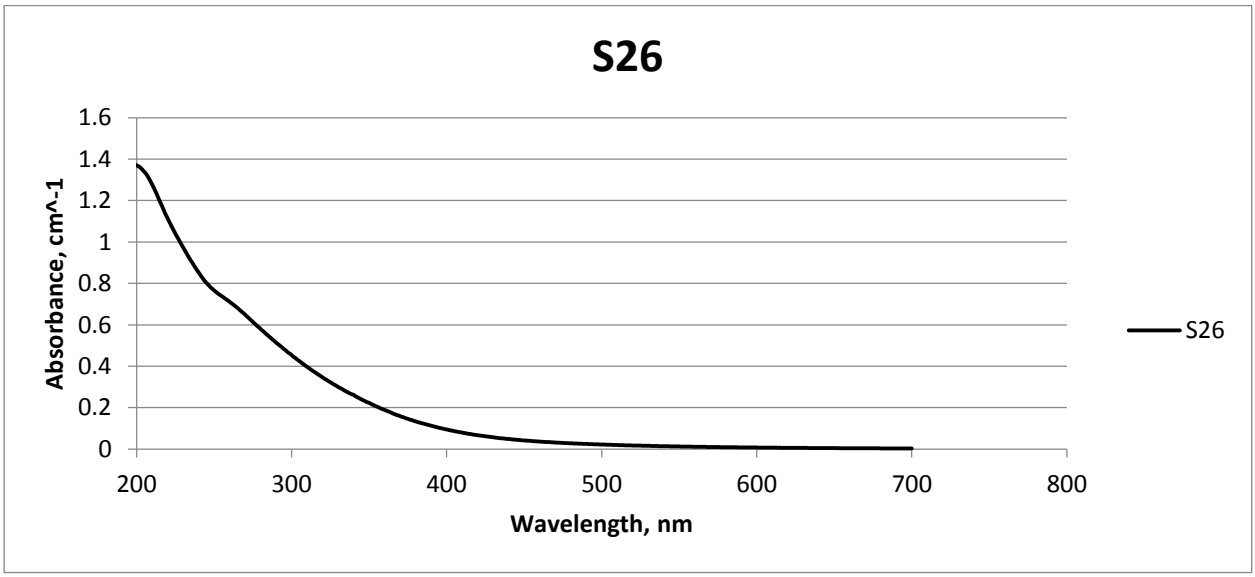

Figure 8.35: UV-/ViS absorbance spectra for Sample 26.

8.3.2 Fluorescence. Instrument settings and EEM spectra

Table: Instrument parameters for the fluorescence measurements.

Instrument parameters	
Instrument	Cary Eclipse Fluorescence Spectrophotometer
Producer	Agilent Technologies
Instrument settings	
PMT voltage	Medium
3D-mode	ON
Cuvette	1 cm quartz
Scan mode, Excitation	
Range, wavelength	240-450 nm
Scan interval	5 nm
Scan slit	5 nm
Scan mode, Emission	
Range, wavelength	250-600 nm
Interval	2 nm
Scan slit	5 nm
Scan time	0.0125 s
Scan speed	9600 nm/min.

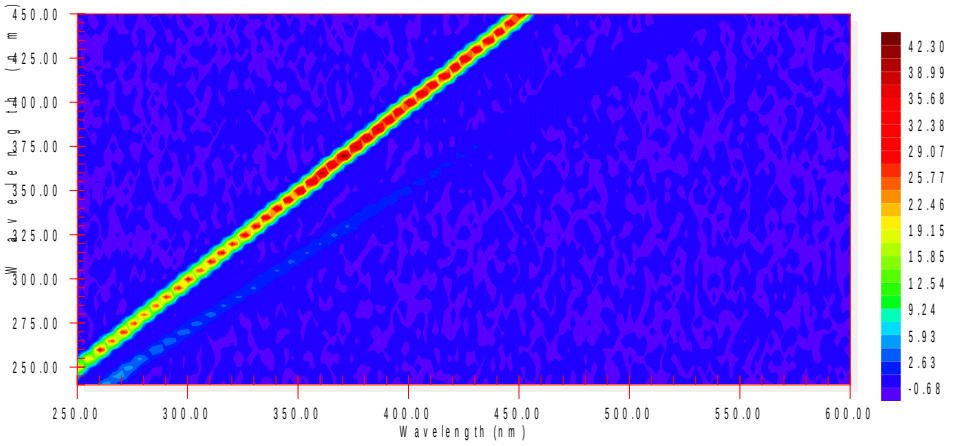

Figure 8.36: EEM-spectra of a blank sample.

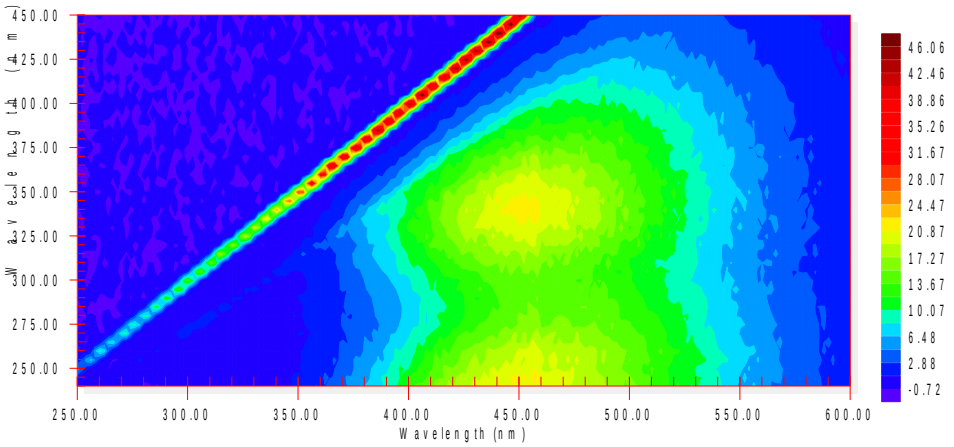

Figure 8.37: EEM-spectra of S1.

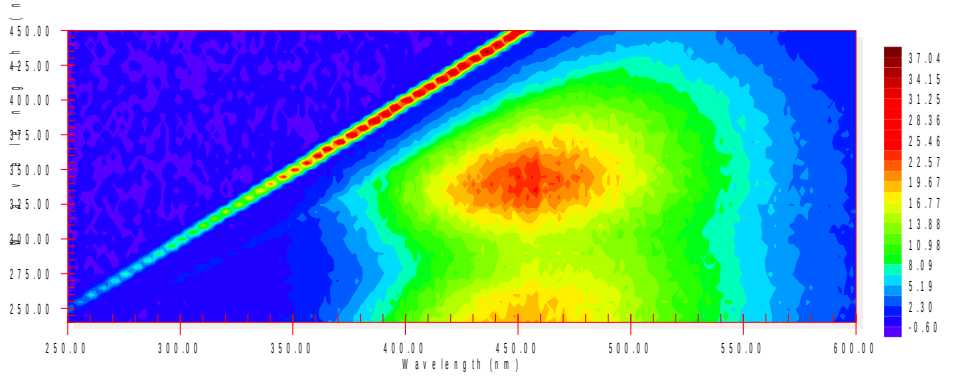

Figure 8.38: EEM-spectra of S2.

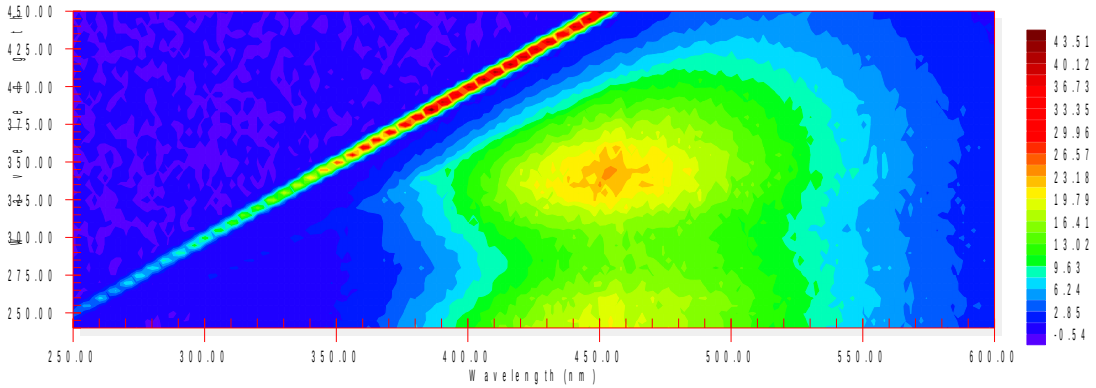

Figure 8.39: EEM-spectra of S3.

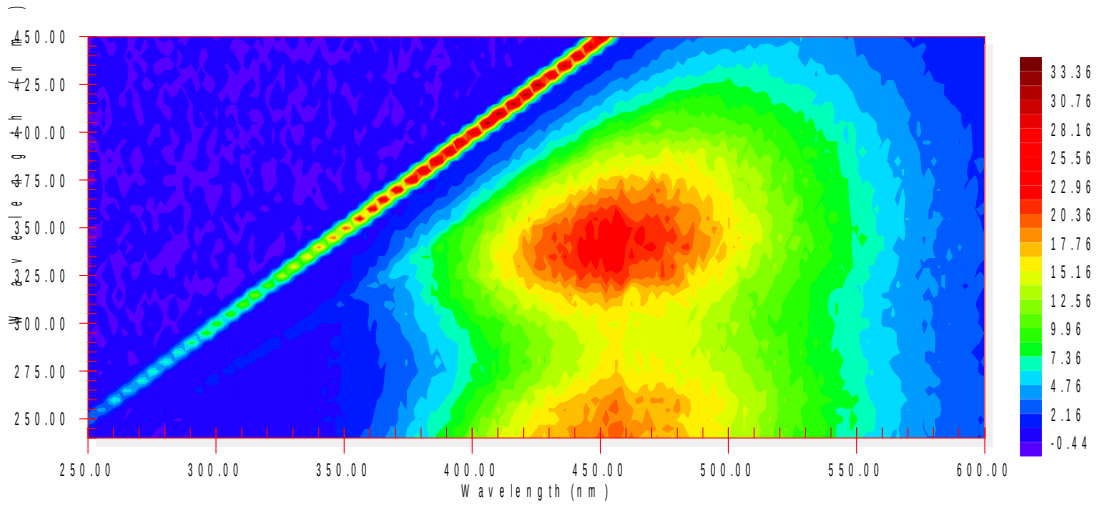

Figure 8.40: EEM-spectra of S4.

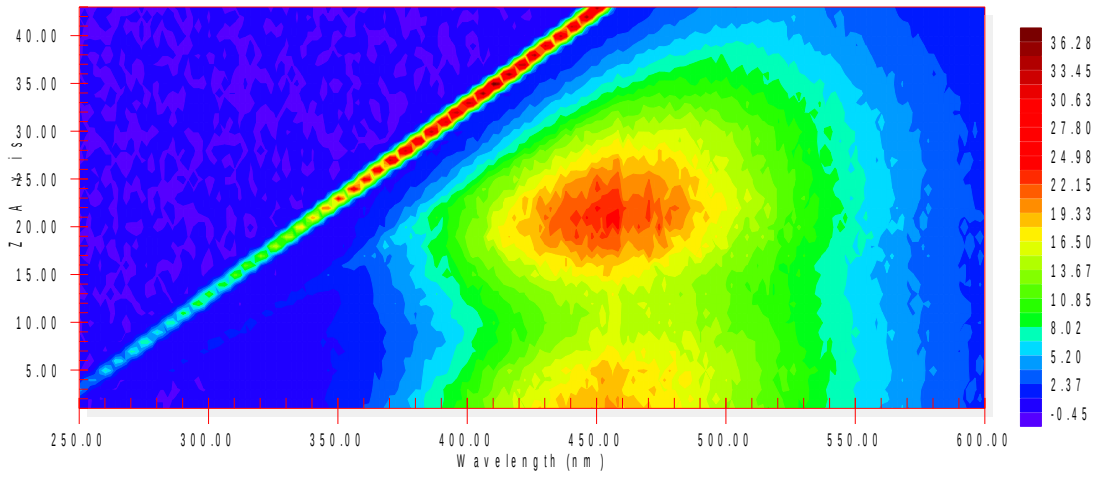

Figure 8.41: EEM-spectra of S5.

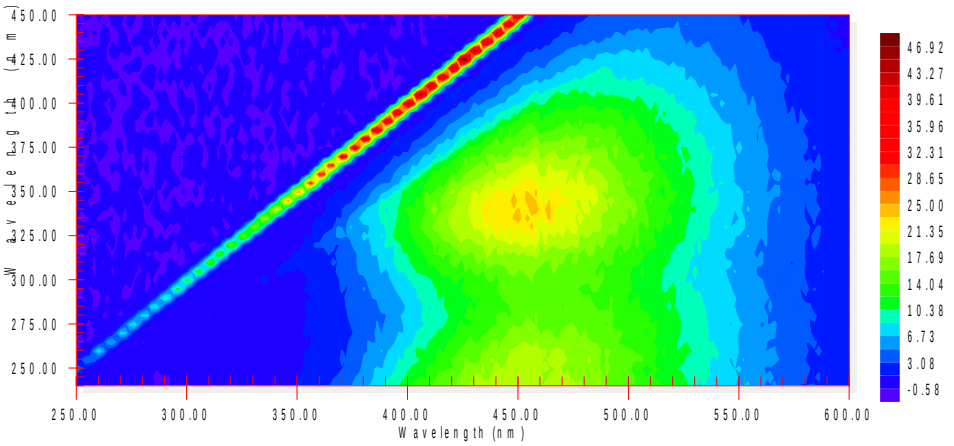

Figure 8.42: EEM-spectra of S6

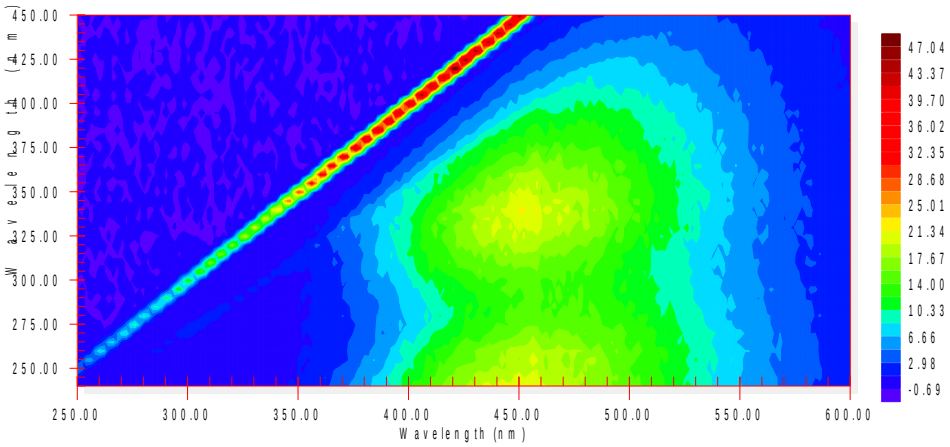

Figure 8.43: EEM-spectra of S7.

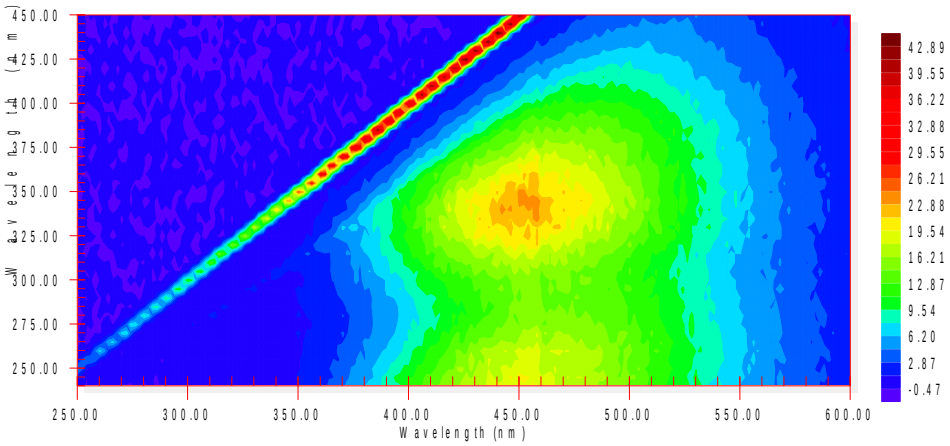

Figure 8.44: EEM-spectra of S8

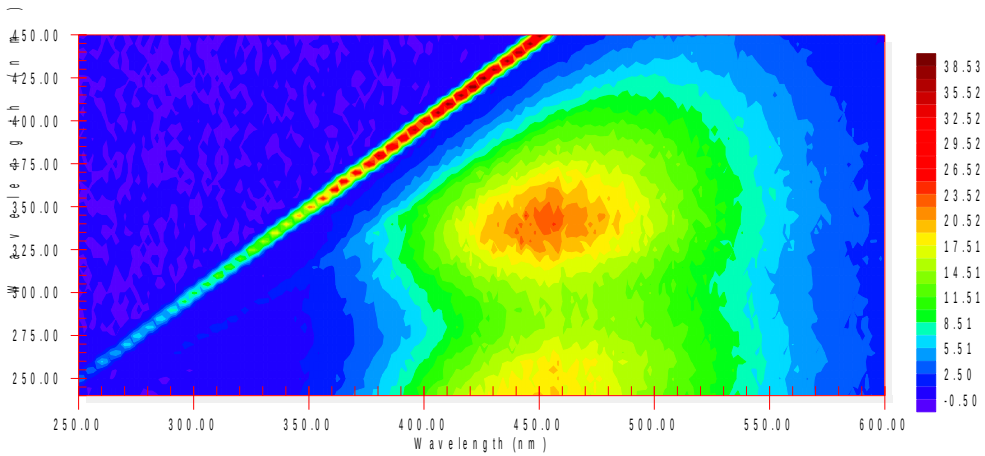

Figure 8.45: EEM-spectra of S9.

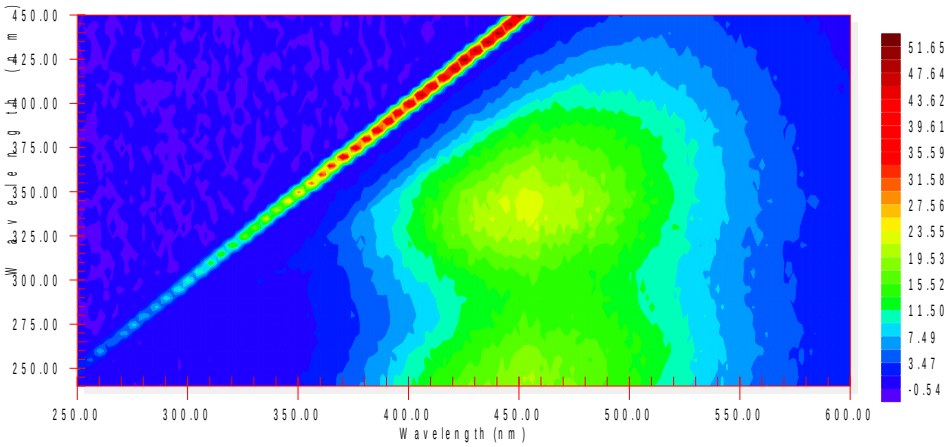

Figure 8.46: EEM-spectra of S10.

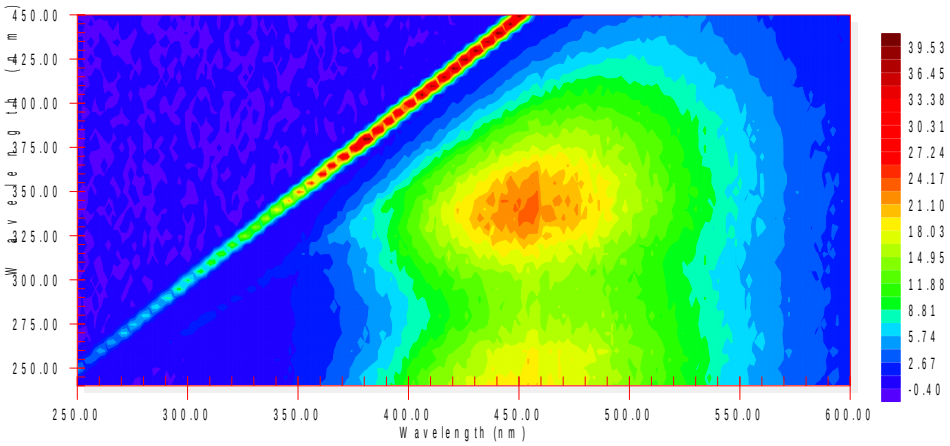

Figure 8.47: EEM-spectra of S11.

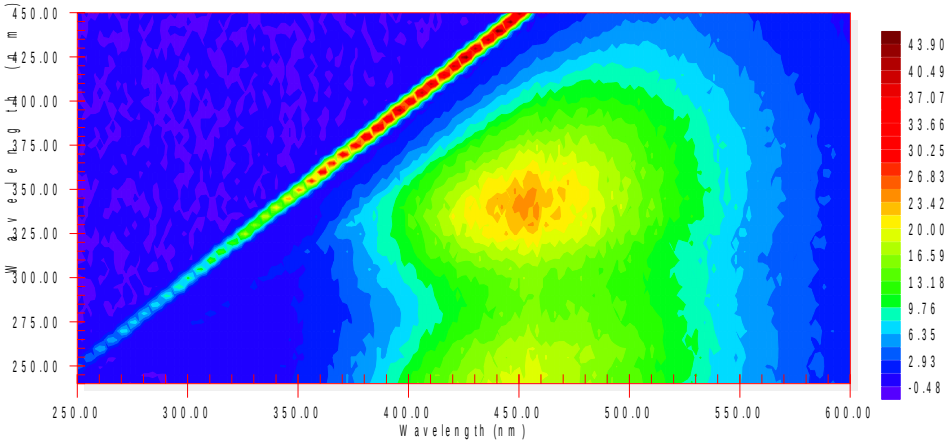

Figure 8.48: EEM-spectra of S12.

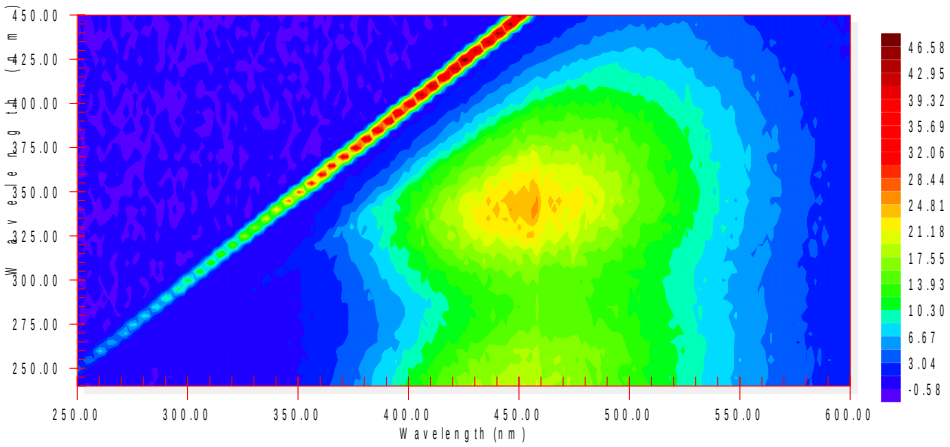

Figure 8.49: EEM-spectra of S13.

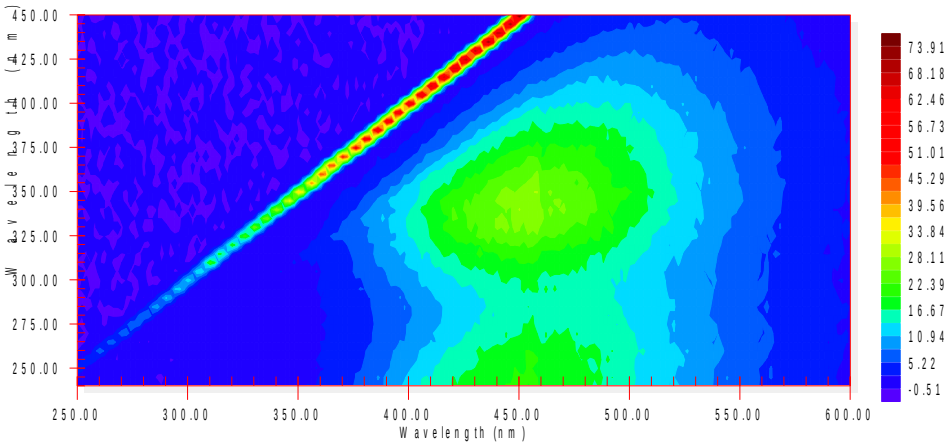

Figure 8.50: EEM-spectra of S14.

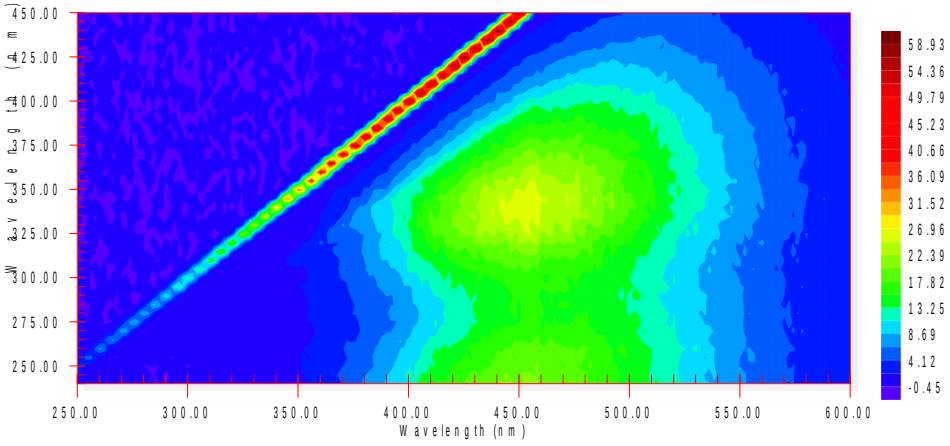

Figure 8.51: EEM-spectra of S15.

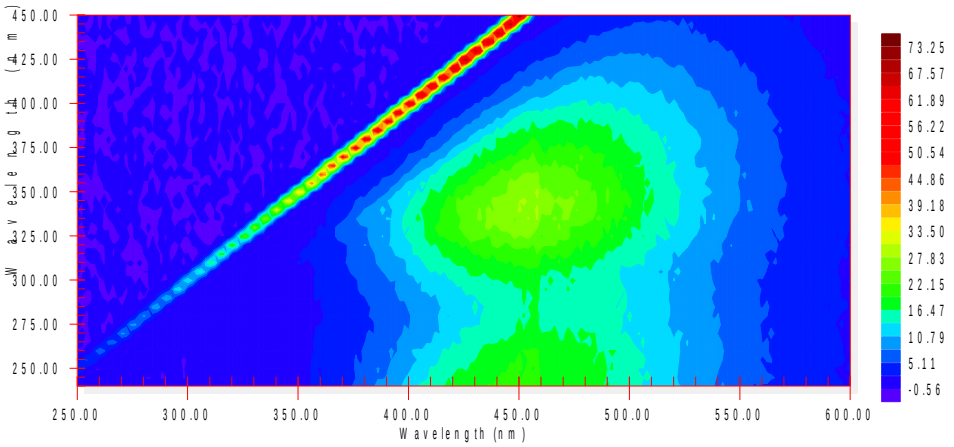

Figure 8.52: EEM-spectra of S16.

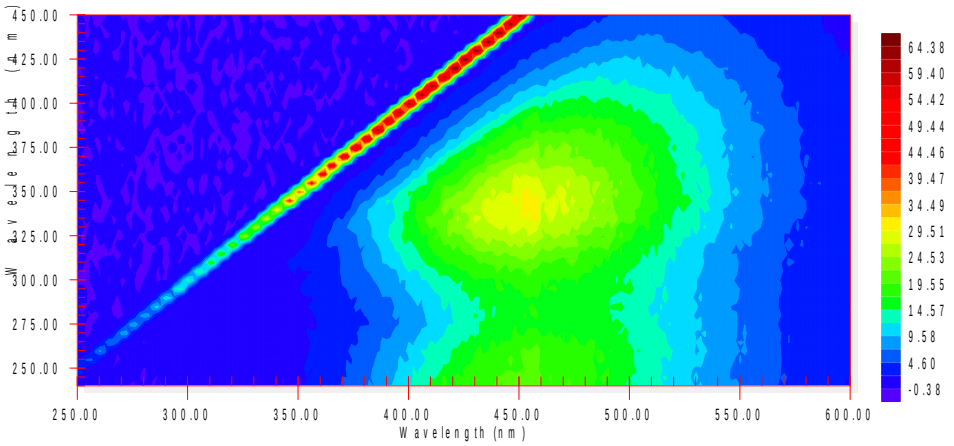

Figure 8.53: EEM-spectra of S17.

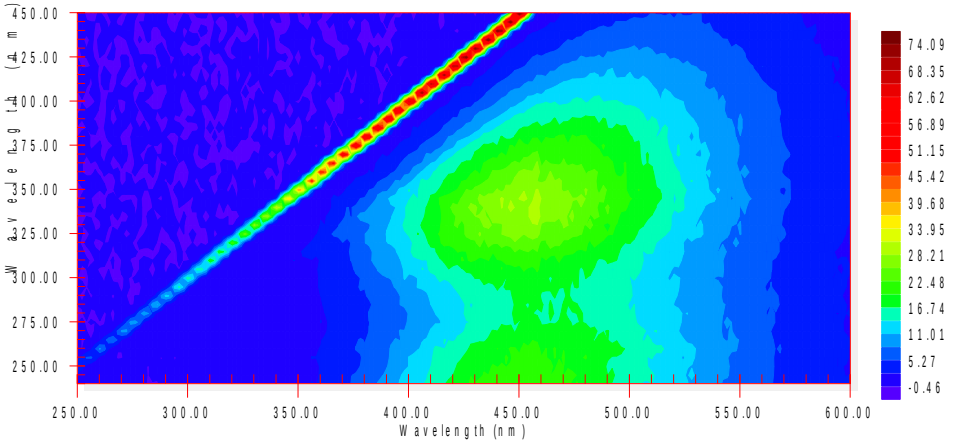

Figure 8.54: EEM-spectra of S18.

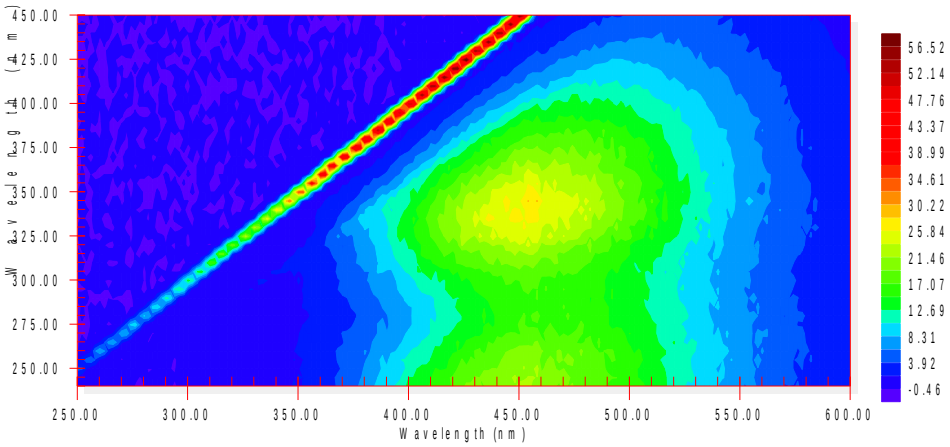

Figure 8.55: EEM-spectra of S19.

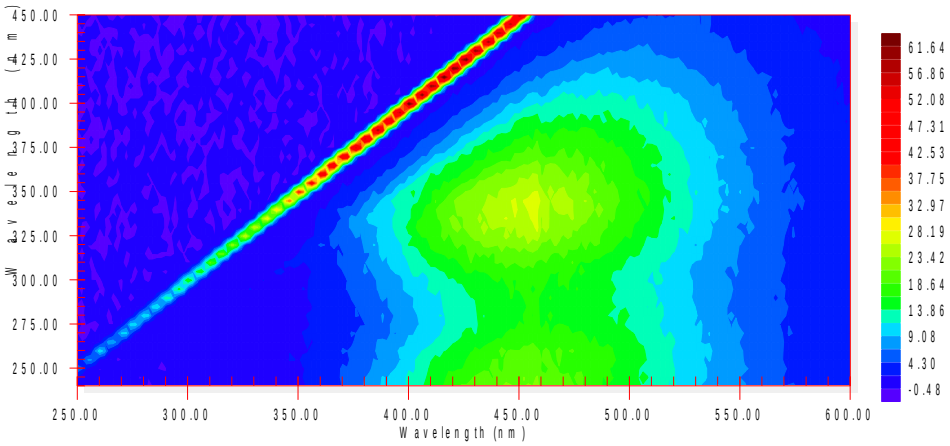

Figure 8.56: EEM-spectra of S20.

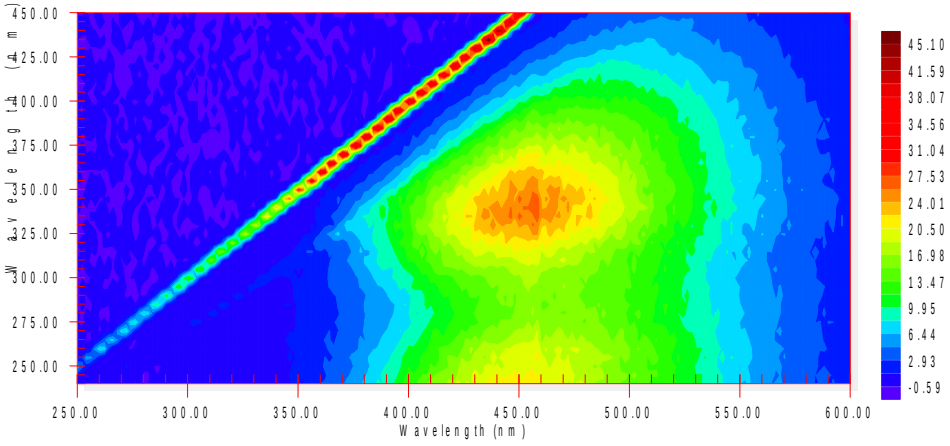

Figure 8.57: EEM-spectra of S21.

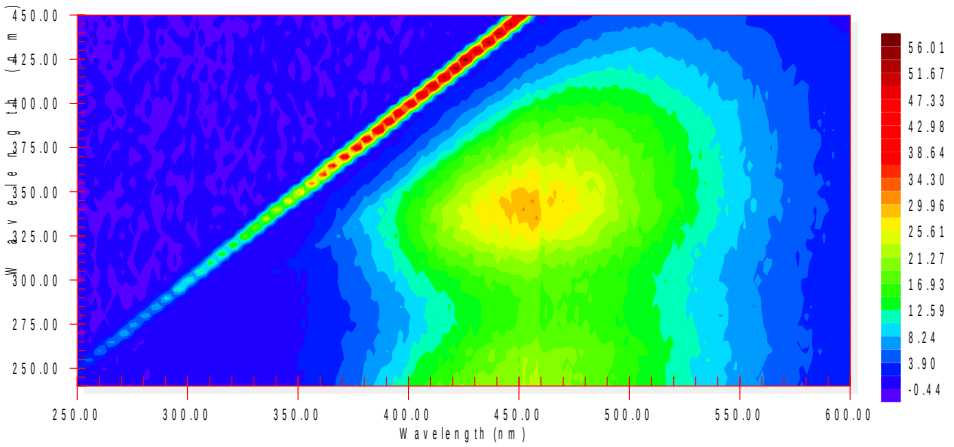

Figure 8.58: EEM-spectra of S22.

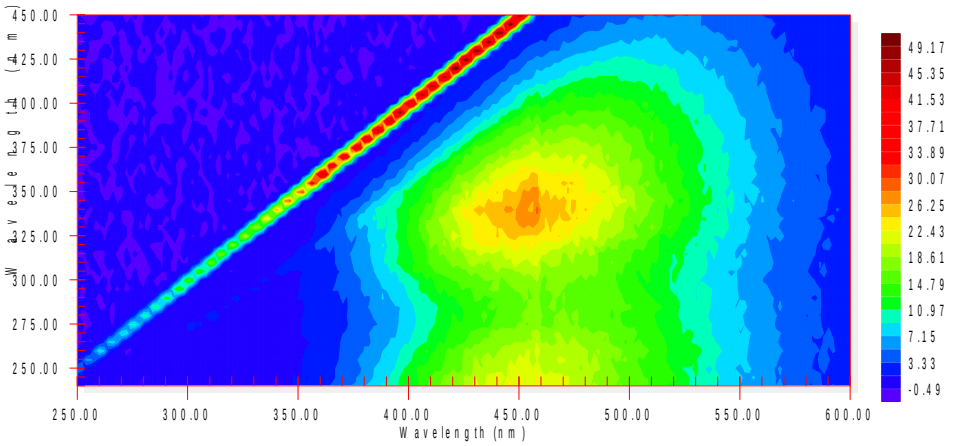

Figure 8.59: EEM-spectra of S23.

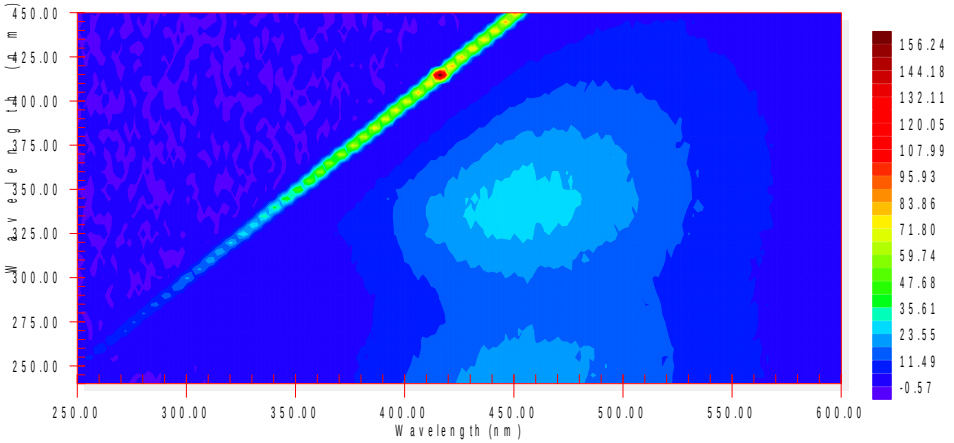

Figure 8.60: EEM-spectra of S24.

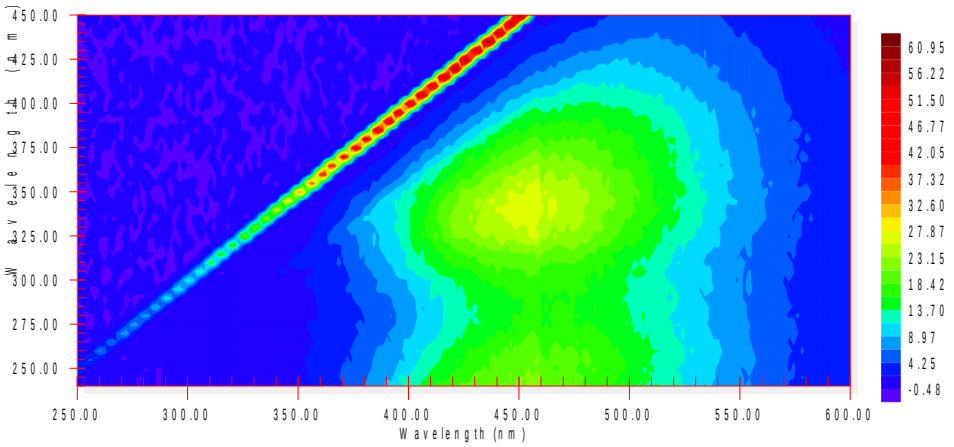

Figure 8.61: EEM-spectra of S25.

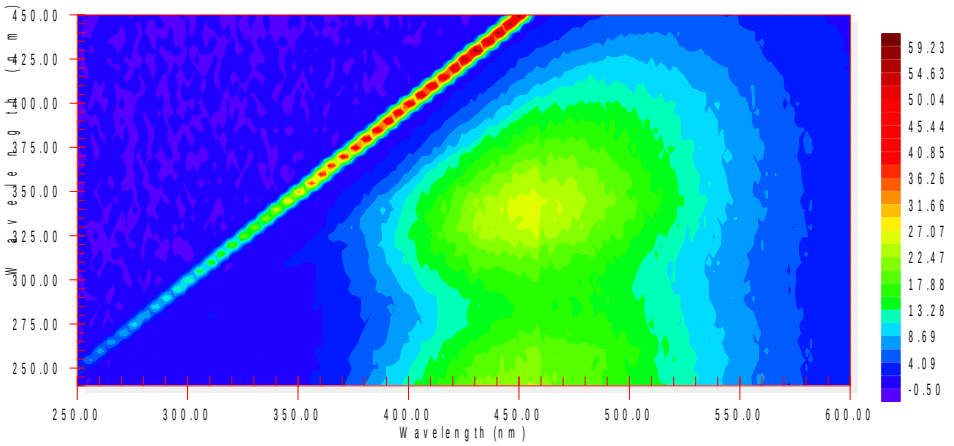

Figure 8.62: EEM-spectra of S26.

8.3.3 Biodegradation.

The following graphs are the results from the biodegradation experiments using the optimized method outlined in Table 3.5. Each graph represents one of a total of four replicates pr. sample to illustrate the variations in response.

The red coloured data points in the graphs represent the area used to calculate the respiration rate (RR) using Equation 3.3. In some of the graphs significant fluctuations were observed in the measurements during the initial lag phase. This made it difficult to determine from which point to start calculating RR, i.e. at which point should the red area start? This was determined by calculating the standard deviation of the blue coloured points (from beginning of measurement to max value). The red area starts from the point in which value is below 3 x standard deviation of blue area. Calculations were performed using RStudio® to ensure all datasets were treated consistently. Sample 7, 18, 23 and 26 were omitted due to contamination. Sample 1, 8 and 25 is missing as no measurements were performed on these.

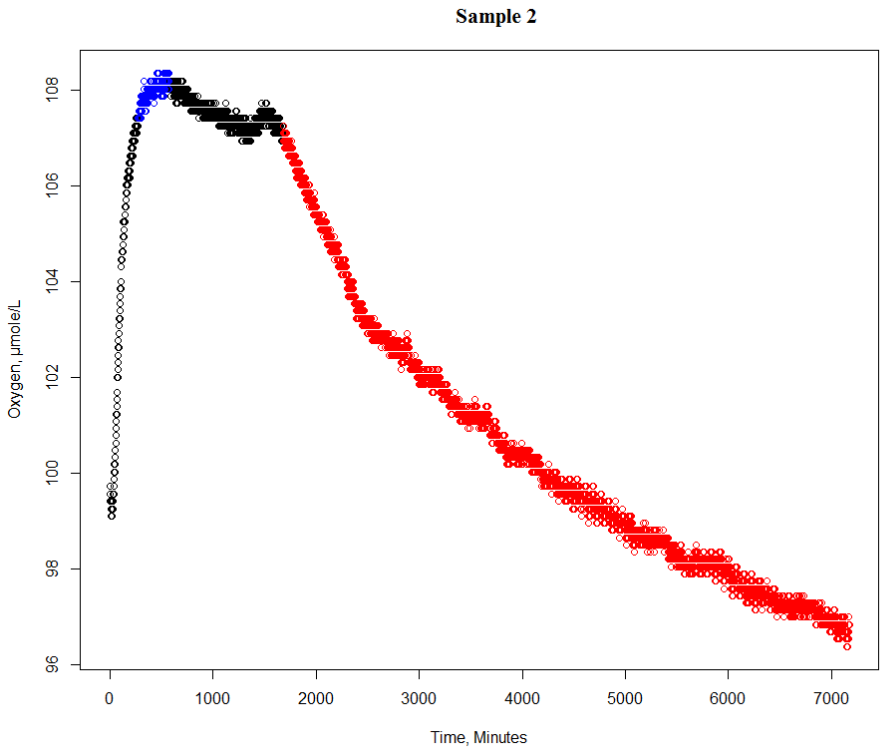

Figure 8.63: Graph illustrating oxygen consumption in Sample 2 as a result of bioactivity. Used as a measurement for biodegradation of DNOM.

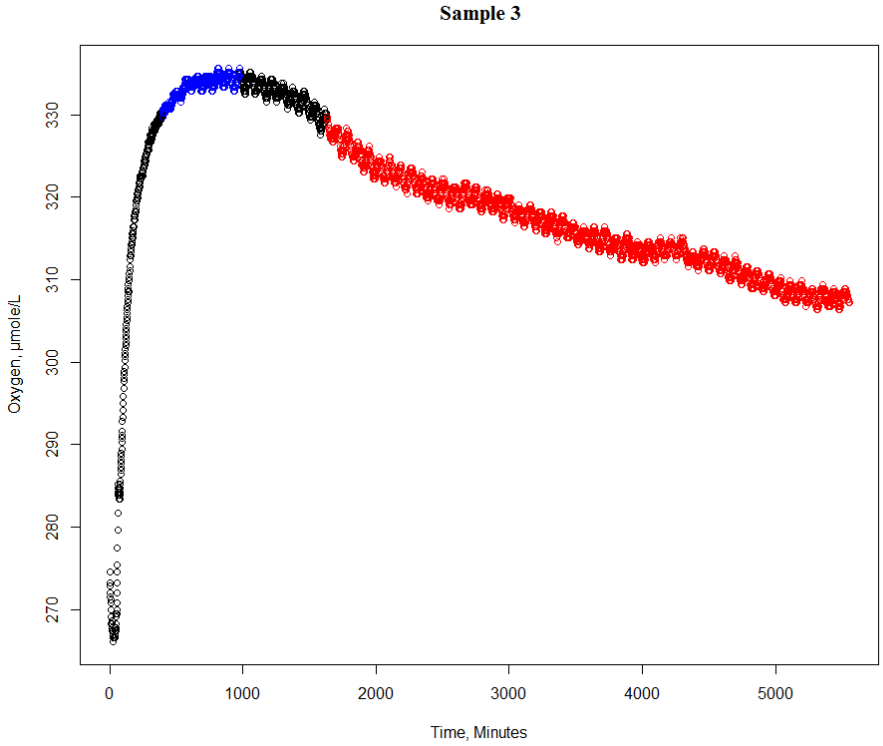

Figure 8.64: Graph illustrating oxygen consumption in Sample 3 as a result of bioactivity. Used as a measurement for biodegradation of DNOM.

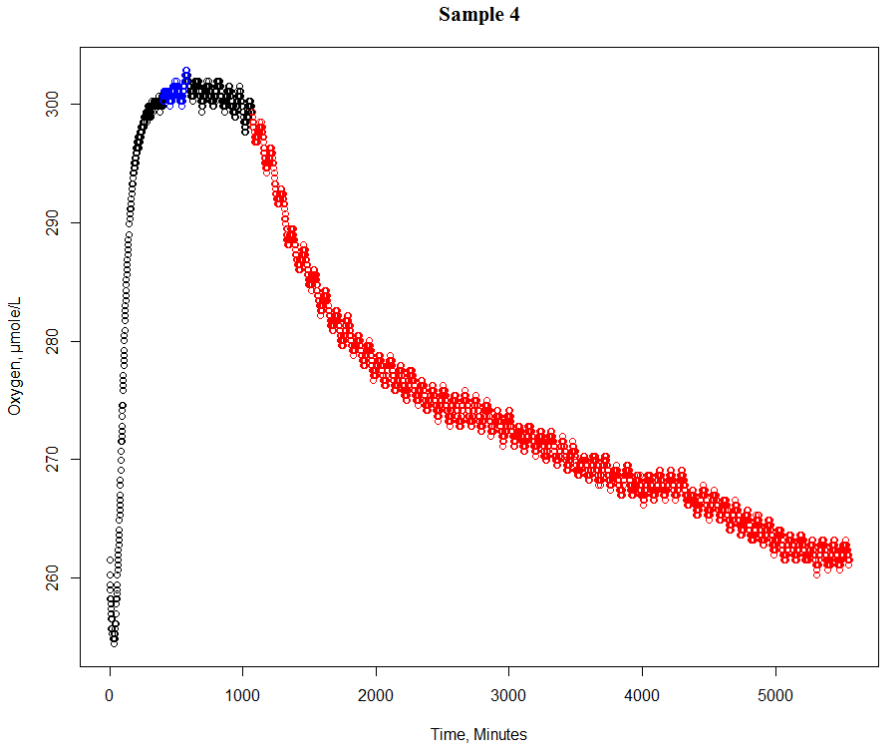

Figure 8.65: Graph illustrating oxygen consumption in Sample 4 as a result of bioactivity. Used as a measurement for biodegradation of DNOM.

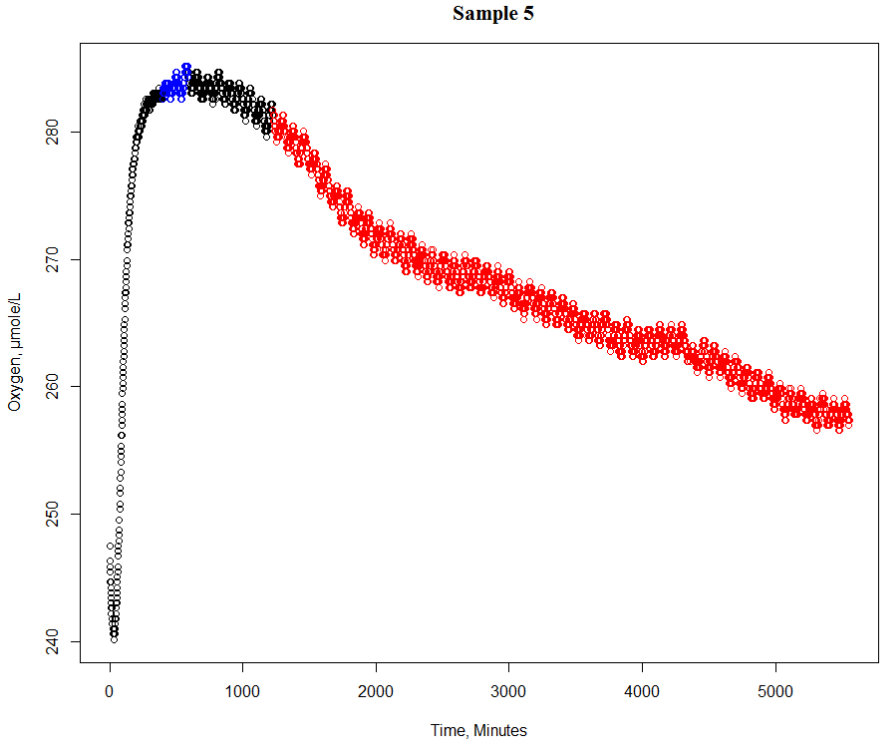

Figure 8.66: Graph illustrating oxygen consumption in Sample 5 as a result of bioactivity. Used as a measurement for biodegradation of DNOM.

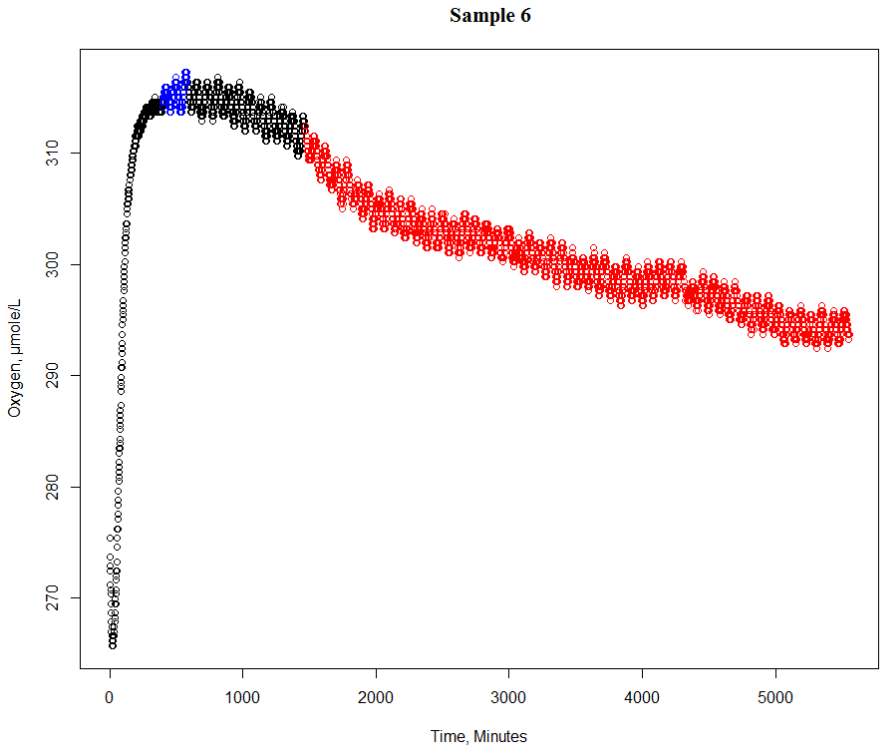

Figure 8.67: Graph illustrating oxygen consumption in Sample 6 as a result of bioactivity Used as a measurement for biodegradation of DNOM.

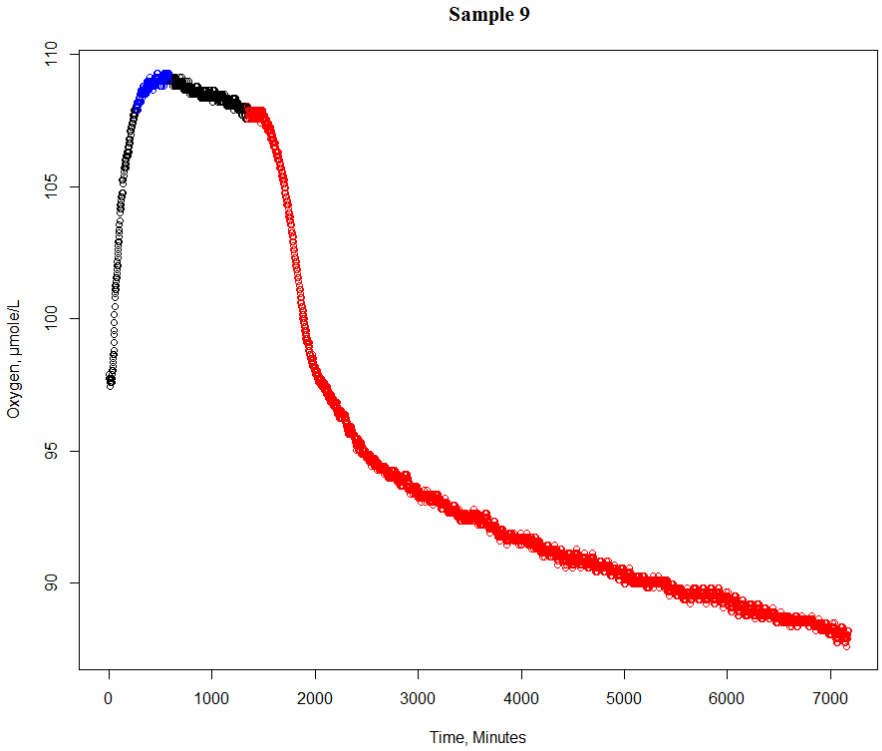

Figure 8.68: Graph illustrating oxygen consumption in Sample 9 as a result of bioactivity Used as a measurement for biodegradation of DNOM.

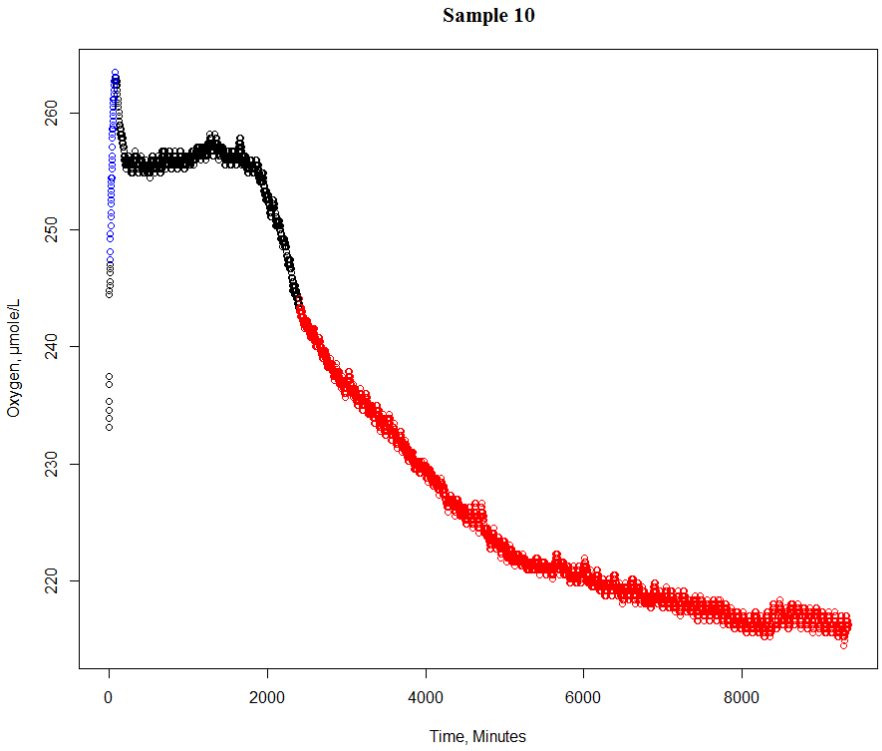

Figure 8.69: Graph illustrating oxygen consumption in Sample 10 as a result of bioactivity. Used as a measurement for biodegradation of DNOM.

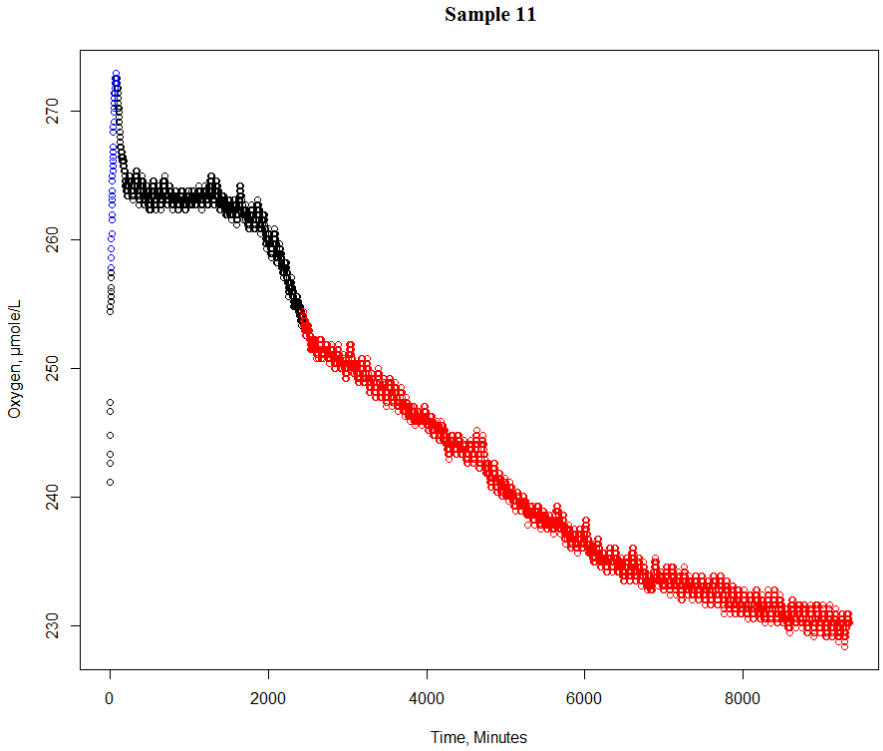

Figure 8.70: Graph illustrating oxygen consumption in Sample 11 as a result of bioactivity Used as a measurement for biodegradation of DNOM.

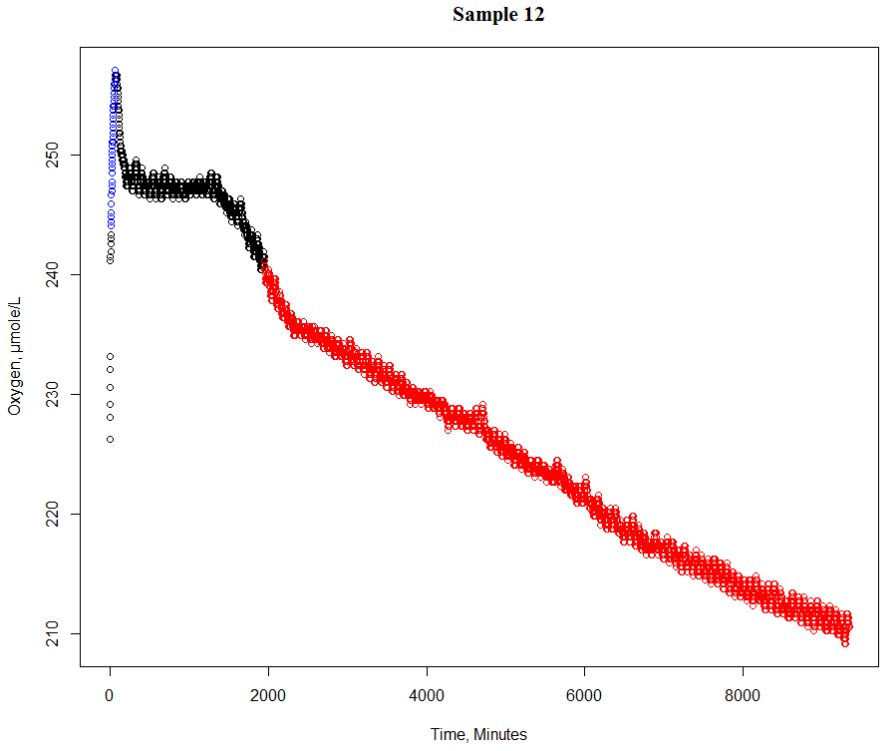

Figure 8.71: Graph illustrating oxygen consumption in Sample 12 as a result of bioactivity. Used as a measurement for biodegradation of DNOM.

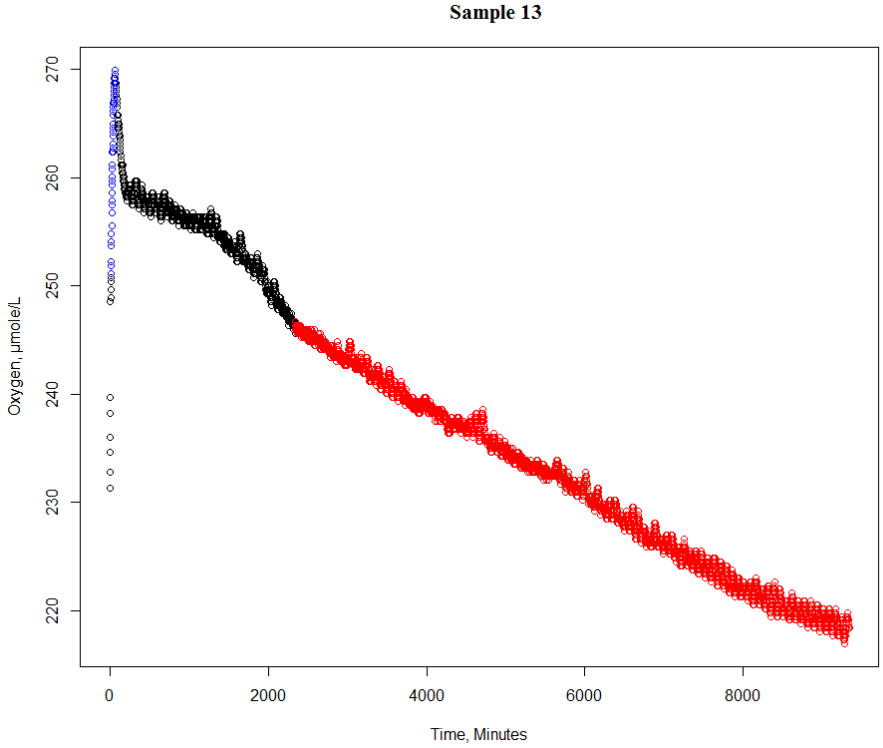

Figure 8.72: Graph illustrating oxygen consumption in Sample 13 as a result of bioactivity. Used as a measurement for biodegradation of DNOM.

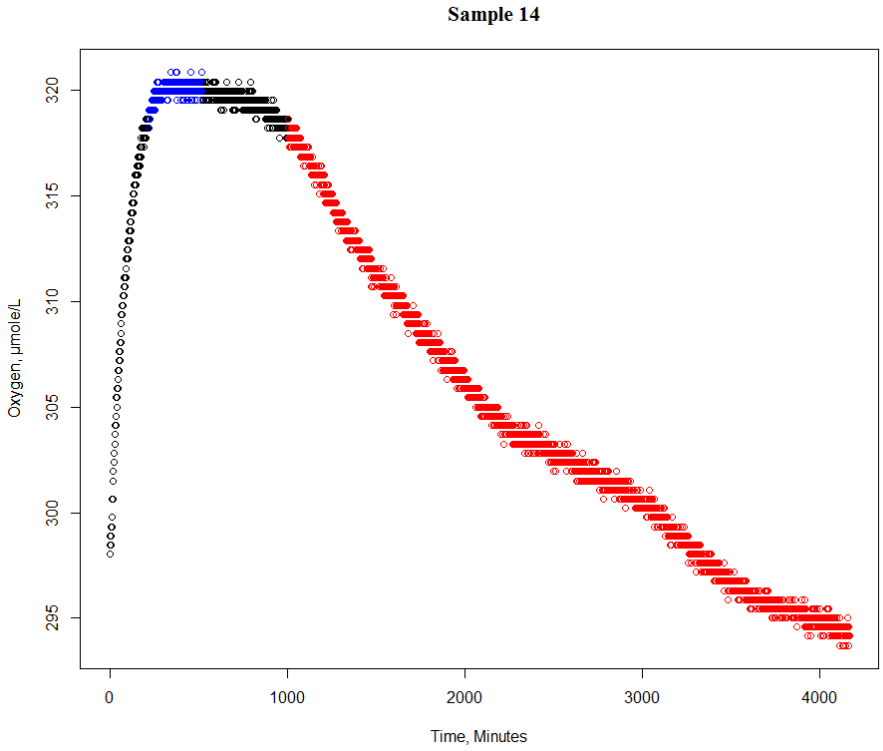

Figure 8.73: Graph illustrating oxygen consumption in Sample 14 as a result of bioactivity. Used as a measurement for biodegradation of DNOM.

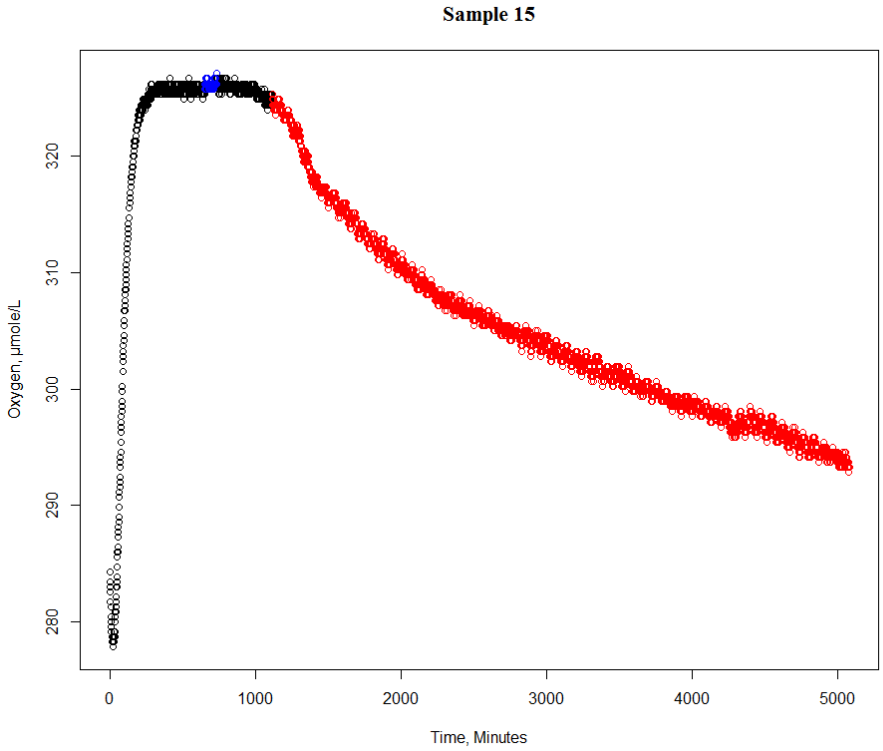

Figure 8.74: Graph illustrating oxygen consumption in Sample 15 as a result of bioactivity. Used as a measurement for biodegradation of DNOM.

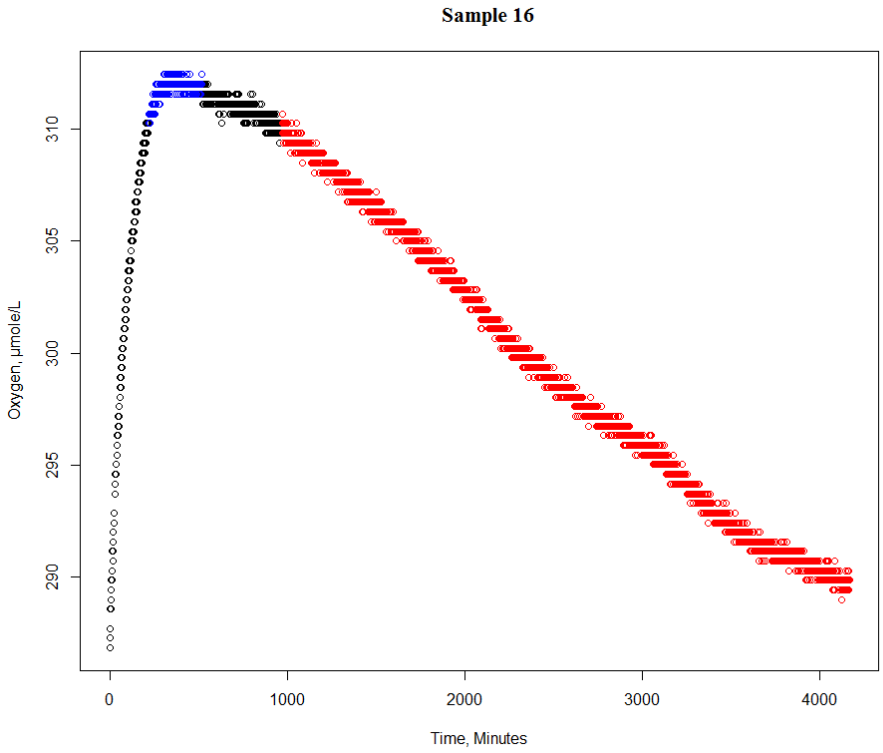

Figure 8.75: Graph illustrating oxygen consumption in Sample 16 as a result of bioactivity. Used as a measurement for biodegradation of DNOM.

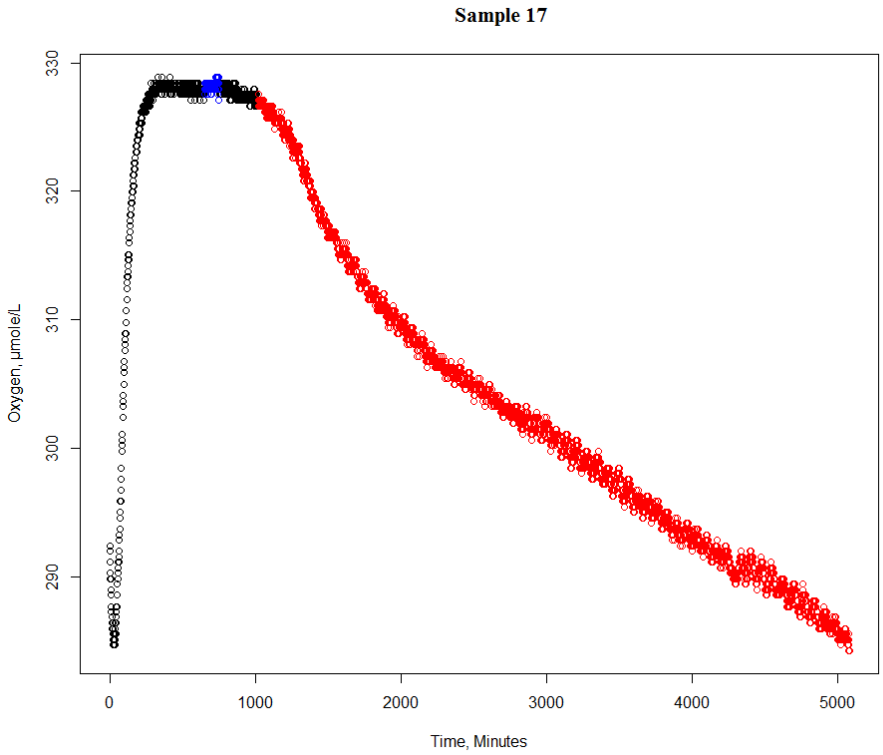

Figure 8.76: Graph illustrating oxygen consumption in Sample 17 as a result of bioactivity. Used as a measurement for biodegradation of DNOM.

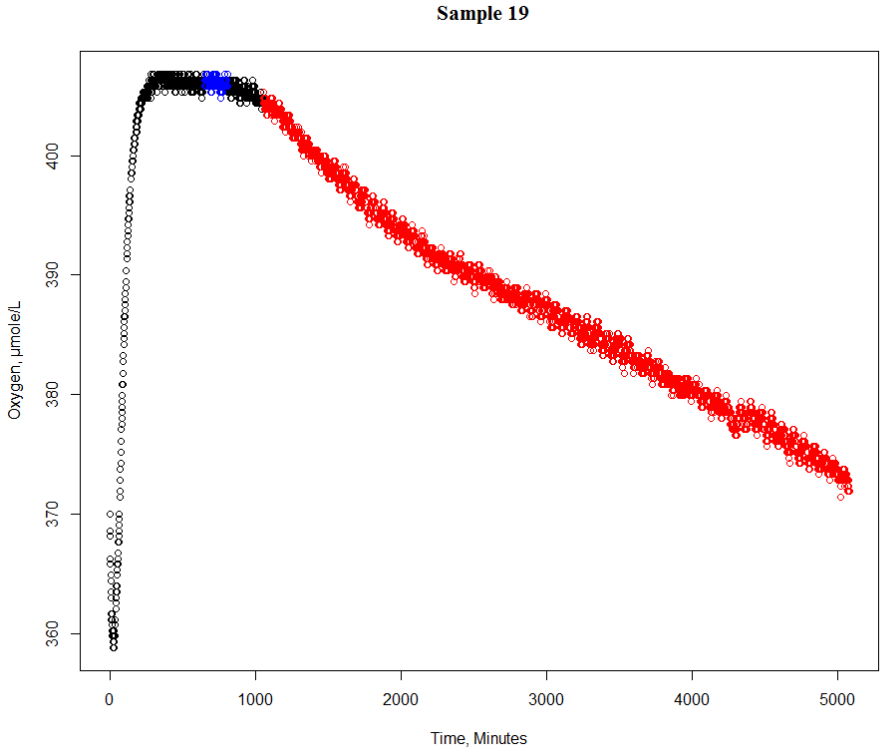

Figure 8.77: Graph illustrating oxygen consumption in Sample 19 as a result of bioactivity. Used as a measurement for biodegradation of DNOM.

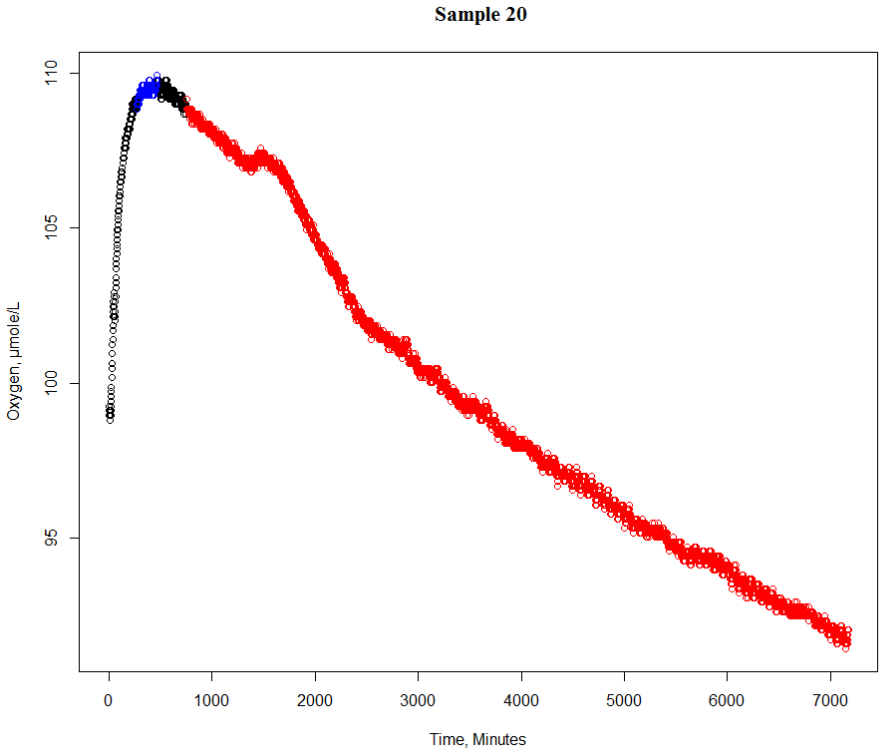

Figure 8.78: Graph illustrating oxygen consumption in Sample 20 as a result of bioactivity. Used as a measurement for biodegradation of DNOM.

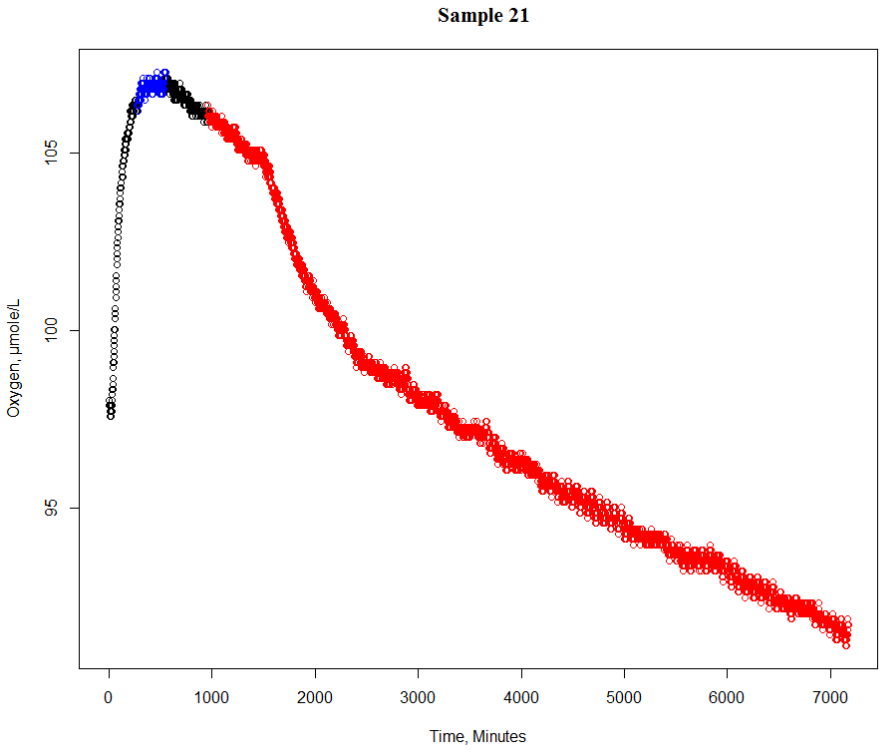

Figure 8.79: Graph illustrating oxygen consumption in Sample 21 as a result of bioactivity. Used as a measurement for biodegradation of DNOM.

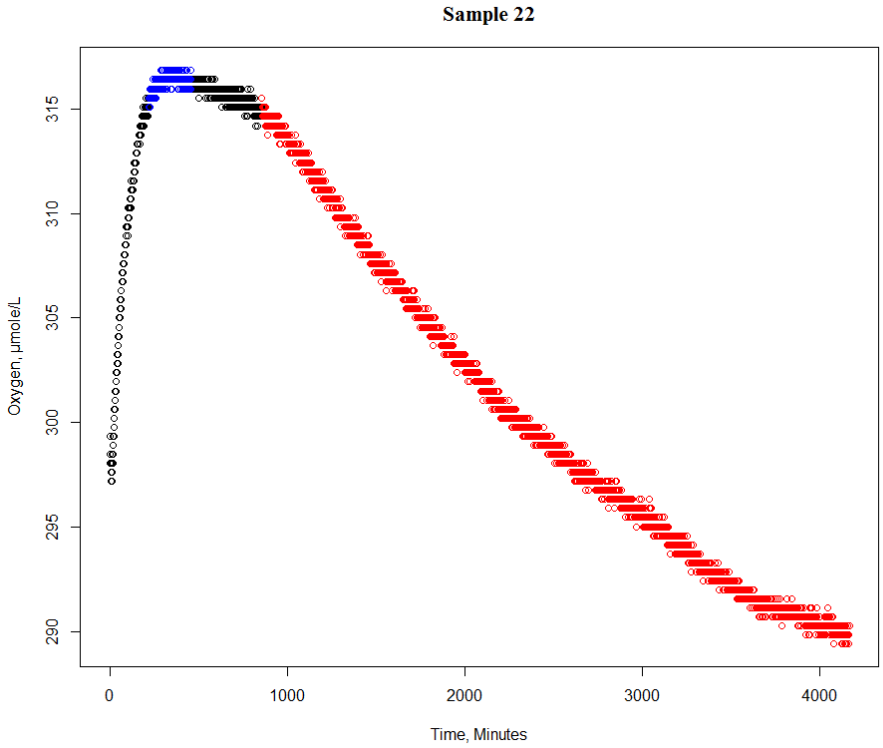

Figure 8.80: Graph illustrating oxygen consumption in Sample 22 as a result of bioactivity. Used as a measurement for biodegradation of DNOM.

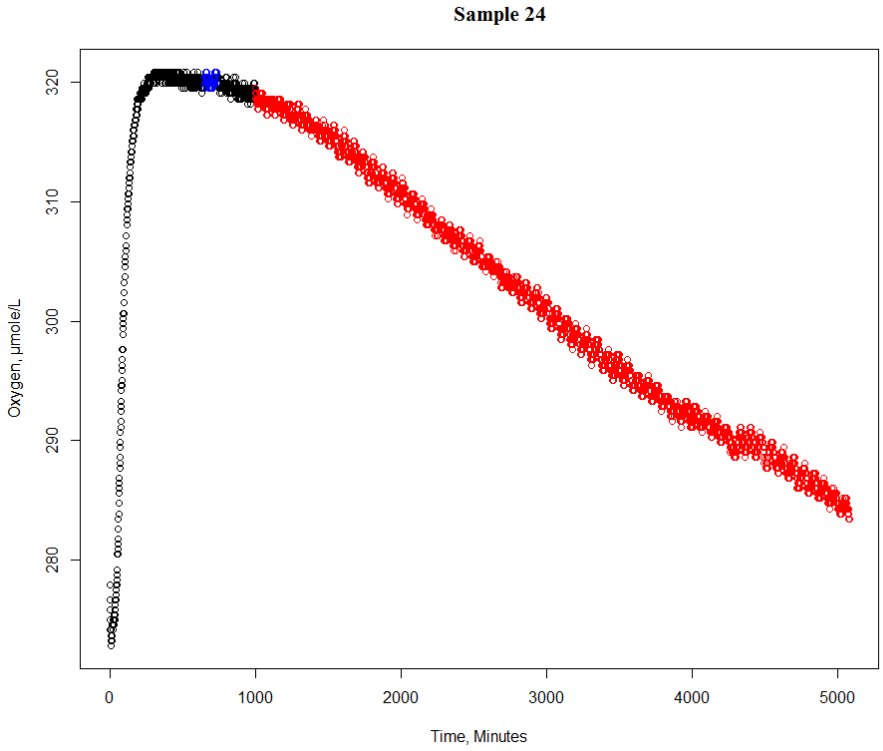

Figure 8.81: Graph illustrating oxygen consumption in Sample 24 as a result of bioactivity. Used as a measurement for biodegradation of DNOM.